

CONTROL ORIENTED MODELING OF AN AUTOMOTIVE DRIVETRAIN
FOR ANTI-JERK CONTROL

By

Gurijala Venkat Prithvi Reddy

A THESIS

Submitted in partial fulfillment of the requirements for the degree of

MASTER OF SCIENCE

In Mechanical Engineering

MICHIGAN TECHNOLOGICAL UNIVERSITY

2018

© 2018 Gurijala Venkat Prithvi Reddy

This thesis has been approved in partial fulfillment of the requirements for the Degree of MASTER OF SCIENCE in Mechanical Engineering.

Department of Mechanical Engineering - Engineering Mechanics

Thesis Advisor: *Dr. Mahdi Shahbakhti*

Thesis Co-advisor: *Dr. Darrell Robinette*

Committee Member: *Dr. Jason Blough*

Committee Member: *Dr. Jeremy Worm*

Committee Member:

Committee Member:

Department Chair: *Dr. William W. Predebon*

Contents

List of Figures	ix
List of Tables	xvii
Acknowledgments	xix
Nomenclature	xxi
List of Abbreviations	xxv
Abstract	xxvii
1 Introduction	1
1.1 Motivation	1
1.2 Technical terms used in this work	6
1.3 Literature review	11
1.3.1 Driveline modeling	11
1.3.2 AJC state estimators and parameter observers	16
1.3.3 AJC torque shaping controllers	21
1.4 Research scope and Thesis organization	24

2	Full order model development and validation	27
2.1	Model development	27
2.1.1	Amesim [®] and Simulink [®] interface	28
2.1.2	Model assumptions and limitations	32
2.1.3	Engine model	33
2.1.4	Driveline and vehicle dynamics model	36
2.1.4.1	Torque converter model	37
2.1.4.2	Automatic transmission model	40
2.1.4.3	Propeller shaft model	43
2.1.4.4	Final drive model	43
2.1.4.5	Backlash model	44
2.1.4.6	Axle shafts model	46
2.1.4.7	Suspension, tire and vehicle dynamics model	47
2.2	Model validation	52
2.2.1	Case 1: Torque converter lock-up clutch locked	55
2.2.1.1	Sub-case 1: Original vehicle parameters	55
2.2.1.2	Sub-case 2: Modified vehicle parameters - Vehicle mass increased	59
2.2.1.3	Sub-case 3: Effect of engine accessory load	61
2.2.1.4	Sub-case 4: Using crankshaft torque signal from ex- perimental data	63

2.2.1.5	Sub-case 5: Modified coefficient of rolling resistance	66
2.2.1.6	Sub-case 6: Propeller and axle shaft stiffness reduced	69
2.2.1.7	Sub-case 7: Engine, torque converter, and transmission inertia adjusted	70
2.2.1.8	Sub-case 8: Implementation of filter for propeller shaft torque	73
2.2.2	Case 2: Torque converter lock-up clutch open	75
2.2.3	Case 3: Torque converter lock-up clutch slipping	78
3	Parametric Analysis of Driveline Response	83
3.1	Effect of varying input torque ramp rate	84
3.1.1	Tip-in scenarios	84
3.1.1.1	With backlash in positive contact and TCC locked	85
3.1.1.2	With backlash in negative contact and TCC locked	88
3.1.1.3	With backlash in negative contact and TCC slipping	92
3.1.2	Tip-out scenarios	94
3.1.2.1	With backlash in positive contact and TCC locked	94
3.1.2.2	With backlash in negative contact and TCC locked	95
3.1.2.3	With backlash in negative contact and TCC open .	95
3.1.3	During backlash traversal	98
3.2	Effect of varying backlash size	101
3.2.1	Variation in transmission backlash	101

3.2.2	Variation in final drive backlash	102
3.3	Effect of varying propeller and axle shaft properties	105
3.3.1	Effect of varying propeller shaft stiffness	105
3.3.2	Effect of varying axle shaft stiffness	106
3.4	Effect of varying propeller and axle shaft damping coefficient	110
4	Reduced-order model (ROM): Development and validation	113
4.1	Introduction	113
4.2	ROM with lumped tire parameters	115
4.2.1	ROM I development	115
4.2.2	ROM I validation	117
4.3	ROM with separate tire parameters	119
4.3.1	ROM II development	119
4.3.2	ROM II validation	122
4.3.3	Effect of lumping backlashes in the ROM	122
4.4	Estimation of model parameters for ROM	126
4.5	Application of ROM for controls	128
5	Conclusion and Future work	133
5.1	Conclusions	133
5.2	Future work	137
	References	139

A	Amesim-Simulink Interface	147
B	Engine Torque Uncertainty	149
C	Program and Data File Summary	153
C.1	Chapter 1	153
C.2	Chapter 2	154
C.3	Chapter 3	155
C.4	Chapter 4	156
C.5	Appendix B	157

List of Figures

1.1	Segment wise sale of new automobiles in the United States in 2016 [1].	2
1.2	Projected vehicle sales in American, European and Chinese markets between 2017 - 2030, classified based on propulsion technology [2]. .	3
1.3	Projected sales of autonomous vehicles in American, European, and Chinese markets between 2017 - 2030, classified by the level of automation [3].	4
1.4	Motivation behind the current research.	6
1.5	Backlash in gears [4].	7
1.6	Representative output of propeller shaft torque showing clunk and shuffle, and backlash traversal in driveline.	10
1.7	Timeline of some of the prior AJC works in research literature. . . .	14
1.8	Some of the estimator design approaches used in the AJC literature[5][6][7][8][9].	20
1.9	Some of the torque shaping controller design approaches given in the AJC literature[10][11][12].	22
1.10	Thesis organization	26

2.1	Components of the full-order model. Top box represents components modeled in Simulink, and bottom box represents components modeled in Amesim.	29
2.2	Overview of Amesim [®] - Simulink [®] interface. Adapted from [13]. . .	31
2.3	Amesim [®] model showing the torque converter with lock-up clutch and spring hysteresis blocks.	38
2.4	Schematic diagram showing the 10-speed transmission[14].	41
2.5	Amesim [®] model showing the 10-speed automatic transmission blocks.	42
2.6	Representative model of backlash.	45
2.7	Amesim [®] model showing the propeller and axle shafts, along with the rear differential and final drive backlash.	46
2.8	Amesim [®] model showing the suspension, tire and the vehicle dynamics blocks.	49
2.9	Overview of the Amesim [®] vehicle model.	51
2.10	Overview of the model validation work done.	53
2.11	Results for sub-case 1 of model validation: Comparison between experimental and simulation data with <u>initial driveline parameters</u> (Table 2.2).	57
2.12	Results for sub-case 2 of model validation: Comparison between experimental and simulation data with <u>increased vehicle mass</u> (Table 2.4).	60

2.13	Results for sub-case 3 of model validation: Comparison between experimental and simulation data after increasing vehicle mass, and <u>subtracting engine accessory load torque</u> (Table 2.6).	62
2.14	Results for sub-case 4 of model validation: Comparison between experimental and simulation data with experimental crankshaft torque trajectory as input.	65
2.15	Results for sub-case 5 of model validation: Comparison between experimental and simulation data with <u>reduced coefficient of rolling resistance</u> (Table 2.10.	68
2.16	Results for sub-case 6 of model validation: Comparison between experimental and simulation data with <u>reduced axle and propeller shaft stiffness</u> (Table 2.12).	71
2.17	Results for sub-case 7 of model validation: Comparison between experimental and simulation data with crankshaft torque as input, reduced vehicle mass, reduced coefficient of rolling resistance, reduced drive shaft stiffness, and <u>increased inertia of engine, torque converter and transmission</u> (Table 2.14).	74

2.18	Simulation output in 5th gear with estimated crankshaft torque compensated for error as input to Amesim [®] , modified vehicle mass, modified coefficient of rolling resistance, modified propeller shaft and axle shaft stiffness, and modified engine, torque converter and transmission inertia, and <u>filtered driveshaft torque</u>	76
2.19	Results for the case of open torque converter clutch. Comparison between experimental and simulation data with adjusted parameters from previous section, <u>with TCC status open</u> (Table 2.16).	79
2.20	Results for the case of slipping torque converter clutch. Comparison between experimental and simulation data, with adjusted parameters from previous section, and <u>with TCC status slipping</u> (Table 2.17).	81
3.1	Driveline response for tip-in scenario with <u>150 Nm/s ramp rate</u> , backlash in positive contact, and locked TCC.	86
3.2	Driveline response for tip-in scenario with <u>500 Nm/s ramp rate</u> , backlash in positive contact, and locked TCC.	87
3.3	Driveline response for tip-in scenario with 150 Nm/s ramp rate, backlash in negative contact, and locked TCC.	90
3.4	Driveline response for tip-in scenario with 500 Nm/s ramp rate, backlash in negative contact, and locked TCC.	91
3.5	Driveline response for tip-in scenario with 500 Nm/s ramp rate, backlash in negative contact, and slipping TCC.	93

3.6	Driveline response for tip-out scenario with 150 Nm/s ramp rate, backlash in positive contact, and locked TCC.	96
3.7	Driveline response for tip-out scenario with 150 Nm/s ramp rate, backlash in negative contact, and locked TCC.	97
3.8	Driveline response for tip-out scenario with 150 Nm/s ramp rate, backlash in negative contact, and open TCC.	99
3.9	Driveline response for tip-in scenario with torque ramp rate varying during backlash traversal. The backlash is initially in negative contact, and TCC is locked.	100
3.10	Effect of changing the transmission backlash on driveline response. Case A represents condition where transmission backlash is 10 deg. Case B represents condition where transmission backlash is 20 deg.	103
3.11	Effect of increasing the final drive backlash on driveline response. Case A represents condition where final drive backlash is 4 deg. Case B represents condition where final drive backlash is 8 deg.	104
3.12	Effect of changing propeller shaft stiffness on overall driveline response. Case A represents condition where propeller shaft stiffness is decreased by 25%. Case B represents condition where propeller shaft stiffness is increased by 25%.	107

3.13	Effect of changing axle shaft stiffness on overall driveline response. Case A represents condition where axle shaft stiffness is increased by 25%. Case B represents condition where axle shaft stiffness is decreased by 25%.	109
3.14	Effect of changing axle shaft damping on driveline response. Case A represents condition where axle shaft damping is increased by 25%. Case B represents condition where axle shaft damping is decreased by 25%.	111
4.1	ROM with lumped tire parameters.	116
4.2	<u>Comparison of ROM I</u> with lumped tire parameters' driveline response with FOM, for a tip-in scenario.	118
4.3	ROM with separate tire parameters.	119
4.4	<u>Comparison of ROM II</u> with separate tire parameters' driveline response with FOM, for a tip-in scenario.	121
4.5	Comparison of ROM with separate tire parameters' driveline response with FOM, <u>in 3rd gear</u> , for a tip-in scenario.	123
4.6	Comparison of lumped and split backlash models in full-order and reduced-order models.	125
4.7	Schematic showing a simple control system, utilizing the output of the ROM, for controlling the torque delivered to the plant(Full-order model).	128

4.8	Comparison of driveline response for two cases of torque input. Case A: Torque input without shaping. Case B: Torque input with shaping.	131
B.1	Observed engine torque response for a throttle input of 0 → 100% .	150
B.2	Observed engine torque response for a throttle input of 0 → 60% .	150
B.3	Observed engine torque response for a throttle input of 0 → 20% .	151
B.4	Observed response for a throttle tip-out scenario	151

List of Tables

2.1	Frequency of driveline oscillations in sub-case 1	56
2.2	Simulation parameters for Case 1	58
2.3	Frequency of driveline oscillations in sub-case 2	59
2.4	Simulation parameters for Case 2	59
2.5	Frequency of driveline oscillations in sub-case 3	61
2.6	Simulation parameters for sub-case 3	63
2.7	Frequency of driveline oscillations in sub-case 4	64
2.8	Simulation parameters for sub-case 4	64
2.9	Frequency of driveline oscillations in sub-case 5	67
2.10	Simulation parameters for sub-case 5	67
2.11	Frequency of driveline oscillations in sub-case 6	70
2.12	Simulation parameters for sub-case 6	72
2.13	Frequency of driveline oscillations in sub-case 7	73
2.14	Simulation parameters for sub-case 7	73
2.15	Filter parameters used for filtering simulated propeller shaft torque	75
2.16	Simulation parameters for Case 2: TCC open condition	78

2.17 Simulation parameters for Case 3: TCC slipping condition	80
C.1 Chapter 1 figure files	153
C.2 Chapter 2 figure files	154
C.3 Chapter 2 model files	154
C.4 Chapter 2 model validation files	155
C.5 Chapter 3 figure files	155
C.6 Chapter 3 model files	156
C.7 Chapter 4 figure files	156
C.8 Chapter 4 model files	157
C.9 Appendix B figure files	157

Acknowledgments

This work would not have been possible without the excellent guidance, and patient support of Dr. Mahdi Shahbakhti, and Dr. Darrell Robinette. Their mentorship has taught me invaluable lessons, in subject and life, for which I am grateful to them.

I would like to thank Dr. Maruthi Ravichandran, and Dr. Jeffrey Doering, of Ford Motor Company, for their valuable technical insights, and patience during the many meetings that took place through the course of this work. Thanks are also due to Vehicle Controls and Systems Engineering (VCSE) department of Ford Research and Advanced (R&A) Engineering Organization. I would like to thank Mary Farmer (Technical Expert, Ford Motor Co.), for her help with experimental data collection, and inputs towards making this project better. I would also like to thank Imad Khan, Hsun-Hsuan Huang, Vladimir Ivanovic, Dan Nagelhout, Natalie Remisoski, and Kalyan Addepalli for their help in obtaining vehicle parameters.

I am grateful to Dr. Jason Blough and Dr. Jeremy Worm, for accepting to be on my thesis defense committee and for their support in the weeks preceding my defense. Their feedback on this work will help in improving the future work of this project.

I graciously acknowledge Prince Lakhani and Kaushal Darokar for their contributions, and for the meaningful discussions that took place during the course of this project.

Thanks are also due to my roommates Sampath Rallapalli, and Vishnu Durgam, who helped in creating a lively, fun-filled atmosphere at home.

I owe everything in my life to the love, and support I received from my parents, Radha and Prakash, and my family members, Kedar, and Hasitha. Their belief in my abilities has always motivated me to be a better person, and for that I can not thank them enough.

Nomenclature

α	Backlash angle [<i>deg.</i>]
δ	Road slope for use in longitudinal vehicle dynamics [<i>rad</i>]
θ_{ax}	Angular position of axle shaft [<i>rad</i>]
θ_b	Angular position of backlash [<i>rad</i>]
θ_e	Angular position of the engine [<i>rad</i>]
θ_s	Angular position of shaft [<i>rad</i>]
θ_t	Angular position of transmission output shaft [<i>rad</i>]
θ_{ps}	Angular position of propeller shaft at final drive end [<i>rad</i>]
θ_{ti}	Angular position of tire [<i>rad</i>]
$\dot{\theta}_{ax}$	Angular speed of axle shaft at tire end [<i>rad/s</i>]
$\dot{\theta}_e$	Angular speed of the engine [<i>rad/s</i>]
$\dot{\theta}_{ps}$	Angular speed of propeller shaft at final drive end [<i>rad/s</i>]
$\dot{\theta}_{ti}$	Angular speed of tire [<i>rad/s</i>]
$\dot{\theta}_{tr}$	Angular speed of transmission output shaft [<i>rad/s</i>]
$\dot{\theta}_w$	Angular speed of wheel hub [<i>rad/s</i>]
$\ddot{\theta}_e$	Angular acceleration of the engine [<i>rad/s</i> ²]
a_{veh}	Longitudinal acceleration of the vehicle [<i>m/s</i> ²]
A_f	Frontal area of the vehicle [<i>m</i> ²]

C_D	Coefficient of drag $[-]$
c_{ax}	Damping of the axle shaft $[N.m/RPM]$
c_{ps}	Damping of the propeller shaft $[N.m/RPM]$
c_s	Damping of shaft $[N.m/RPM]$
c_{ti}	Damping of the tire $[N.m/RPM]$
F	Multiplication factor used in section 4.5 $[-]$
F_{aero}	Aerodynamic force on the vehicle $[N]$
F_{engine}	Propulsive force developed by the engine $[N]$
F_{roll}	Rolling resistance force on the vehicle $[N]$
F_{slope}	Slope force on the vehicle $[N]$
g	Acceleration due to gravity $[m/s^2]$
i_{tr}	Gear ratio of current gear state of the transmission $[-]$
i_{fd}	Gear ratio of the final drive $[-]$
J_e	Rotational inertia of the engine $[kg.m^2]$
J_w	Rotational inertia of the wheel hub $[kg.m^2]$
K	Capacity factor of torque converter $[RPM/\sqrt{N.m}]$
k_{ax}	Stiffness of the axle shaft $[N.m/deg]$
k_{ps}	Stiffness of the propeller shaft $[N.m/deg]$
k_s	Stiffness of shaft $[N.m/deg]$
k_{ti}	Stiffness of the tire $[N.m/deg]$
N	Engine speed $[RPM]$

r_{veh}	Coefficient of viscous friction $[-]$
r_{ti}	Radius of the tire $[m]$
SR	Speed ratio of torque converter $[-]$
t	Time $[sec]$
$\tau_{e,base}$	Time constant of first-order lag $[msec]$
$t_{(d,base)}$	Time delay in base path $[sec]$
$t_{(d,inst)}$	Time delay in instantaneous path $[sec]$
T_{ax}	Torque output from axle shaft $[N.m]$
T_{driver}	Driver requested torque $[N.m]$
T_{fric}	Friction losses of engine torque $[N.m]$
TR_{spk}	Torque ratio due to spark modulation $[-]$
T_{fd}	Torque output from final drive $[N.m]$
T_{im}	Torque input at torque converter impeller $[N.m]$
T_{ps}	Torque output from propeller shaft $[N.m]$
T_{shaped}	Shaped engine torque output in ROM $[N.m]$
T_{tcc}	Torque through the torque converter lock-up clutch $[N.m]$
T_{ti}	Torque output at the tire $[N.m]$
T_{tu}	Torque output at torque converter turbine $[N.m]$
T_{tr}	Torque output from transmission $[N.m]$
$T_{gearloss}$	Torque loss inside the transmission $[N.m]$
TR	Torque ratio of torque converter $[-]$

T_{unc} Uncertainty in engine delivered torque [$N.m$]

V Velocity of the vehicle [m/s]

V_{wind} Wind velocity acting on the vehicle [m/s]

List of Abbreviations

2WD	Two Wheel Drive
4WD	Four Wheel Drive
AT	Automatic Transmission
AJC	Anti-Jerk Control
CAN	Controller Area Network
CV	Constant Velocity
CVT	Continuously Variable Transmission
DKF	Discrete Kalman Filter
ECU	Electronic Control Unit
EKF	Extended Kalman Filter
FOM	Full Order Model
HEV	Hybrid Electric Vehicle
HIL	Hardware in Loop
IC	Internal Combustion
LO	Luenberger Observer
LQR	Linear Quadratic Regulator
MT	Manual Transmission
MPC	Model Predictive Control

MPT	Multi Parametric Toolbox
NVH	Noise Vibration and Harshness
PI	Proportional Integrator
PWA	Piecewise Affine
ROM	Reduced Order Model
SKF	Scented Kalman Filter
SMO	Sliding Mode Observer
SP	Smith Predictor
SUV	Sports Utility Vehicle
TCC	Torque converter lock-up clutch
TCU	Transmission Control Unit

Abstract

Drivability is an important metric during the development of an automobile. Calibration engineers spend a significant amount of time trying to improve the drivability of vehicles for various driving conditions. With an increase in the available computational power in an automobile, novel model-based methods are being implemented for further improving the drivability, while reducing calibration time and effort. Phenomenon known as clunk and shuffle, which are caused due to backlash and compliance in the driveline, are a major cause of issues related to drivability and noise, vibration and harshness (NVH) during tip-in and tip-out scenarios.

This thesis focuses on developing a high-fidelity, control-oriented vehicle driveline model, which can be used for developing systems, to improve the drivability of a vehicle, during tip-in and tip-out events. A first principle physics-based model is developed, which includes the engine as a torque generator, backlash elements as discontinuities, and driveshafts as compliant elements. Experimental validation results showed that the accuracy of the developed model, in representing shuffle oscillation frequency, during the tip-in scenarios, with locked torque converter clutch, is approximately 99 %.

A parametric analysis is performed to characterize the behavior of the model during

different input conditions, and to study the effect of backlash size, and driveshaft compliance on the response of the driveline. Based on the observations from the parametric analysis, the high-fidelity model is later condensed into a reduced-order model, and comparative analysis is carried out between two reduced-order model (ROM) designs. The comparative results between the full-order model and ROM show that the ROM with separate tire parameters is better in predicting the frequency and amplitude of shuffle oscillations during tip-in events.

Chapter 1

Introduction

1.1 Motivation

Ever since the first production automobile was built by Karl Benz in 1885, there have been plenty of innovations with respect to performance, safety, efficiency and comfort of an automobile. With the advent of the electronic control unit (ECU) in automobiles, developments in the automotive industry took new heights. Cars today have dozens of ECUs on-board to manage tasks as simple as controlling the headlights, to complicated transient emission control of engines. As the computational power and reliability of electronic control systems in automobiles increase, it opens up new avenues for implementing innovative technologies.

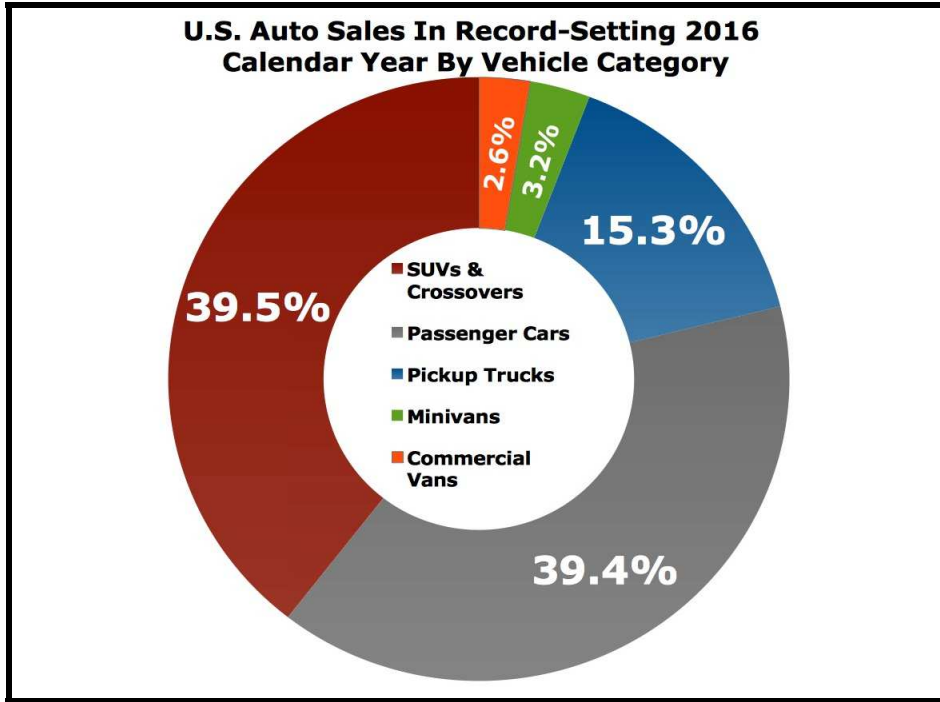


Figure 1.1: Segment wise sale of new automobiles in the United States in 2016 [1].

With crossovers, and pick-up trucks dominating the market share in the United States (Fig. 1.1), automotive manufacturers are increasingly focusing on refining these segments, which includes improving the drivability of these vehicles. Drivability can be defined as the qualitative evaluation of the powertrain's (interchangeably referred to as driveline in this thesis) operational characteristics which includes aspects like smooth acceleration, seamless gear shifts, etc. The current work is motivated by the need to reduce undesirable jerks that are experienced due to the oscillations induced into the powertrain, caused by: (i) the presence of backlash within elements of the driveline like the transmission, final drive, constant velocity (CV) joints etc., and (ii) the flexibility of axle shafts.

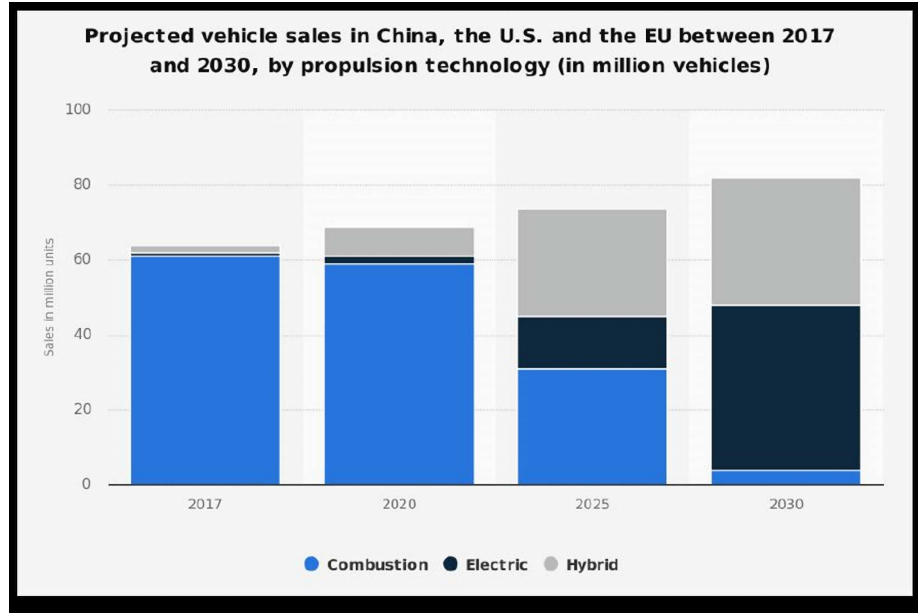


Figure 1.2: Projected vehicle sales in American, European and Chinese markets between 2017 - 2030, classified based on propulsion technology [2].

While the perception of backlash induced oscillations is subjective, it is also dependent on factors like the source of propulsion (IC engine, electric motor, hybrid system), and configuration of the driveline (2WD, 4WD, etc.). With an increase in the sales of hybrid electric vehicles (HEVs) and electric vehicles (EVs) (Fig. 1.2), the torque delivery characteristics of an electric motor is playing an important role in determining the drivability of the vehicle. An IC engine is subject to delays in torque generation and delivery due to the dynamics of manifold filling and fuel combustion. The electric motor however, does not have such delays, and therefore, torque generation and delivery is quite instantaneous, which may lead to higher impact velocities at backlash zones, causing harsh vibrations throughout the driveline.

Also, with increasing availability of driver-assistance technologies, semi-autonomous

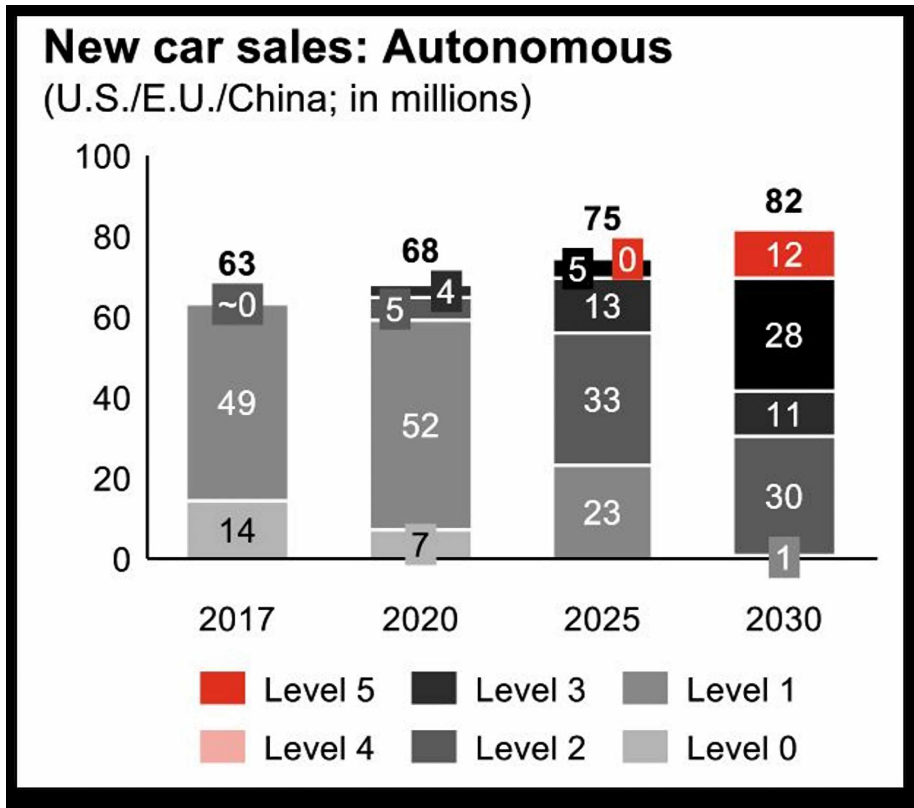


Figure 1.3: Projected sales of autonomous vehicles in American, European, and Chinese markets between 2017 - 2030, classified by the level of automation [3].

and fully-autonomous vehicles are making a slow but steady entry into the automotive market. Predictions indicate that by 2030 (Fig. 1.3), there would be significant market for Level 5 autonomy vehicles, making the concept of a driver obsolete. Most of the people using automobiles would spend a major portion of their time in the vehicle, working or entertaining themselves. Motion sickness while looking at screens/books inside a moving vehicle is already an established problem [15]. Undesirable jerks in the vehicle would further aggravate the problem, and negatively affect the experience inside an autonomous vehicle.

Fig. 1.4 shows an overview of the motivation behind the current research. Considering these scenarios, it was recognized that an effective control strategy is crucial in reducing unwanted oscillations in the driveline, and consequently improving drivability. Rule based strategies, for this application, lead to plenty of calibration parameters, in order to account for all the possible scenarios that the vehicle may experience. Calibrating such a system requires significant amount of time, and effort, leading to increased development time of an automobile. Model based strategies, on the other hand, provide a more efficient method of developing a control system, and are preferred as long as an accurate, and robust model of the system to be controlled is available, and computational power requirements are met.

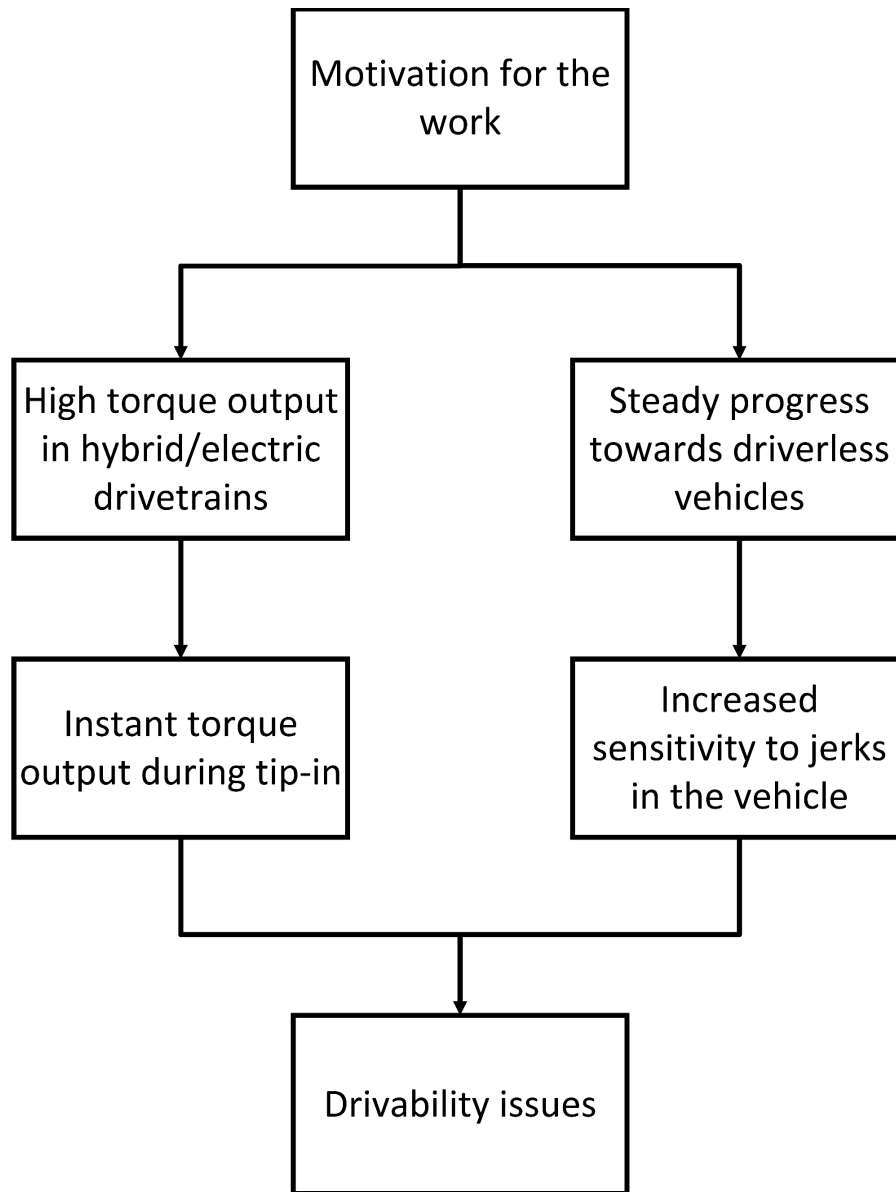


Figure 1.4: Motivation behind the current research.

1.2 Technical terms used in this work

For understanding the objective and results of this work properly, it is necessary to briefly describe some of the technical terms that are used throughout this thesis.

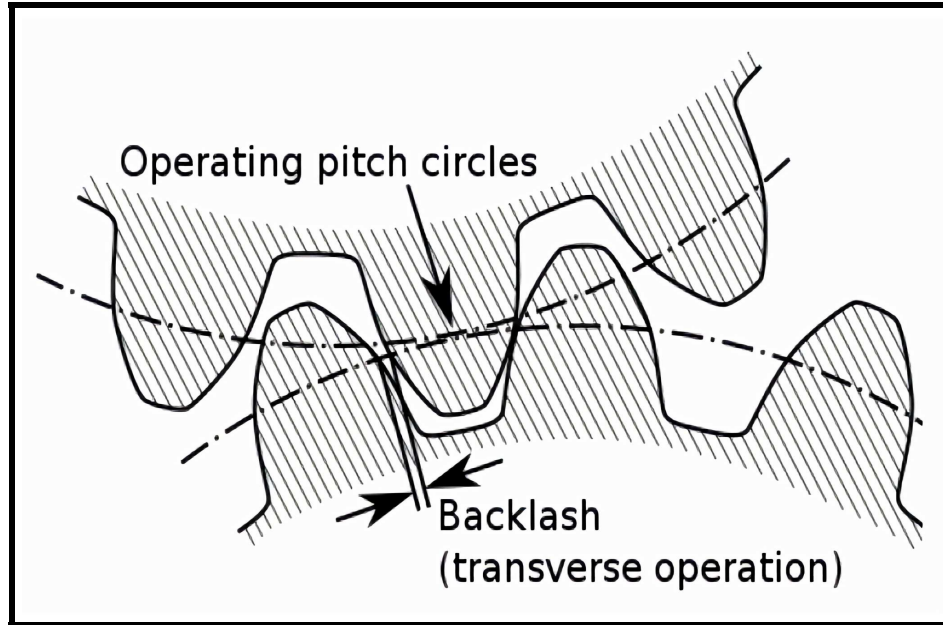


Figure 1.5: Backlash in gears [4].

For any gear set, it is a design choice to have some play/clearance between the teeth of gears meshing with each other. This is to allow the meshing to be free, and to provide a clearance for the lubricant to create a film on the surface of gear teeth. This gap between the meshing faces of two gears in a gear set is known as backlash (Fig. 1.5). With respect to an automotive powertrain, this backlash is primarily observed in the transmission and the final drive on the driven axle. The magnitude of transmission backlash is dependent on the gear in use during vehicle operation.

The main cause of concern with gear backlash, in automotive drivetrains, is during driving maneuvers which are referred to as tip-in and tip-out. Usually, tip-in occurs when there is a rise in driver requested torque, and tip-out occurs when there is a drop in driver requested torque. This rise or drop may take place either through

the accelerator pedal, or through other systems like cruise controller. These tip-in and tip-out scenarios cause the meshing gear teeth to hit against each other in an impact, as torque flow direction through the driveline changes. The audible aspect of this impact is called *clunk*. A significant change in the magnitude of torque delivered by the propulsive source, causes longitudinal oscillations in the driveline, which are referred to as *shuffle*, and causes the undesired feeling of jerk to the driver/passenger. The frequency of these oscillations is generally in the range of 2 - 10 Hz, depending on the gear selected in the transmission, and corresponds to the resonant frequency of human organs [16], causing serious NVH issues in an automobile. Shuffle phenomenon can occur independent to clunk, and it is significantly influenced by engine inertia, and the compliance of the driveline [17].

Backlash states can be classified as negative, positive and inlash based on its position in the driveline [18]. When torque is flowing from the wheels to the engine, backlash is said to be in ‘negative’ contact. When torque is flowing from the engine to the wheels, backlash is said to be in ‘positive’ contact. During transition from negative contact to positive contact, the backlash is said to be ‘inlash’. These classifications are useful when developing control strategies to mitigate backlash induced jerks in the driveline.

The phenomenon of clunk and shuffle are shown in Fig. 1.6. The first subplot shows the trajectory of engine torque, the second subplot shows the corresponding response

of the propeller shaft torque, and the third subplot shows the traversal of backlash in the driveline. Initially, the engine is coasting and the backlash is in negative contact. As soon as the engine torque starts rising, the driveshafts start untwisting. Once the shafts finish untwisting, the backlash start traversing from negative contact to positive contact, which is represented by the propeller shaft torque being zero for a brief period of time. Clunk is heard as soon as positive contact is made by the gear teeth, and then shuffle is felt in the driveline. This complete scenario takes place in the order of milliseconds, and Fig. 1.6 shows a magnified view for representational purposes.

While it is possible to observe the effect of backlash induced driveline oscillations in a manual transmission, this work only focuses on automatic transmissions.

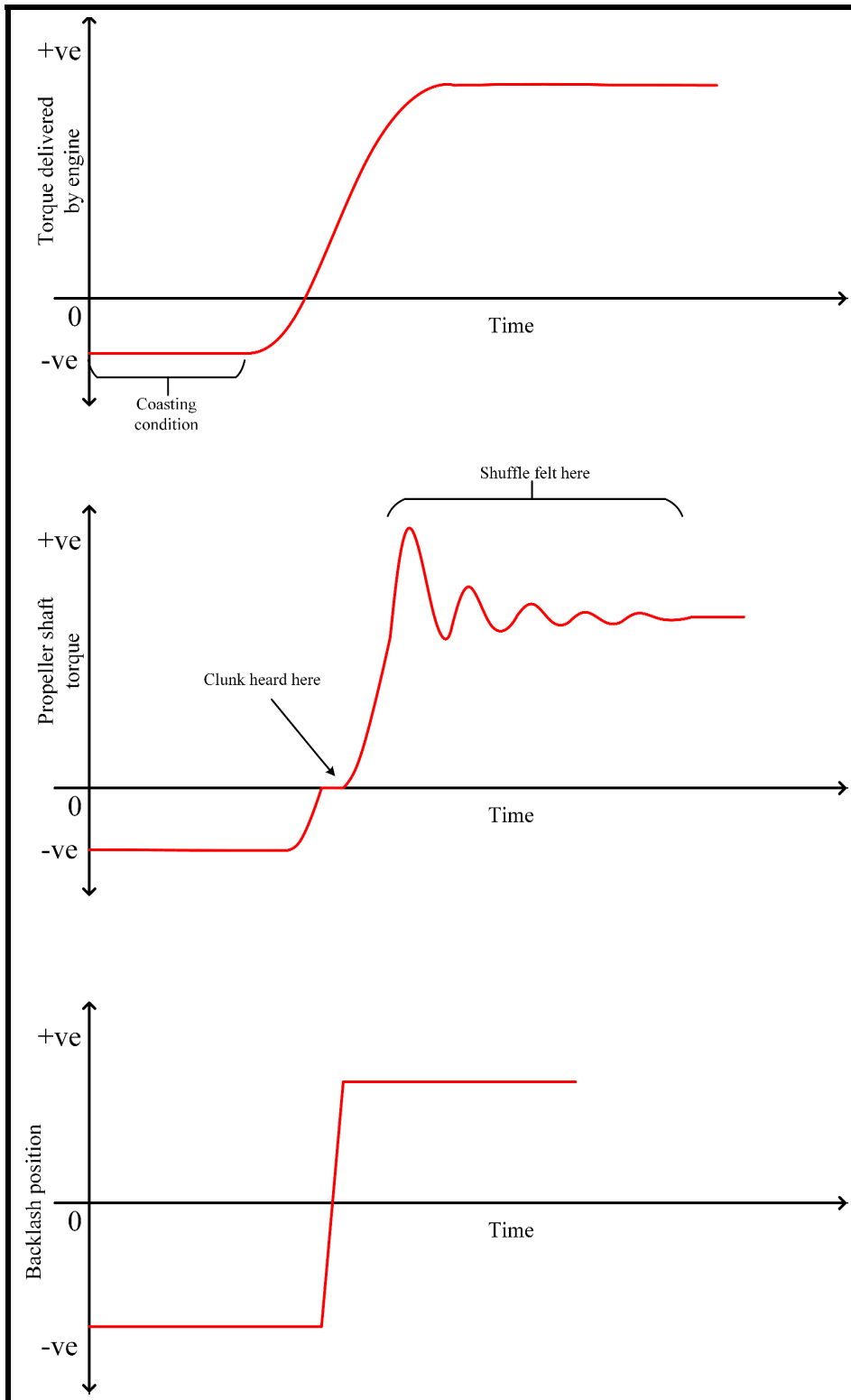


Figure 1.6: Representative output of propeller shaft torque showing clunk and shuffle, and backlash traversal in driveline.

1.3 Literature review

The topic of Anti-Jerk Control (AJC) has been of interest to a number of researchers in the past four decades. Fig. 1.7 shows a timeline for some of the studies that have been carried out in this field. The existing literature can be classified into three parts. The first part focuses on driveline modeling related to control system development, the second part focuses on the observer design to estimate the states and parameters for AJC (e.g., position in backlash, size of backlash, etc.), while the third part focuses on controller design and implementation.

1.3.1 Driveline modeling

Driveline modeling can be carried out for various applications, and depending on the application, the level of accuracy expected from the model is determined. Literature relevant to driveline models for observing shuffle oscillations, and developing state estimators and controllers was reviewed and an overview of some of the works is provided here.

Cho and Hedrick, in [19], developed an eight state mathematical model, based on engine, transmission and driveline states for powertrain dynamics. Their model was

experimentally validated, and was found to be suitable for developing closed-loop control systems. Their technique had the advantage of being easily configurable for any vehicle. Hrovat and Tobler, in [20], developed a bond graph based, simple driveline model for analyzing shuffle oscillations in a manual transmission vehicle. Their work includes components that are relevant for observing dominant shuffle modes in an automobile. Also, their work was experimentally validated and showed good agreement with the developed model.

Pettersson's [21] thesis is a good source for understanding the basic principles of powertrain modeling for control applications. He developed three models with increasing complexity from model to model. The first model was a linear model with the transmission and final drive considered with viscous friction, and the clutch, propeller shaft and drive shafts were modeled as stiff elements. For the next two models, he added flexibility to the clutch and included static nonlinearity in the clutch respectively. Hayat et. al., in [22], carry out an in-depth analysis on various models that are best suited for different aspects of drivability (e.g., tip-in or tip-out, take off, and during gear shifts). They also propose different modeling techniques based on the stage of vehicle design cycle. A full-order linear model is proposed during the design and development phase. A reduced order model is proposed for the control strategy formulation phase, and a full-order nonlinear model is proposed for the validation phase of the vehicle development.

Karlsson et. al., in [23], compare the suitability of a cylinder-by-cylinder engine model, and a mean value engine model for use in powertrain control applications. Their work suggests that the mean value engine model is a good choice for powertrain simulations and control, as it is less complicated compared to the cylinder-by-cylinder engine model.

Sorniotti, in [24], developed five nonlinear models of the vehicle driveline, and differentiated the models based on the components of the driveline that were assumed to be stiff and flexible. The stiffness of the driveshaft and half-shafts were identified to be the main factors affecting the low-frequency vibrations in the vehicle. Bartram et. al., in [25], studied the relation between road surface and vibrations in the driveline, and observed that depending on the road conditions, there may be significant effect on the oscillation amplitude and frequency of a driveline.

Dridi et. al., in [26], compared the performance of a nonlinear automotive model developed using Bond Graph and Block Diagram technique, and found that both the approaches showed approximately similar accuracy while representing the vehicle speed for an electrical powertrain. Sun et. al., in [27], from Nanjing University of Aeronautics and Astronautics, developed a dynamic model for automotive powertrain simulations in Amesim platform. Their model was validated through laboratory data for different operating conditions of an IC engine.

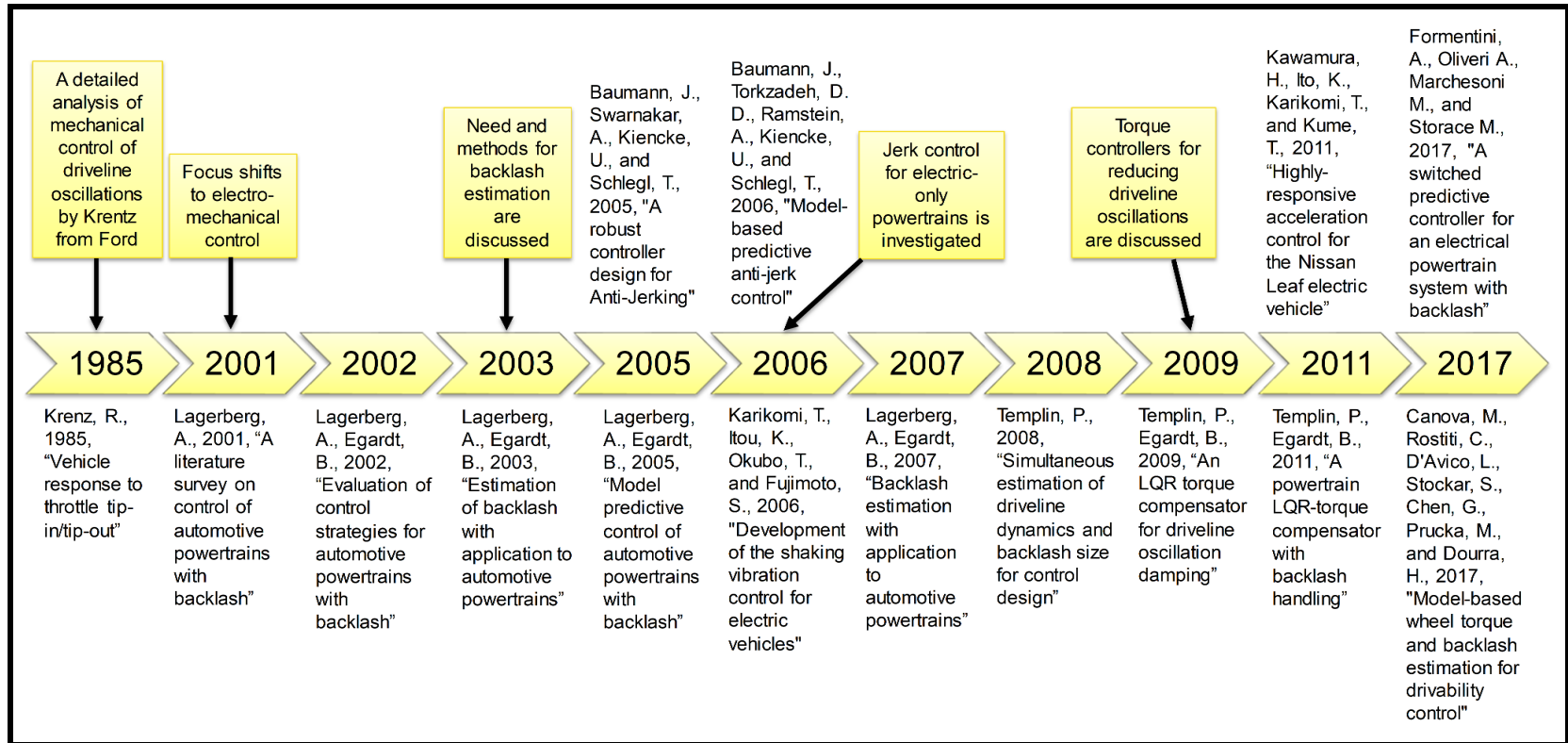


Figure 1.7: Timeline of some of the prior AJC works in research literature.

Lagerberg et al. [28],[8],[18],[10],[9] from Chalmers University, were amongst the first researchers who worked on design of real-time estimators and controllers to shape the torque delivered to the drivetrain. Their work on this topic, during the years 2001-2007, provides a good insight into the challenges involved in AJC. They have validated their work via simulations as well as vehicle testing, which was done under collaboration with Volvo Cars. Moreover, their work has served as the basis for most of the publications in this topic in the past decade.

Templin et al. [29],[30],[11] built upon the work of Lagerberg et al., and designed torque shaping controllers that were implemented in heavy duty trucks. The controllers in these works, [30] and [11], were developed using the Linear Quadratic Regulator (LQR) design methodology. Baumann et al. (see [12] and [6]) explored two approaches for AJC design: In [12], they developed an H_∞ controller for robust AJC under different driving scenarios; In [6], they designed a model-based predictive controller for quick torque response while mitigating driveline oscillations. These works, [12] and [6], were carried out in collaboration with Siemens Automotive.

Karikomi et al. [31] and Kawamura et al. [32] from Nissan Motor Company designed and evaluated an AJC system for electric powertrains. Their approach involved a combined feedforward and feedback compensator, which shapes the torque of the electric motor such that the driver demand is delivered quickly and driveline oscillations are maintained at an acceptable level. Their results showed the need for having

a feedback compensator designed specifically for the lash crossing condition, since the controller designed for the contact mode does not mitigate clunk as much as desired.

Batra et. al [33] from the University of Waterloo, designed and evaluated a nonlinear model predictive control based system to prevent jerk induced due to changing road conditions, causing sudden activation of the traction control system. Their work was based on an electric powertrain, and their focus was on reducing jerk caused due to tire slip, and flexibility in the driveline. They developed a full-order driveline model, and validated the model through experimental tests, and reduced the order of the model. They demonstrated the real-time capability of their system using a hardware-in-loop (HIL) setup.

1.3.2 AJC state estimators and parameter observers

Typically, the state estimators take as inputs the actuator (i.e., engine or motor) torque command and the measured actuator and wheel angular positions or the measured actuator and wheel angular speeds, and provide as outputs the estimates of the shaft twist angle (i.e., torsion angle), position in backlash, actuator torque, etc. The parameter estimators take similar inputs and provide as outputs the estimates of driveline parameters, such as backlash size, shaft stiffness, etc. Fig. 1.8 shows some of the different approaches for estimator design, given in the AJC literature.

On a production vehicle, angular speeds of the engine and the wheel can be measured and recorded through the CAN bus. The studies in references [31] and [29] make use of these measurements in their control strategies. Some other works, e.g., [18], utilize the angular position measurements of the engine and the wheel to estimate the position and size of the backlash.

In [18] and [9], a Switched Kalman Filter (SKF) was designed for estimating the backlash size, and an Extended Kalman Filter (EKF) was designed for estimating the driveline state variables. The SKF and EKF are nonlinear variants of the Kalman Filter and are used in AJC due to the nonlinear behavior caused by the backlash in the vehicle drivetrain.

An SKF approximates the nonlinear dynamic system as a combination of linear dynamic models. These linear models can then be used, either individually or as a weighted average of a combination of linear models, to closely represent the nonlinear dynamics. In addition to multiple linear state space models, the SKF method also uses a switch variable, whose value defines the state space model to be selected and applied for prediction.

The EKF is a widely used estimation technique for nonlinear systems. It uses the Taylor series expansion to linearize the system dynamics about the last estimated values. A Kalman filter approach is then applied for state prediction and filtering,

based on current measurement values. Since, as part of the above mentioned linearization, the Taylor series is truncated to the first two terms of expansion, the EKF is an approximation and thus is not an optimal estimator.

The authors in [34] utilize a Discrete Kalman filter (DKF) for estimating the wheel torque and the backlash angle in a discrete plant model. Due to the transformation of differential equations, involved in the continuous plant models, to difference equations, involved in the discrete plant models, the dynamics of the plant are modified, which gives rise to differences between continuous and discrete Kalman filters. These differences disappear as the sample period of DKF goes to zero in other words, the continuous Kalman filter may be viewed as a limiting case of the DKF. The major benefit of the DKF is its realizability, due to the digital nature of implementation on ECU processors.

IC engines have an inherent time delay, from the moment at which the torque command changes until the sensors measure the resulting engine and wheel speed variations. This time delay is associated with, among other factors, the combustion cycles of the engines. To design an effective AJC system, which takes into account the delay, several works, e.g., [6], have utilized the approach of Smith Predictor (SP). The benefit of SP is that it separates the time delay from the dynamics of the plant, and, therefore, facilitates the design of the state observer and the controller without having to consider the delay. The authors of [6] applied this SP approach, wherein

they designed a Luenberger Observer (LO) based on the separated plant dynamics. The outputs of LO were the inputs of their torque shaping control system, which was applied in a vehicle ECU.

Overall, different state and parameter estimator design approaches have been used in the AJC literature, depending on the focus of the study, measurements available, and plant model structure and accuracy. All the methods have their own benefits and limitations. While LOs work well when the driveline model is accurate and the measurement data is not noisy, Kalman filter-based techniques operate well under noisy measurement data and, to some extent, inaccurate plant models. The EKF, as a nonlinear version of Kalman filter, is more suited for driveline control due to the nonlinear system response arising from backlash. In terms of robustness to model/parameter uncertainty, sliding mode observers (SMOs) are inherently more robust than LOs and EKFs. Tuning LO and SMO is typically easier than EKF, since finding appropriate initial values for the covariance matrices of EKF can be challenging. In addition, EKF is more computationally demanding than LO and SMO, since it requires matrix product and inverse operations. However, EKF is significantly more robust to measurement noise, compared to LO and SMO.

While the above methods were applied to estimate the states and the parameters in real time, the nonlinear least squares optimization-based approach [7] can be used to estimate the parameters offline. This method of [7] is advantageous in scenarios

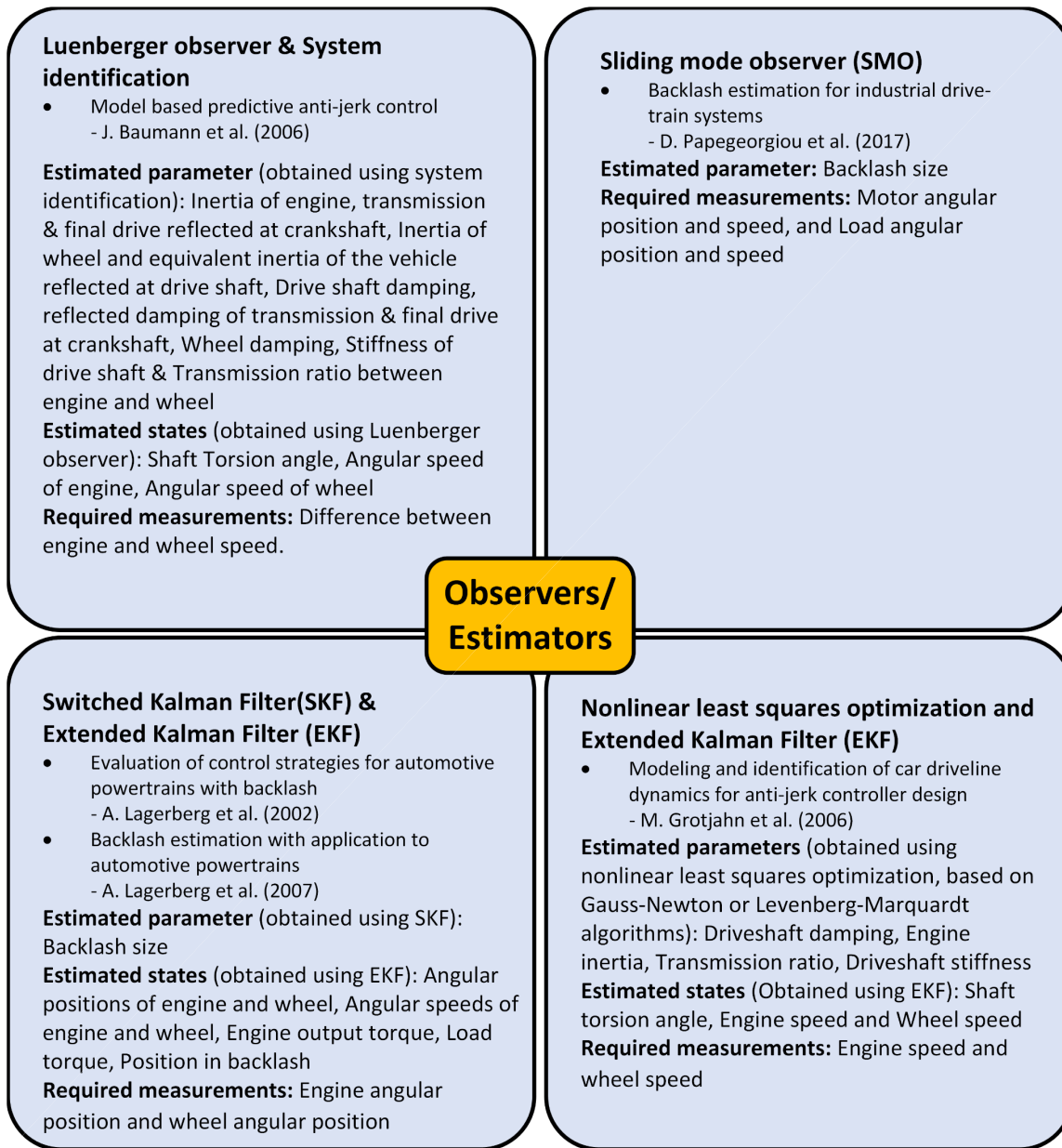


Figure 1.8: Some of the estimator design approaches used in the AJC literature[5][6][7][8][9].

where parameters are time-invariant or the estimation of these parameters online is computationally demanding. Here, the driveline parameters (e.g., backlash size) are determined by minimizing the error between the predicted and measured signals, such as shaft torque and vehicle acceleration.

1.3.3 AJC torque shaping controllers

Fig. 1.9 shows some of the approaches for AJC design that have been published in the literature. Below, a brief overview of these works is provided.

The authors in references [30] and [11] developed a LQR to shape the engine torque command in the contact mode, such that shuffle is mitigated during transients and driver torque command is satisfied in the steady state. To mitigate shuffle, the derivative of the shaft torque is penalized in the LQR cost function. Additionally, to achieve steady state tracking of the driver command, integral control is included in the LQR design. Furthermore, this work [11] also includes a backlash control mode, which mitigates clunk by regulating the lash crossing speed during backlash traversal. The performance of the overall control system was evaluated on a Volvo truck.

Another approach for AJC design is based on the H_∞ mixed-sensitivity synthesis technique [12]. This work focused on shaping the engine torque in the contact mode (backlash was not explicitly considered in the driveline model), under uncertainties in parameters such as driveline stiffness and damping. The H_∞ design involves the computation of a state feedback controller that minimizes the H_∞ norm of the closed loop weighted mixed sensitivity functions. The weights involved in the design are selected to ensure robustness to uncertainties and good performance. This H_∞ torque

Anti-Jerk Controllers		
<p>Model Predictive Control (MPC)</p> <ul style="list-style-type: none"> Model predictive control of automotive powertrains with backlash - A. Lagerberg, B. Egardt (2005) <p>Advantages: Indicates the performance ceiling of optimization-based control strategies; State and actuator constraints can be directly incorporated in the controls design.</p> <p>Limitations: Accurate plant model is required for effective performance; Significant amount of time (ranging from several hours to days) is required to compute the explicit MPC solution.</p>	<p>Linear Quadratic Regulator (LQR)</p> <ul style="list-style-type: none"> A powertrain LQR torque compensator with backlash handling - P. Templin, B. Egardt (2011) <p>Advantages: Easy to implement; Effective in damping shuffle and mitigating clunk.</p> <p>Limitations: Does not directly take into account the state and actuator constraints in the controls design.</p>	<p>H_∞ control</p> <ul style="list-style-type: none"> A robust controller design for Anti-Jerking - J. Baumann et al. (2005) <p>Advantages: Robust to uncertainties in the system parameters.</p> <p>Limitations: Does not take into account the state and actuator constraints in the controls design.</p>

Figure 1.9: Some of the torque shaping controller design approaches given in the AJC literature[10][11][12].

shaping controller was validated using a Siemens vehicle.

Model Predictive Control (MPC) is another approach for AJC design, which has been investigated by Lagerberg et. al. [10]. The dynamics of the powertrain were formulated as a Piecewise Affine (PWA) system, and, as part of the MPC problem formulation, target sets were defined in the state space of the model. These target sets were selected such that the steady state desired acceleration is met, the speed at the end of lash crossing is small, and the driveline jerk is constrained. The actuator

constraints, such as the maximum rate of increase of the engine torque, were also considered in the problem formulation. The explicit solution to the MPC problem was obtained using the Multi-Parametric Toolbox (MPT) in MATLAB. The performance of the MPC system was evaluated using simulations.

Formentini et. al. in [35] designed a switched control system to shape the torque of electric drivetrains. The control system consisted of four MPC controllers, and each of these controllers was designed specifically for one of the following scenarios: Contact mode during tip-in, backlash mode during tip-in, contact mode during tip-out, and backlash mode during tip-out. The system selected one of these controllers to shape the motor torque based on the estimated condition of the driveline operation. Since the four MPC systems were independently designed, the overall control strategy is sub-optimal as compared to a single optimal MPC system, designed for all the driveline operating conditions. However, the complexity involved in the design of these four controllers is smaller than that of the single optimal MPC system. The performance of the above switched torque shaping controller was evaluated using experiments and was compared with that of a PI controller.

To summarize some of the key aspects of the above control design approaches,

† the H_∞ and the LQR methodologies are advantageous from the point of view of ease of implementation and robustness to plant uncertainties - however, their

design approaches do not directly take into account the state and the actuator constraints, which may lead to calibration complexities;

† the MPC methodology directly takes into account these constraints, but it is difficult to calibrate due to the long wait times involved in calculating the explicit MPC anti-jerk control solution (see, e.g., [10]). Moreover, the effectiveness of MPC may be limited by the accuracy of the plant models.

1.4 Research scope and Thesis organization

The work presented in this thesis is a part of an Alliance Project between Ford Motor Company and Michigan Technological University. The main objective of this project is to develop an effective and robust estimator and controller, that work in tandem to reduce the undesirable jerks mentioned in the previous subsections. Before the estimator and controller can be developed, an accurate model of the vehicle driveline for controls purpose, has to be developed and validated. This thesis deals with developing a full-order, high-fidelity vehicle model, that captures the required dynamics of the driveline during tip-in and tip-out scenarios. This full-order model is validated using experimentally obtained data from the sponsoring organization, and then parametric analysis is carried out to select the important components of the driveline. Later, two reduced-order models are derived from the full-order model,

and their response is comparatively analyzed, and one of them is selected for further validation.

This thesis is organized as shown in Fig. 1.10. The second chapter of the thesis deals with the full-order vehicle model that was developed in Amesim[®] and Simulink[®] modeling environments. A brief overview of the powertrain elements that were modeled is presented, followed by the governing equations, and the model validation results are discussed. The third chapter discusses the parametric analysis of the model, the results of which are used for deciding on the reduced-order model. The fourth chapter deals with the development of the reduced-order model, and presents comparative results with respect to the full-order model. The fifth and final chapter provides a conclusion of this thesis, and discusses the planned future work as part of the Alliance project.

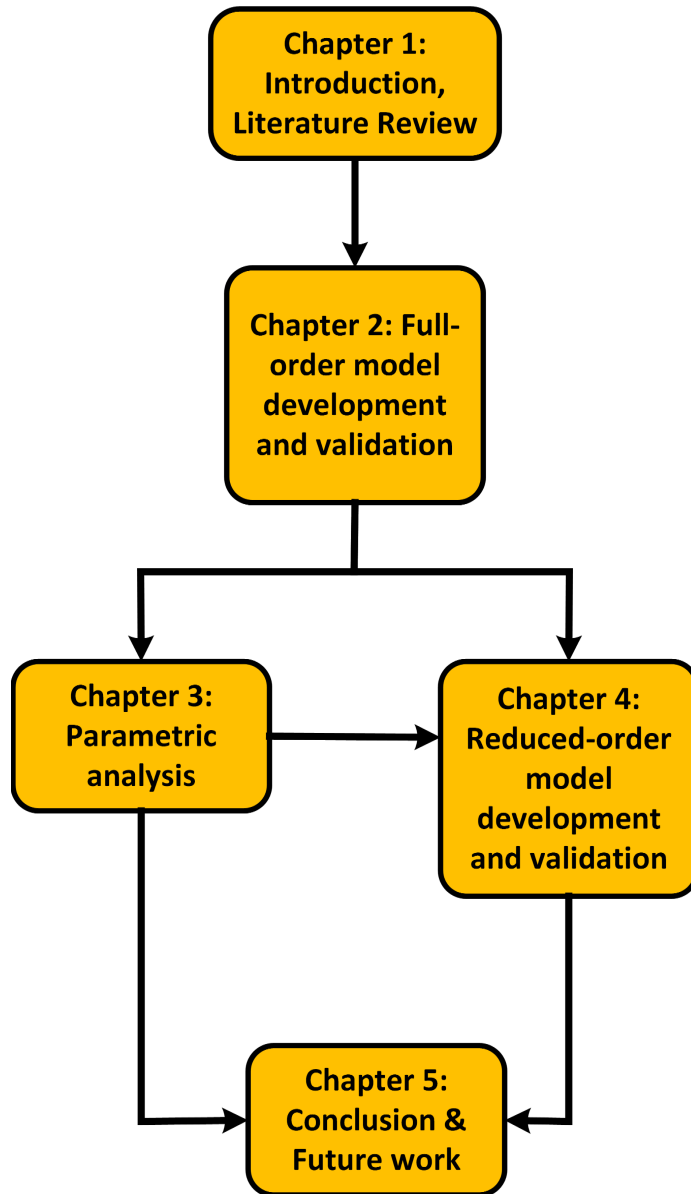


Figure 1.10: Thesis organization

Chapter 2

Full order model development and validation

2.1 Model development

This section describes the development of a full-order, control oriented vehicle model, to replicate driveline dynamics observed during tip-in and tip-out scenarios. Based on the technical insight provided by the sponsoring organization, and comments from [20], it is assumed that the capability of the model should be aligned towards representing the amplitude and frequency of driveline oscillations, through driveshaft torque, engine speed and vehicle longitudinal acceleration, during tip-in and tip-out

scenarios, and an error of 10 - 20 % in parameter magnitudes is acceptable as long as the frequencies are matching. The reason behind this assumption is the fact that a well designed closed-loop control system, would have the advantage of feedback operations, and would be robust to modeling errors.

The developed model can be classified into: a) the engine as the torque source and b) the torque converter, 10-speed automatic transmission, propeller shaft, final drive, backlash elements, rear differential, axle shafts, suspension, tires and vehicle longitudinal dynamics. The schematic of the model is shown in Fig. 2.1.

The engine model was developed in Simulink[®] in order to replicate the torque including the source dynamics which affect driveline oscillations. The remaining vehicle model was developed in LMS Amesim[®] due to the availability of pre-defined powertrain blocks which only required model parameters like inertia, stiffness, damping coefficient etc., to build the model. An interface was designed between the models such that the Amesim[®] part of the model was imported into Simulink[®] and Simulink[®] solver was used for running the simulations.

2.1.1 Amesim[®] and Simulink[®] interface

The Amesim[®] - Simulink[®] standard interface provides a lucrative option for utilizing the individual benefits of each software package, through the usage of S-functions

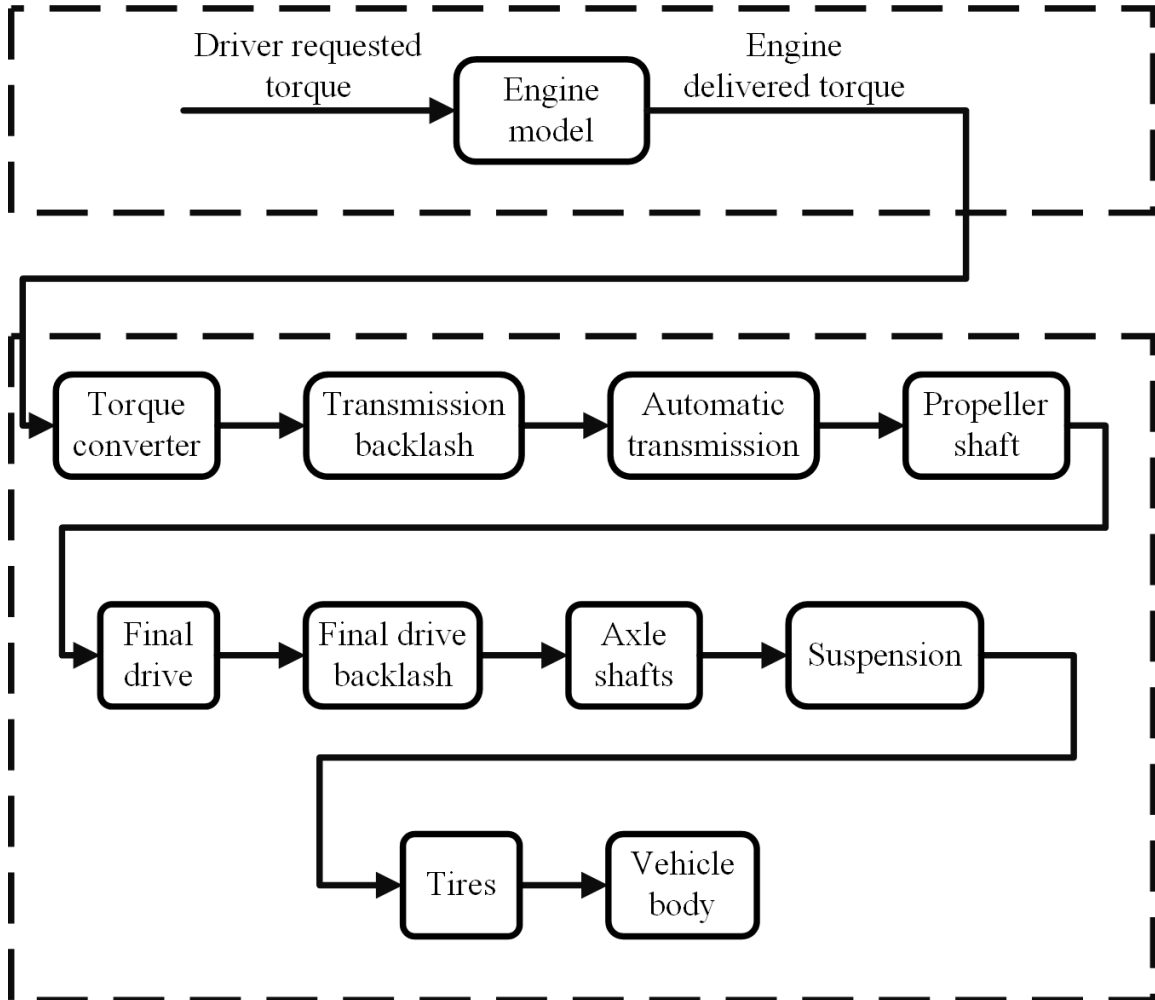


Figure 2.1: Components of the full-order model. Top box represents components modeled in Simulink, and bottom box represents components modeled in Amesim.

(system-functions). MathWorks[®] documentation defines S-function as “a computer language description of a Simulink block written in MATLAB[®], C, C++ or FORTRAN.” For setting up the interface between Amesim[®] and Simulink[®], some prerequisites need to be taken care of. The files required for converting the Amesim[®] model for use in Simulink[®] can only be generated using a C-compiler. The default GNU gcc compiler provided with Amesim[®] is not suitable for this purpose. Therefore, for

a Windows platform machine, Microsoft[®] Visual C++ is a mandatory requirement. It was also observed that Amesim[®] had limited compatibility with some versions of Visual C++, and therefore, a specific version compatible with the Amesim[®] version had to be used. More details about the software packages, and the compiler are provided in Appendix A. Also, it is essential to ensure that Amesim[®] is able to “locate” MATLAB[®] on the machine used for simulations, using environment variables. Without this, Amesim[®] will not be able to generate the files required for the S-function that would be used in Simulink[®].

For utilizing this interface, first, the model is developed individually in each of the packages. Then, the submodel parameters of the Amesim[®] model blocks are defined. Later, the Amesim[®] model is compiled to an S-function using the C++ compiler. This S-function file is generated as a “.mex” format file. Before this can be imported into Simulink[®], the required libraries for enabling the interface have to be loaded in MATLAB[®]. The code for loading these libraries is provided in Appendix A. These libraries provide an interface block in Simulink[®] which is used for calling the “.mex” file that is generated through Amesim[®]. Once the “.mex” file is loaded, Simulink[®] solvers can be used for simulating the entire model. The generated results are automatically updated in Amesim[®], and Amesim[®]'s in-built analysis tools can be used just as in a regular simulation. For the model developed in this work, ‘ode15s(stiff/NDF)’ solver was used in Simulink[®] with a variable time step. An overview of this process is shown in Fig. 2.2.

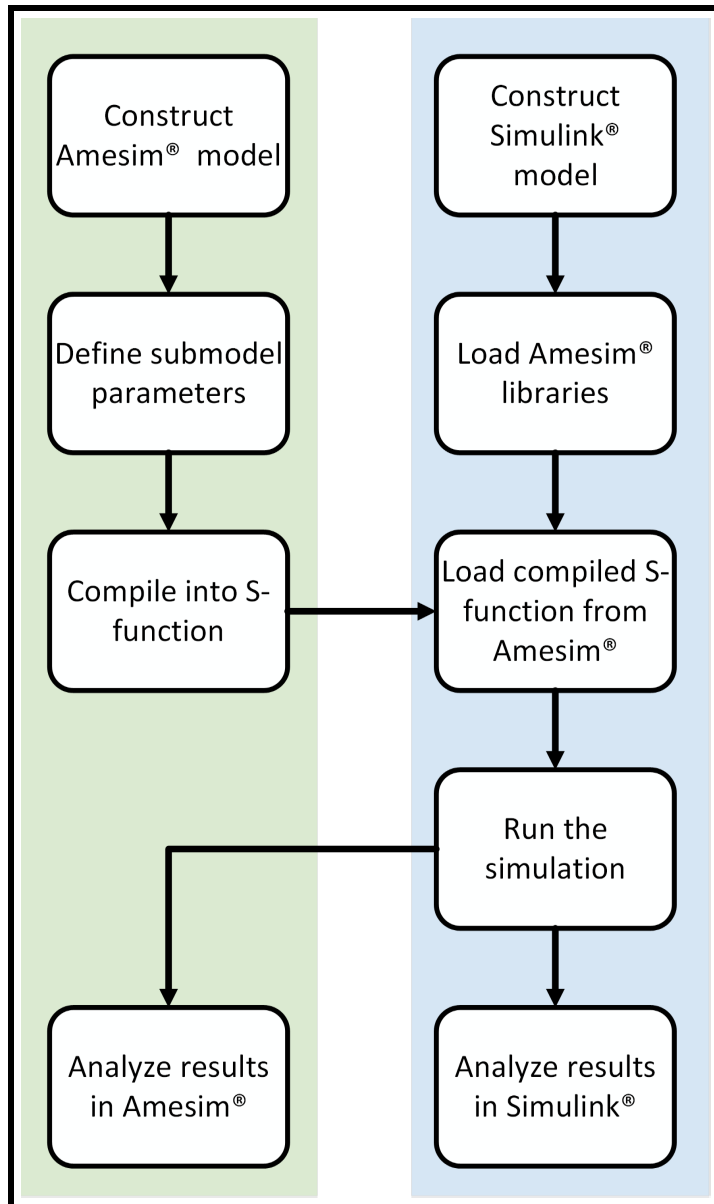


Figure 2.2: Overview of Amesim[®] - Simulink[®] interface. Adapted from [13].

Amesim[®] also offers a co-simulation interface, where both Amesim[®] and Simulink[®] solvers are used in parallel. This interface is suitable when the models in both the softwares are discrete-time based. Consequently, the S-function block in co-simulation is seen as a discrete block whereas in the standard interface, it is

seen as a continuous block.

During the course of simulations, using this interface, it was observed that the Amesim[®] model's results file may get corrupted over time, due to continuous overwriting during each simulation. If the files are corrupted, the results of the subsequent simulations do not change even when the model parameters are changed in Amesim[®]. This can be remedied by using the 'Purge' function in Amesim[®] regularly, which will clean Amesim[®]'s buffer and remove all the auxiliary and result files that Amesim[®] generates during each simulation, and "clean" the model for subsequent runs.

2.1.2 Model assumptions and limitations

As mentioned in the beginning of this chapter, the focus of this work is on developing a driveline model which would be utilized in control system development. Therefore, some assumptions and simplifications were made in the model, without compromising its fidelity for controls work. The vehicle model represents a full-size, engine driven SUV/pick-up truck platform, with an automatic transmission and RWD architecture. Vehicle jerk during the tip-in and tip-out maneuvers is of prime interest, which in general occurs only during longitudinal motion of the vehicle, and therefore, this model represents only the longitudinal dynamics of the vehicle. Also, gear shift

dynamics are not considered in this work, as the objective was limited to fixed gear states. Consequently, all the results presented in this work were simulated with a fixed gear state and for tip-in and tip-out scenarios only. While an actual vehicle powertrain experiences some torsion due to flexible engine and transmission mounts, it is assumed that the powertrain mounts are stiff in this model. The differential is also assumed to be locked throughout the simulations. The suspension elements are located between the axle shafts and tires, and are assumed to be stiff in this model.

2.1.3 Engine model

The engine model in Simulink[®] was used to generate the torque profiles that were required to replicate various driving scenarios for the powertrain model in Amesim[®]. The engine model in this work is adapted from the information provided in [36]. Two torque input commands are considered, and they are referred to as base torque command, and instantaneous torque command. Base torque command is defined as the maximum possible indicated torque that the engine can generate, based on the air inflow at a given moment. Since it is dependent on intake charge into the engine, it is constrained by the throttle body flow dynamics, intake manifold flow dynamics and other actuator dynamics like the wastegate valve (for a turbocharged engine), EGR valve etc [37], [38]. These dynamics can be represented as a lag, using a first order transfer function, with a time constant of $\tau_{e,base}$. Further, this torque command

is affected by a combustion time delay $t_{(d,base)}$, which is assumed to be one complete rotation of the engine crankshaft. Therefore, the time delay is a function of engine speed and can be represented as $60/N$, where N is the engine speed [36].

The equations used for calculating the base path torque are:

$$T_{(e,base,ind)}^*(t) = T_{(e,base,brake)}^*(t) + T_{fric}(t) \quad (2.1)$$

$$\dot{T}_{e,base,ind}(t) = \frac{1}{\tau_{e,base}}(T_{(e,base,ind)}^* \times (t - t_{(d,base)}) - T_{(e,base,ind)}(t)) \quad (2.2)$$

where, $T_{(e,base,ind)}^*$ is the base torque command in the indicated domain, $T_{(e,base,brake)}^*$ is the base torque command in the brake domain and $T_{fric}(t)$ is the friction losses of the engine.

Instantaneous torque command is defined as the maximum possible base torque that can actually be generated, after spark modulation. This torque command is also affected by a delay which can be attributed to the discrete firing of each cylinder. The vehicle in this work has a 6 cylinder engine and therefore, the time delay associated with the firing of the cylinders $t_{(d,inst)}$, can be represented as $60/3N$, where N is the engine speed. A torque ratio command, TR_{spk}^* , is defined based on the base and instantaneous torque commands. The torque ratio delivered, TR_{spk} , includes the time

delay of the instantaneous path, and is given by:

$$TR_{spk}(t) = TR_{spk}^*(t - t_{(d,inst)}) \quad (2.3)$$

Therefore, the torque delivered by the engine, $T_{(e,inst,brake)}$, can be represented as:

$$T_{(e,inst,brake)}(t) = (T_{(e,base,ind)}(t) \times TR_{spk}(t)) - T_{fric}(t) \quad (2.4)$$

Uncertainty in the engine torque delivery:

Due to uncertainty in engine charge estimation, variation among production engines and variation in tuning engine torque controller to cover all engine speed and load conditions, there is usually a difference between the actual torque delivered by the engine and estimated torque delivery by the engine. This variation is further amplified during transient operation conditions like tip-in scenarios. The sponsoring organization had carried out an in-depth technical analysis using multiple sensors, and measurement techniques, to analyze and quantify this variation. The findings of their study was made available for this work, and therefore an uncertainty term ($T_{unc}(t)$) was included, as shown in Eq. 2.5:

$$T_{(e,inst,brake)}(t) = (T_{(e,base,ind)}(t) \times TR_{spk}(t)) - T_{fric}(t) + T_{unc}(t) \quad (2.5)$$

The calculation of T_{unc} is based on the magnitude of rate of change of torque, with highly dynamic events leading to T_{unc} being of higher magnitude (15-20% of delivered torque), and less dynamic events leading to T_{unc} being of smaller magnitude (5% of delivered torque). The upper and lower bounds of these uncertainties are identified based on the limits noted by the technical document shared by the sponsoring organization. Further details about the calculation of T_{unc} are shown in Appendix B.

2.1.4 Driveline and vehicle dynamics model

The Amesim[®] model includes the following components of the vehicle: torque converter including the lock-up clutch, a 10-speed automatic transmission, propeller shaft, final drive, rear differential, axle shafts, stiff suspensions, tires, longitudinal vehicle dynamics and two sources of backlash, modeled one each at the input of the transmission and output of final drive. Equations for each of these components are provided in this section, to give a better understanding of the physics behind the driveline oscillations.

The torque delivered by the engine, $T_{(e,inst,brake)}(t)$, is used to calculate its angular speed $\dot{\theta}_e$, using the rotational inertia of the engine:

$$J_e \ddot{\theta}_e = T_{(e,inst,brake)} - T_{im} \quad (2.6)$$

where, J_e is the rotational inertia of the engine, $\ddot{\theta}_e$ is the rotational acceleration of the engine and T_{im} is the load torque at the impeller of the torque converter.

2.1.4.1 Torque converter model

The torque converter consists of an impeller, stator, turbine, and a lock-up clutch with damper springs, set inside a metal housing. The lock-up clutch can operate in one of its three modes when the vehicle is running: locked, open, or slipping. In general, when the vehicle starts from a stationary state, the lock-up clutch is open and complete torque transmission takes place through the fluid between the impeller and turbine. When the vehicle reaches a set of pre-defined conditions (e.g., impeller speed, vehicle speed and transmission fluid temperature), the lock-up clutch can operate in either slipping or locked positions. The transmission control unit (TCU) defines the position of the lock-up clutch based on drivability target while minimizing fuel consumption [39]. The modeled torque converter (Fig. 2.3) includes both, the fluid path dynamics (due to the fluid inside the converter), and the lock-up clutch dynamics. The fluid path dynamics are represented using look-up tables which define the torque ratio and capacity factor of the converter based on its speed ratio. The lock-up clutch dynamics are modeled based on its assumed clutch capacity. Additionally, the hysteresis caused by the damper springs of the lock-up clutch inside the torque converter are also modeled.

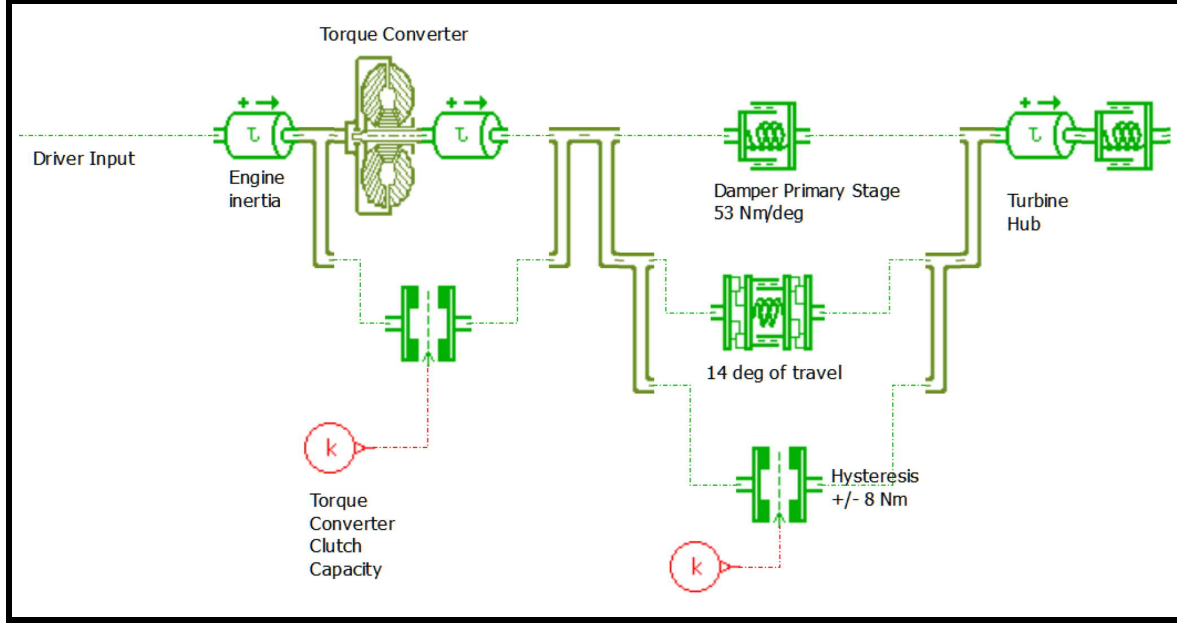


Figure 2.3: Amesim[®] model showing the torque converter with lock-up clutch and spring hysteresis blocks.

When the torque converter lock-up clutch operates in locked condition, it is assumed that there are no losses in torque transmission, and that the impeller torque, T_{im} , is completely transmitted to the torque converter turbine:

$$T_{tu} = T_{im} \quad (2.7)$$

where, T_{tu} is the turbine torque of the torque converter.

The speed ratio (SR), torque ratio (TR) and capacity factor (K) of the torque converter are defined as:

$$SR = \frac{\dot{\theta}_{tu}}{\dot{\theta}_{im}} \quad (2.8)$$

where, $\dot{\theta}_{tu}$ is the angular speed of the torque converter turbine and $\dot{\theta}_{im}$ is the angular speed of the torque converter impeller.

$$TR = \frac{T_{tu}}{T_{im}} \quad (2.9)$$

$$K = \frac{\dot{\theta}_{im}(9.55)}{\sqrt{T_{im}}} \quad (2.10)$$

where, $\dot{\theta}_{im}$ is the angular speed of the torque converter impeller.

When the torque converter lock-up clutch operates in open condition, the turbine torque, T_{tu} , is given by:

$$T_{tu} = \left(\frac{\dot{\theta}_e(9.55)}{K(SR)} \right)^2 (TR(SR)) \quad (2.11)$$

where, $\dot{\theta}_e$ is the angular speed of the engine which is equal to the angular speed of the torque converter impeller, K is the capacity factor of the torque converter as a function of speed ratio SR , and TR is the torque ratio as a function of speed ratio SR , of the torque converter.

When the torque converter lock-up clutch operates in slipping condition, the equation

is a combination of fluid path dynamics and clutch path dynamics and the turbine torque, T_{tu} , is given by:

$$T_{tu} = T_{tcc} + \left(\frac{\dot{\theta}_e(9.55)}{K(SR)} \right)^2 (TR(SR)) \quad (2.12)$$

where T_{tcc} is the torque through the lock-up clutch.

It is important to note that the equations for the torque converter, discussed in this work, are simplified equations and do not consider the effect of geometrical parameters (like number of blades on the impeller and turbine, and their blade angles) and fluid properties of the converter.

2.1.4.2 Automatic transmission model

Torque output from the torque converter flows through a 10-speed automatic transmission whose schematic is shown in Fig. 2.4. It consists of 4 planetary gears and 6 clutch packs. Certain nodes for the transmission have been defined by the manufacturer, and inertias at these nodes were used for capturing its dynamics. A truth table was defined in Amesim[®] which locks certain clutch packs, based on the gear selected, leading to relevant torque multiplication.

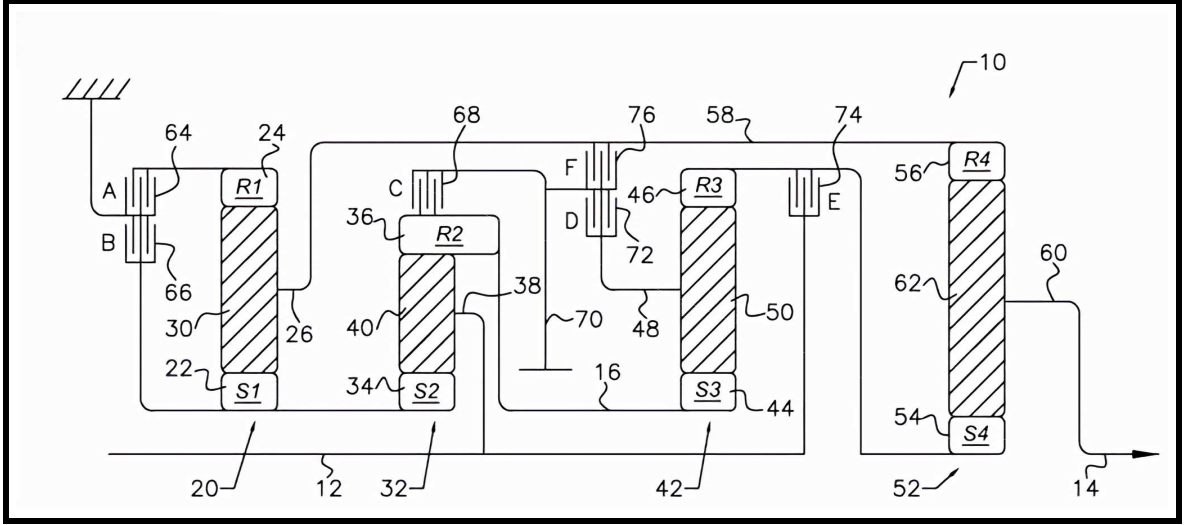


Figure 2.4: Schematic diagram showing the 10-speed transmission[14].

The torque losses within the transmission (including transmission pump losses) have been considered in the model, and are calculated based on engine speed, and gear selected. These losses are subtracted from the torque converter output, and therefore, the equation for torque flowing through the transmission, T_{tr} , is given by:

$$T_{tr} = (T_{tu} - T_{gearloss})i_{tr} \quad (2.13)$$

where, $T_{gearloss}$ is the transmission torque loss, and i_{tr} is the gear ratio of the selected gear.

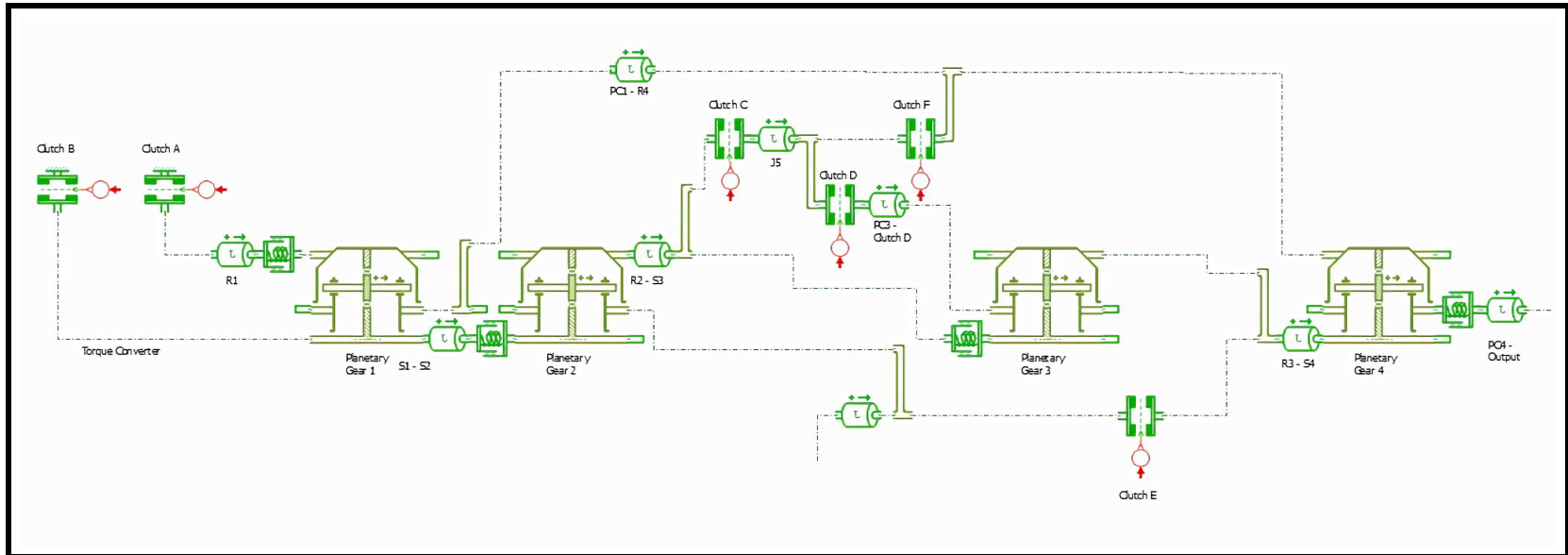


Figure 2.5: Amesim[®] model showing the 10-speed automatic transmission blocks.

2.1.4.3 Propeller shaft model

The propeller shaft was modeled using a shaft element in Amesim[®], which is essentially an elastic rotary shaft, which behaves like a rotary spring damper. Stiffness for this shaft element was provided by the sponsoring organization as part of the model parameters, and damping coefficient had to be assumed. Torque output at the propeller shaft, T_{ps} can be represented by:

$$T_{ps} = T_{tr} = k_{ps}(\theta_{tr} - \theta_{ps}) + c_{ps}(\dot{\theta}_{tr} - \dot{\theta}_{ps}) \quad (2.14)$$

where θ_{tr} is the angular position of the transmission output shaft, and θ_{ps} is the angular position of the propeller shaft on its output side.

2.1.4.4 Final drive model

The torque at the propeller shaft output is sent through the final drive, for further torque multiplication, and speed reduction. The equation governing the flow of torque through the final drive is given by:

$$T_{fd} = T_{ps}i_{fd} \quad (2.15)$$

where, T_{fd} is the torque output at the final drive, T_{ps} is the torque output at the propeller shaft, which is also the torque input to the final drive and i_{fd} is the final drive ratio.

2.1.4.5 Backlash model

Two rotary clearance blocks were placed in the Amesim[®] model for replicating the backlashes, with the first one at the input of the transmission, representative of the transmission backlash and the second one at the output of the final drive, representative of the final drive backlash. The rotary clearance block of the Amesim[®] powertrain library was used for modeling the backlash because it takes into account the clearance as well as impact at the face of gear teeth caused due to an elastic end-stop, providing a more realistic picture of the expected output due to the presence of backlash. Therefore, the stiffness and damping at the backlash element can also be defined, if different, from the material of the shaft at which backlash is modeled.

Backlash is representatively shown in Fig. 2.6. If 2α is considered to be the size of backlash, then the possible positions of the backlash are $-\alpha$ for negative contact of

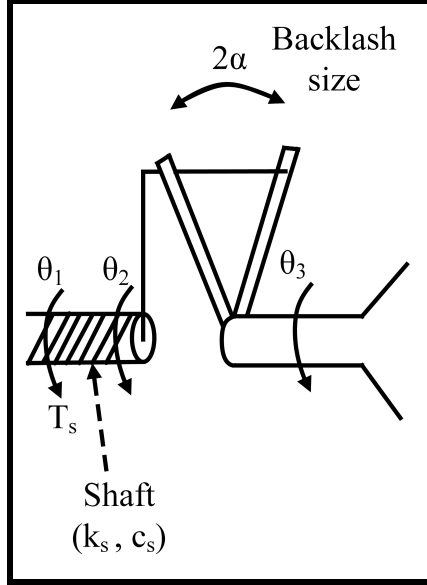


Figure 2.6: Representative model of backlash.

backlash, α for positive contact of backlash, or $(-\alpha, \alpha)$ when traversing backlash.

Also, the displacement of the shaft, θ_s , and position in backlash, θ_b , can be given by:

$$\theta_s = \theta_1 - \theta_3 \quad (2.16)$$

$$\theta_b = \theta_2 - \theta_3 \quad (2.17)$$

where, θ_1 is the angular position at the shaft input, θ_2 is the angular position at the beginning of the backlash, and θ_3 is the angular position at the end of the backlash.

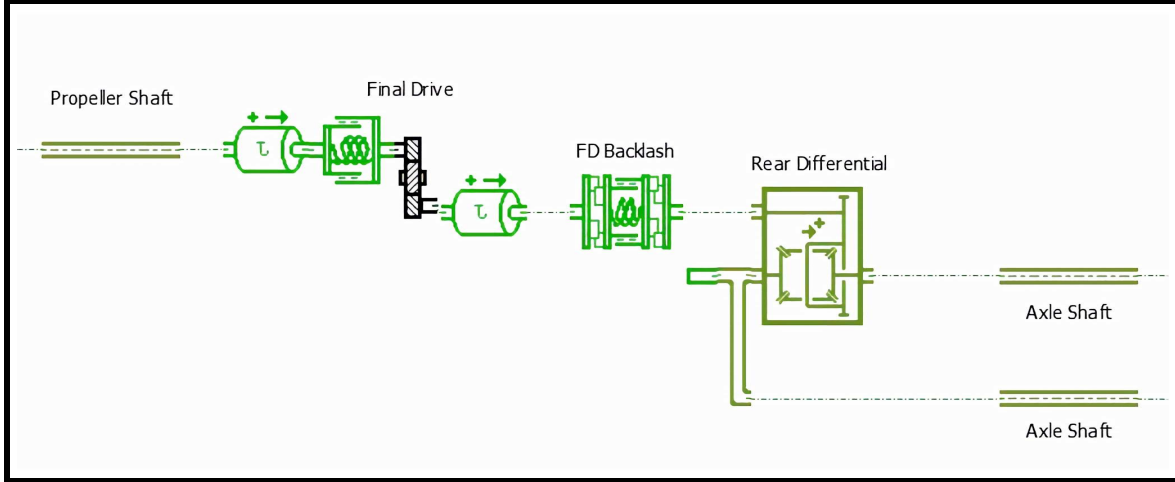


Figure 2.7: Amesim[®] model showing the propeller and axle shafts, along with the rear differential and final drive backlash.

Using equations 2.13 and 2.14, the backlash can be modeled as:

$$\dot{\theta}_b = \begin{cases} \max\{0, \dot{\theta}_d + \frac{k_s}{c_s}(\theta_d - \theta_b)\}, & \text{if } \theta_b = -\alpha \\ \frac{k_s}{c_s}(\theta_d - \theta_b), & \text{if } |\theta_b| < \alpha \\ \min\{0, \dot{\theta}_d + \frac{k_s}{c_s}(\theta_d - \theta_b)\}, & \text{if } \theta_b = +\alpha \end{cases} \quad (2.18)$$

2.1.4.6 Axle shafts model

The rear differential, shown in Fig. 2.7, splits torque from the final drive such that it is distributed between the two axle shafts. The axle shafts are modeled using a shaft element in Amesim[®], similar to the propeller shaft model. The torque, T_{ax} flowing through each axle shaft can be represented by:

$$T_{ax} = \frac{T_{fd}}{2} = k_{ax}(\theta_{fd} - \theta_{ax}) + c_{ax}(\dot{\theta}_{fd} - \dot{\theta}_{ax}) \quad (2.19)$$

where, k_{ax} , is the stiffness of the axle shaft, c_{ax} , is the damping coefficient of the axle shaft, θ_{fd} , is the angular position of the final drive shaft, θ_{ax} is the angular position of the axle shaft at tire end, $\dot{\theta}_{fd}$, is the angular speed of the final drive shaft, and $\dot{\theta}_{ax}$ is the angular speed of the axle shaft at tire end.

2.1.4.7 Suspension, tire and vehicle dynamics model

The suspension was modeled using a stiffness and damping element, that was connected between the axle shafts and the tires. It was assumed stiff by providing a large value to its stiffness and damping parameters in Amesim[®]. Using a detailed suspension model was out of the scope of this work, and simplified parameters for its stiffness and damping were not available during modeling.

The tires were modeled as a simplified stiffness and damping element along with inertia. A Pacejka tire model [40], which is much more detailed than the stiffness and damping element, was also developed as an alternative, but had to be discontinued due to unavailability of some properties that were required by that model. The torque at the tire, T_{ti} , is given by:

$$T_{ti} = T_{ax} = k_{ti}(\theta_{ax} - \theta_{ti}) + c_{ti}(\dot{\theta}_{ax} - \dot{\theta}_{ti}) \quad (2.20)$$

where, k_{ti} , is the stiffness of the tire, c_{ti} , is the damping coefficient of the tire, θ_{ax} is the angular position of the axle shaft, θ_{ti} is the angular position of the tire, $\dot{\theta}_{ax}$, is the angular speed of the axle shaft, and $\dot{\theta}_{ti}$, is the angular speed of the tire.

Longitudinal vehicle dynamics were modeled assuming 1D vehicle with two axles, but with only the rear axle receiving propulsive torque. Aerodynamic force, rolling resistance force, and slope force on the vehicle are considered through this block. The equations for the longitudinal vehicle dynamics are modeled according to reference [13], and are shown below:

Aerodynamic force:

$$F_{aero} = \frac{1}{2} \rho A_f C_D (V)^2 \quad (2.21)$$

where, ρ is the air density, A_f is the frontal area of the vehicle, C_D is the drag coefficient, V is the longitudinal velocity of the vehicle.

Rolling friction force:

$$F_{fric} = r_{veh} V + F_{roll} \text{sign}(V) \quad (2.22)$$

where, r_{veh} is the coefficient of viscous friction, F_{roll} is the rolling resistance force and

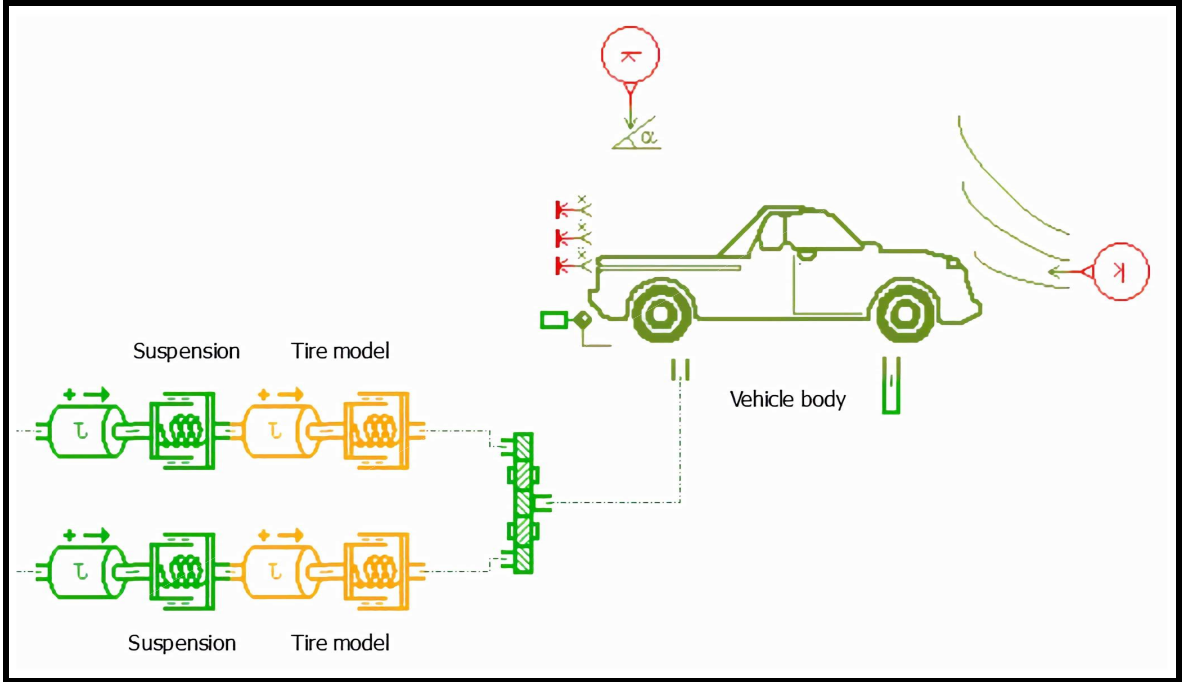


Figure 2.8: Amesim[®] model showing the suspension, tire and the vehicle dynamics blocks.

V is the longitudinal velocity of the vehicle.

$$F_{roll} = R_{roll} m_{veh} g \cos(\delta) \quad (2.23)$$

where R_{roll} is the rolling friction coefficient, m_{veh} is the mass of the vehicle, g is the gravitational acceleration, δ is the slope angle.

Slope force:

$$F_{slope} = m_{veh} g \sin(\delta) \quad (2.24)$$

The traction force generated by the engine, for propelling the vehicle can be given

by:

$$F_{traction} = \frac{T_{ti}}{r_{ti}} \quad (2.25)$$

where, T_{ti} , is the torque developed at the tire, and calculated in Eq. 2.20, and r_{ti} , is the radius of the tire.

The acceleration of the vehicle is calculated according to the following formula:

$$a_{veh} = \frac{F_{traction} - F_{aero} - F_{fric} - F_{slope}}{m_{veh} + \frac{J_w}{\dot{\theta}_w}} \quad (2.26)$$

where, the force components are calculated as per the previous equations, m_{veh} is the mass of the vehicle, J_w is the inertia of wheel hub, and $\dot{\theta}_w$ is the angular speed of the wheel hub, and is equal to the angular speed of the tire.

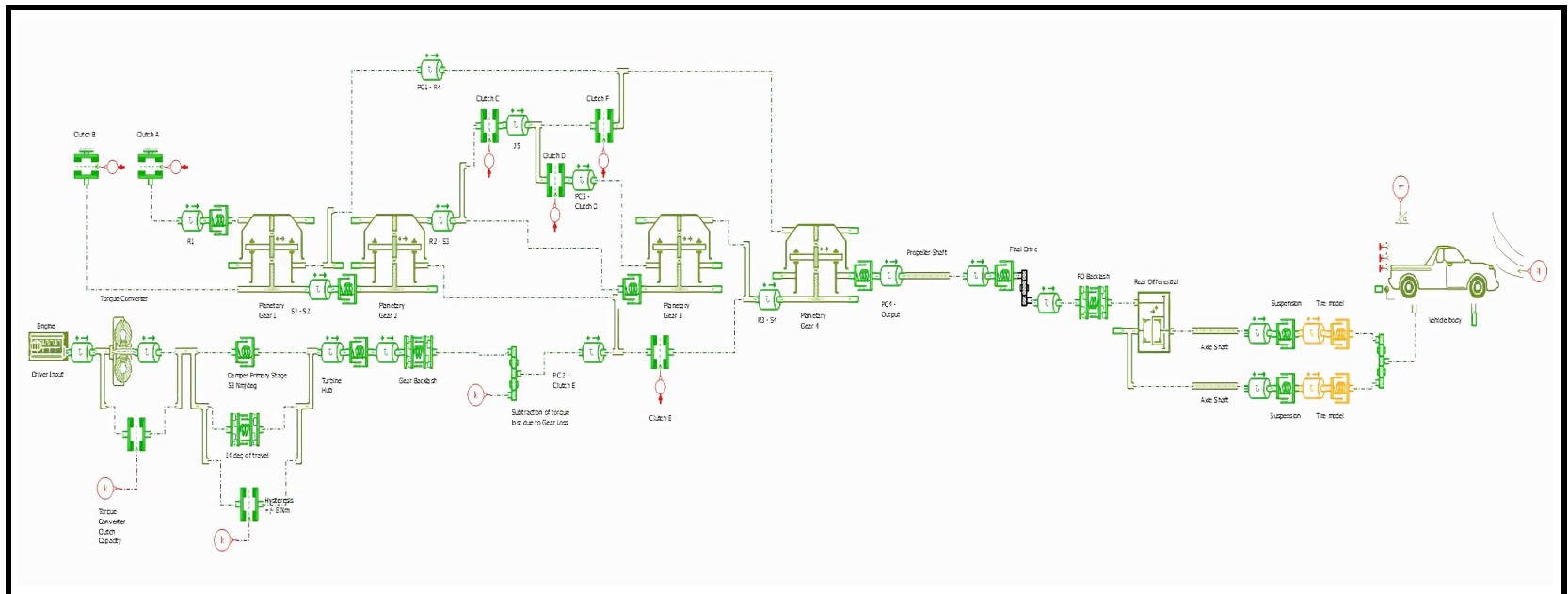


Figure 2.9: Overview of the Amesim[®] vehicle model.

2.2 Model validation

After developing the full-order vehicle model, experimental validation was carried out to ensure that the model is able to capture the dynamics required for driveline anti jerk controls work in the future. It is important to note that while most of the required vehicle parameter data was provided by the sponsoring organization, there were certain components whose detailed data could not be made available. One of those was the torque converter, whose capacity factor, speed ratio, torque ratio curves and inertia values were provided, but geometric properties like the number of blades and blade angles of the impeller and turbine, and torque converter fluid properties could not be made available. Therefore, the current model could only utilize a simple look-up table based torque converter.

For validating the model, experimental tests were carried out by the sponsoring organization on a vehicle whose architecture was similar to the full-order model. The tests involved multiple tip-in and tip-out sequences in three different modes of the torque converter clutch (TCC). Also, the current production level control algorithms in place for reducing the backlash induced oscillations on the test vehicle, were overridden during the test. The experimental vehicle was instrumented with telemetric torque sensors on the propeller shaft, seat-track accelerometers on the driver's seat, and accelerometers on the rear differential of the vehicle. The data from the accelerometers

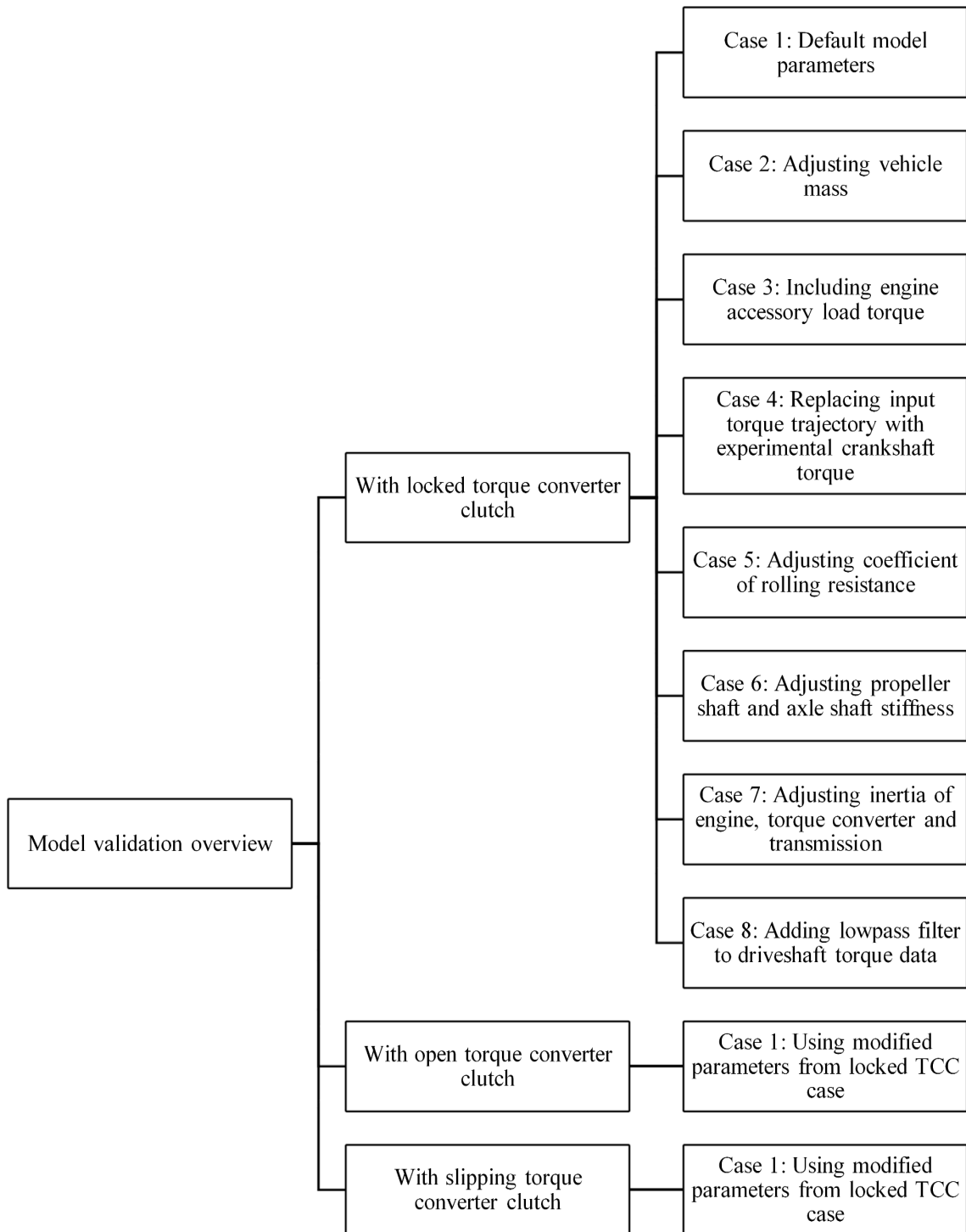


Figure 2.10: Overview of the model validation work done.

has significant noise in it, which is visible in all the validation results' plots. Also, the entire range of CAN bus signals from various control units of the vehicle were recorded, including base and instantaneous torque commands, estimated torque at the crankshaft, engine speed, individual wheel speeds, and estimated torque in the fluid path of the torque converter. These tests were carried out on a cold morning, at a controlled test track.

Data collected from the vehicle can be classified based on the following conditions: a) the torque converter clutch locked throughout the drive cycle, b) the torque converter clutch unlocked or open throughout the drive cycle and c) the torque converter clutch slipping during the tip-in events. While validating the simulation output, importance was given to match parameters that would be of interest in controls related work, like engine speed, wheel speed, vehicle acceleration and driveshaft torque. A step-by-step approach, based on Newton's second law of motion ($F = ma$), was taken to reduce uncertainties in provided/assumed model parameters.

During validation, the case with TCC locked was used for fine-tuning the model parameters in Amesim[®]. The final parameters after fine-tuning with the locked TCC were used while validating scenarios with open and slipping TCC. An overview of the model validation work is provided in Fig. 2.10.

2.2.1 Case 1: Torque converter lock-up clutch locked

In this case, the torque converter lock-up clutch through the TCU was explicitly commanded to be in the locked position, for the entire drive cycle. Therefore, the damping due to the fluid in the torque converter was negligible and consequently the highest amplitude in driveline oscillations was observed in this case. For simulations, the torque converter model was commanded a clutch capacity of 800 Nm, which was well above the output from the engine. Therefore, the entire torque from the engine passed through the lock-up clutch path. Based on the difference between the simulation results and experimental results, model parameters were varied one after another, in order to match the simulation results with the experimental results.

2.2.1.1 Sub-case 1: Original vehicle parameters

Initially, the simulation was run using the original vehicle parameters (Table 2.2), provided by the sponsoring organization, for the modeled components. The torque trajectory for the Amesim[®] model was calculated in Simulink[®], using base and instantaneous torque commands from the experimental data. The results obtained were analyzed to interpret the changes that would be needed to the model. Fig. 2.11(a) shows the estimated crankshaft torque calculated by the ECU, and the simulated

Table 2.1
Frequency of driveline oscillations in sub-case 1

Jerk frequency from test vehicle	Jerk frequency from simulation	Error in jerk frequency
5.88 Hz.	7.40 Hz.	25.85 %

crankshaft torque from the Simulink[®] model. Fig. 2.11(b),(c),(d) show the comparison between the measured engine speed, vehicle speed, vehicle longitudinal acceleration, propeller shaft torque, and respective simulated data.

The estimated and simulated crankshaft torques have a relatively small error during the coasting period until 0.25 seconds. However, as soon as tip-in occurs, the trajectories have significant variation, with the estimated crankshaft torque showing more dynamic behavior compared to the simulated crankshaft torque. This issue is addressed in the forthcoming sub-cases.

The vehicle speeds in Fig. 2.11 (b) show a close match, but the simulated engine speed has considerable error when compared to the measured engine speed. In Fig. 2.11 (c), even though the measured seat-track acceleration is noisy, it is evident that the simulated acceleration value is higher than the measured value. In Fig. 2.11 (d), there is a phase delay between the measured and simulated propeller shaft torques during transients, and a large mismatch during coasting condition.

The errors in engine speed and vehicle longitudinal acceleration were attributed to

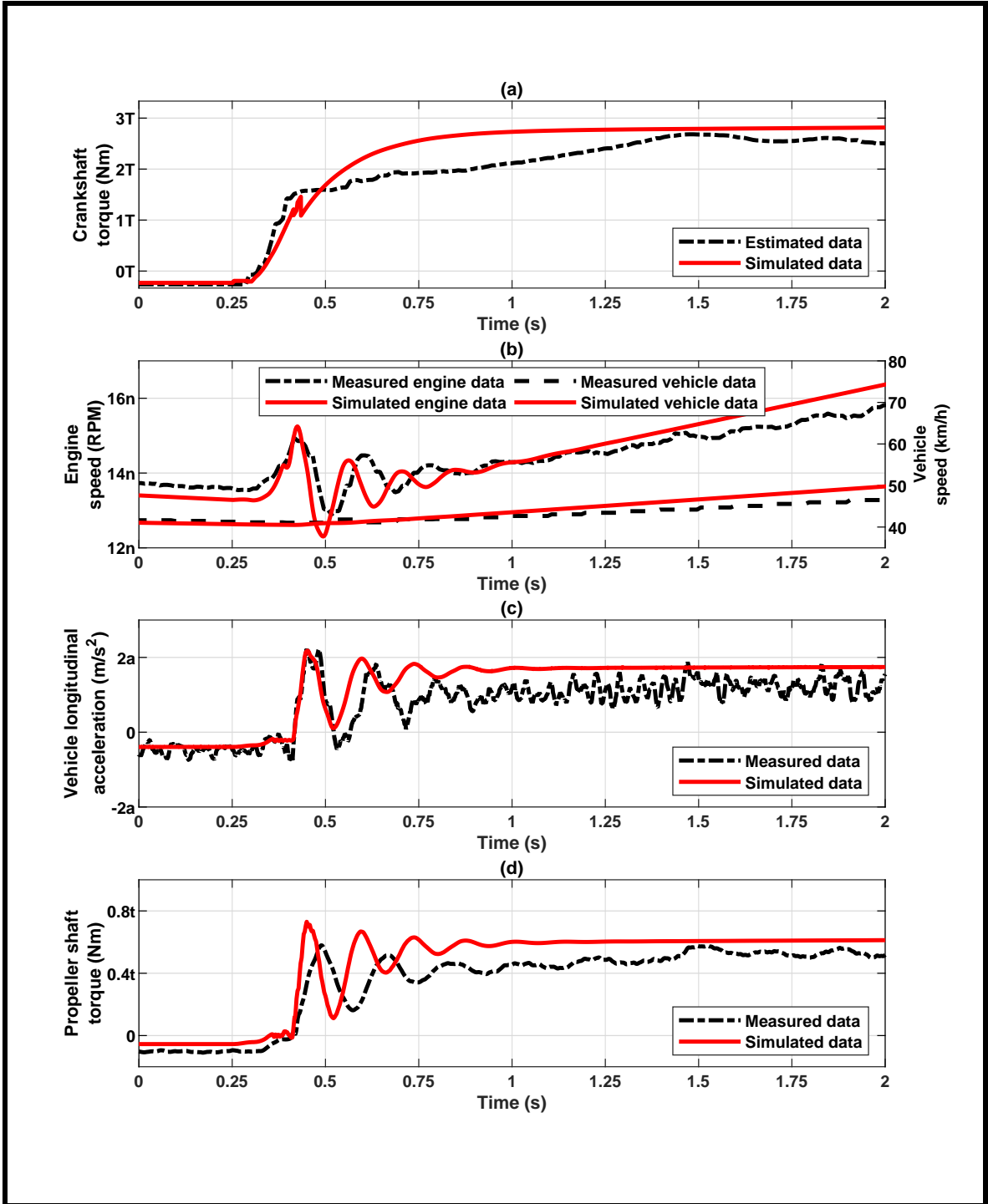


Figure 2.11: Results for sub-case 1 of model validation: Comparison between experimental and simulation data with initial driveline parameters (Table 2.2).

Table 2.2
Simulation parameters for Case 1

Parameter	Value
Gear state	5
TCC status	Locked
Input torque trajectory	Calculated using engine model
Mass of vehicle	2550 kg
Coefficient of rolling resistance	0.02
Propeller shaft stiffness	Default value
Axle shaft stiffness	Default value
Engine inertia	Default value
Torque converter inertia	Default value
Transmission inertia	Default value

the mismatch in chosen value of vehicle mass for simulations, making the model lighter than the actual vehicle, and causing the acceleration to be higher during simulations. Therefore, the mass of the vehicle was recalculated based on inputs from the manufacturer. Table 2.1 shows the difference in the frequencies of shuffle oscillation measured on the vehicle, and in the simulation, for the tip-in scenario shown. The error of 20.65 % in shuffle frequency points to a mismatch in the overall inertia and the stiffness of the driveline model. This is addressed in the forthcoming sub-cases.

Table 2.3
Frequency of driveline oscillations in sub-case 2

Jerk frequency from test vehicle	Jerk frequency from simulation	Error in jerk frequency
5.88 Hz.	7.40 Hz.	25.85 %

Table 2.4
Simulation parameters for Case 2

Parameter	Value
Gear state	5
TCC status	Locked
Input torque trajectory	Calculated using engine model
Mass of vehicle	2884 kg
Coefficient of rolling resistance	0.02
Propeller shaft stiffness	Default value
Axle shaft stiffness	Default value
Engine inertia	Default value
Torque converter inertia	Default value
Transmission inertia	Default value

2.2.1.2 Sub-case 2: Modified vehicle parameters - Vehicle mass increased

The vehicle mass was increased to account for the weight of the instruments used during the tests, and of the three engineers who were present during the tests. The parameters used for this simulation are provided in Table 2.4. The same tip-in scenario as sub-case 1 was simulated again. Fig. 2.12 shows the result of this simulation.

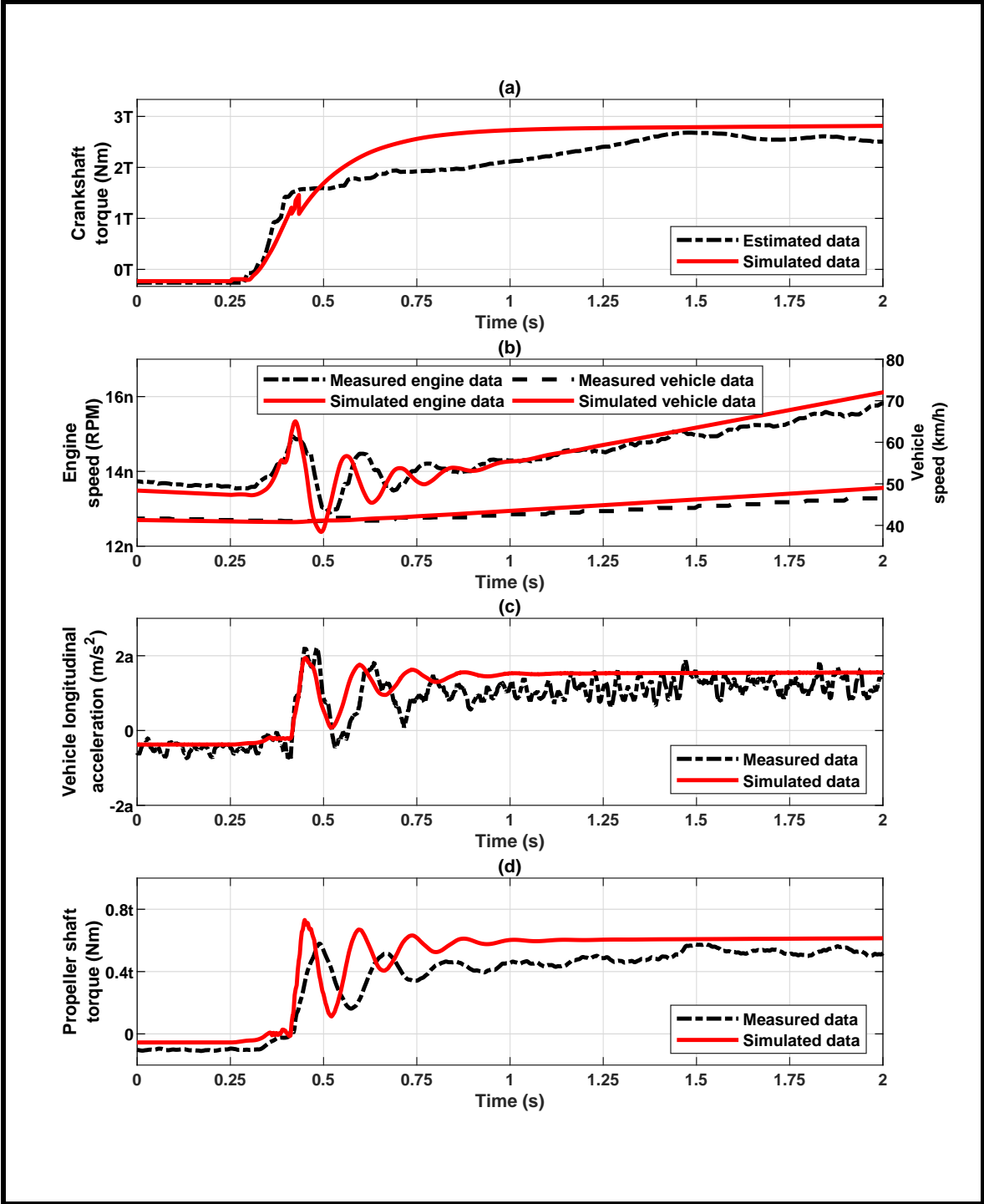


Figure 2.12: Results for sub-case 2 of model validation: Comparison between experimental and simulation data with increased vehicle mass(Table 2.4).

Table 2.5
Frequency of driveline oscillations in sub-case 3

Jerk frequency from test vehicle	Jerk frequency from simulation	Error in jerk frequency
5.88 Hz.	7.40 Hz.	25.85 %

The effect of increasing the mass of the vehicle is evident from the reduced error in vehicle speed and engine speed. However, there is no significant change in the other responses as compared to Fig. 2.11. Table 2.3 shows the oscillation frequency for the experimental data, and simulated data. Next, the force component of Newton's second law of motion was considered for fine-tuning the model.

2.2.1.3 Sub-case 3: Effect of engine accessory load

Engine delivered torque makes up the most significant contribution to the force equation mentioned in the previous sub-case. Based on the observations from sub-case 1, it was suspected that engine accessory load torque was significantly high, due to climatic conditions during the test. Therefore, it was decided to add the effect of engine accessory load torque on the calculated crankshaft torque in Simulink[®]. The actual engine accessory load torque data was available in the CAN signals from the validation data, and it was subtracted from the Simulink[®] calculated torque value.

Fig. 2.13 shows the result of this sub-case, and Table 2.6 shows the parameters used

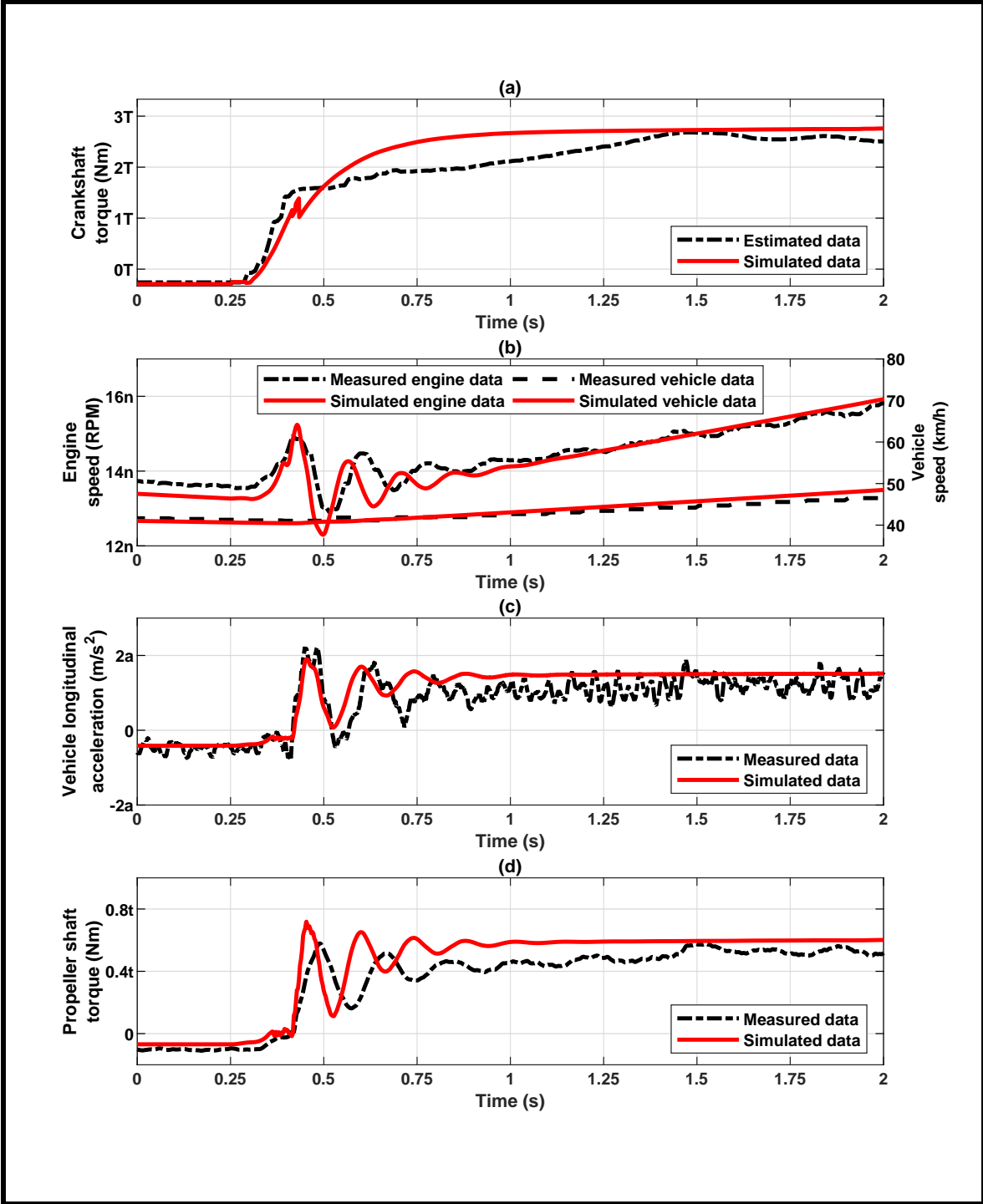


Figure 2.13: Results for sub-case 3 of model validation: Comparison between experimental and simulation data after increasing vehicle mass, and subtracting engine accessory load torque (Table 2.6).

Table 2.6
Simulation parameters for sub-case 3

Parameter	Value
Gear state	5
TCC status	Locked
Input torque trajectory	Calculated using engine model – Engine accessory load torque
Mass of vehicle	2884 kg
Coefficient of rolling resistance	0.02
Propeller shaft stiffness	Default value
Axle shaft stiffness	Default value
Engine inertia	Default value
Torque converter inertia	Default value
Transmission inertia	Default value

for simulation in this sub-case. The results show that the effect of engine accessory load is not as significant as suspected, and the reduction in error between the signals in subplots (b),(c) and (d), is negligible.

2.2.1.4 Sub-case 4: Using crankshaft torque signal from experimental data

Another important difference between the experimental vehicle and the simulation model was related to the engine. While the model utilizes a simplified natural aspirated engine model for calculating the crankshaft torque, the test vehicle was equipped with a turbocharged engine. The initial rise, followed by a lag and rise in the estimated crankshaft torque, evident in subplot (a) of all the model validation plots,

Table 2.7
Frequency of driveline oscillations in sub-case 4

Jerk frequency from test vehicle	Jerk frequency from simulation	Error in jerk frequency
5.88 Hz.	7.40 Hz.	25.85 %

Table 2.8
Simulation parameters for sub-case 4

Parameter	Value
Gear state	5
TCC status	Locked
Input torque trajectory	Test vehicle crankshaft torque
Mass of vehicle	2884 kg
Coefficient of rolling resistance	0.02
Propeller shaft stiffness	Default value
Axle shaft stiffness	Default value
Engine inertia	Default value
Torque converter inertia	Default value
Transmission inertia	Default value

can be attributed to the dynamics of the turbocharger. Therefore, for the remaining cases of validation, the estimated crankshaft torque was directly utilized as an input to the Amesim[®] model. With this approach, the Amesim[®] model can be accurately validated without having to worry about the dynamics of the turbocharger. Fig. 2.14 shows the response of this simulation.

The estimated crankshaft torque, and the simulated crankshaft torque in Fig. 2.14(a) show a variation of 10% over the range of the simulation. This was deliberately

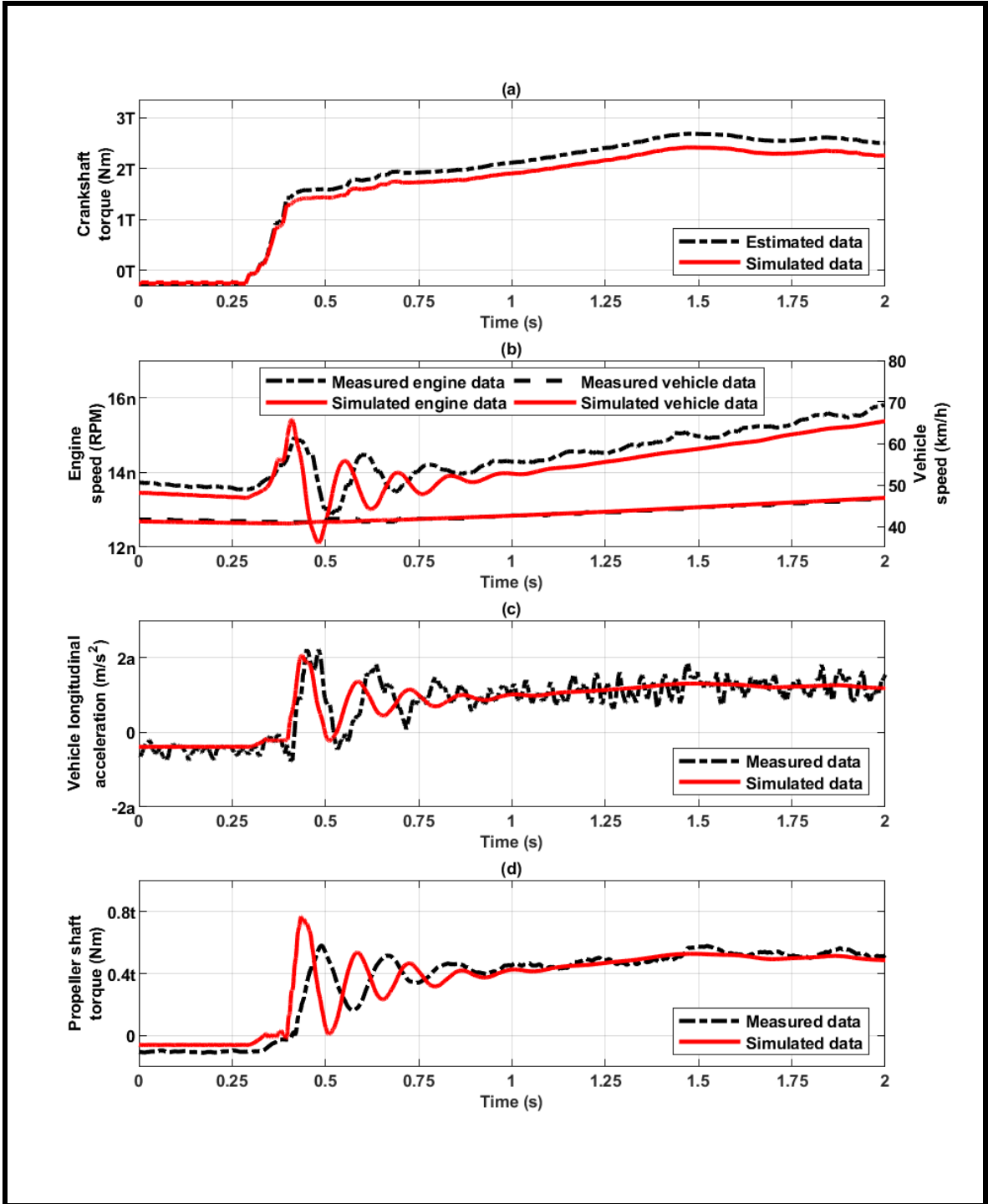


Figure 2.14: Results for sub-case 4 of model validation: Comparison between experimental and simulation data with experimental crankshaft torque trajectory as input.

included, based on the information provided by the sponsoring organization, about the error in the estimated crankshaft torque. Modeling this error, provided some leeway, to tune the input to the Amesim[®] model. In Fig. 2.14(b),(c),(d), the benefit of using the estimated crankshaft torque is noticeable. The longitudinal vehicle acceleration, propeller shaft torque, and vehicle speed show lower percentage of error compared to sub-case 3. Therefore, it can be assumed that the force component developed by the engine, has been reasonably fixed, by using estimated crankshaft torque as the input to the Amesim[®] model. However, the simulated engine speed seems to be less than the actual engine speed, which puts the focus on the resistive forces of the longitudinal vehicle dynamics.

2.2.1.5 Sub-case 5: Modified coefficient of rolling resistance

As mentioned in the beginning of this section, the experimental tests were carried out in a controlled test track, and therefore, any major perturbation in the slope force can be ruled out. Similarly, the frontal area and the drag coefficient that were used for calculating the aerodynamic force were based off calculations from a vehicle similar to the test vehicle. However, there was a degree of uncertainty in the coefficient used for calculating the rolling resistance force. Based on the fact that the coefficient of rolling resistance for tires is dependent on a wide range of factors including the construction of the tire, the speed with which the vehicle is traveling, the air pressure

Table 2.9
Frequency of driveline oscillations in sub-case 5

Jerk frequency from test vehicle	Jerk frequency from simulation	Error in jerk frequency
5.88 Hz.	7.40 Hz.	25.85 %

Table 2.10
Simulation parameters for sub-case 5

Parameter	Value
Gear state	5
TCC status	Locked
Input torque trajectory	Test vehicle crankshaft torque
Mass of vehicle	2884 kg
Coefficient of rolling resistance	0.01
Propeller shaft stiffness	Default value
Axle shaft stiffness	Default value
Engine inertia	Default value
Torque converter inertia	Default value
Transmission inertia	Default value

inside the tires, and the temperature of tires during the test, it was ascertained that the coefficient of rolling resistance being used in the model, was on the higher side for the test conditions in which the data was collected. Also, experimental and simulation results in [[41]], [[42]] and [[43]] indicate that the coefficient of rolling resistance would be closer to 0.01 for the test conditions. Fig. 2.15 shows the result of using 0.01 as the coefficient of rolling resistance. The reduction in engine speed error is significant, and even though the error in vehicle speed and longitudinal acceleration slightly increased, it was assumed to be a reasonable trade-off for the reduction in engine speed error.

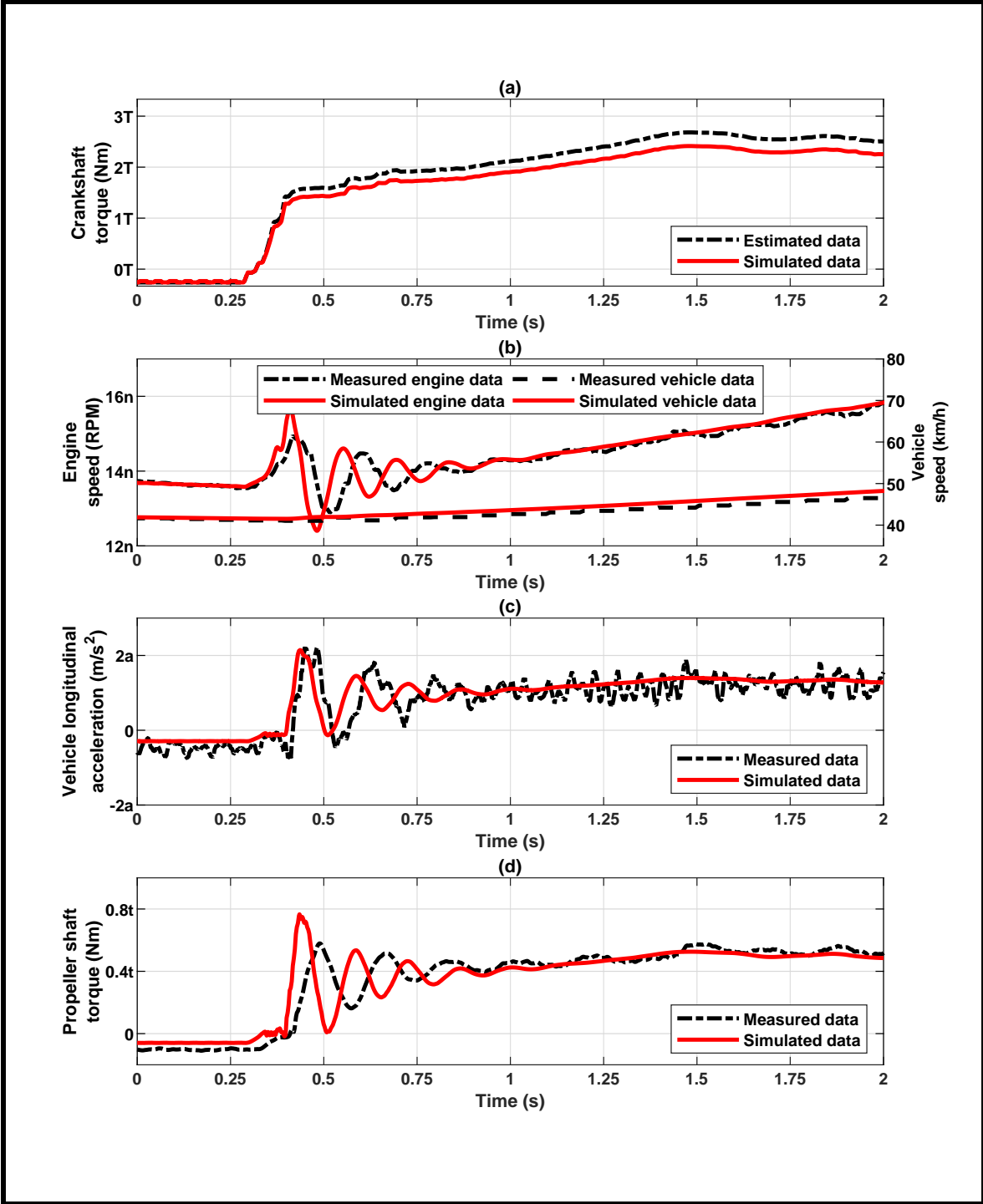


Figure 2.15: Results for sub-case 5 of model validation: Comparison between experimental and simulation data with reduced coefficient of rolling resistance (Table 2.10).

2.2.1.6 Sub-case 6: Propeller and axle shaft stiffness reduced

Model validation steps until this point focused on reducing the error in magnitudes of engine speed, vehicle speed, longitudinal vehicle acceleration and propeller shaft torque using Newton's second law of motion. However, this has no effect on the difference in frequencies of the observed oscillations, in the experimental and simulated data. This is due to the fact that the oscillation frequency ω_n of the system is dependent on

$$\omega_n = \frac{k}{I} \quad (2.27)$$

where, k is the stiffness of the system, and I is the inertia of the system, and both these parameters have not been varied until this point. Based on the technical discussion that took place with the sponsoring organization, it was understood that assuming the suspension to be stiff might be the cause of error in the overall stiffness of the system. However, not modeling the suspension does not affect the controls objective of this model. Since, the propeller shaft and the axle shaft are the most compliant elements within the modeled driveline (Fig. 3.12 and Fig. 3.13), their stiffness was modified to observe the effect on frequency of the jerk oscillations. While a number of iterations were carried out with a range of changes to the propeller and axle shaft stiffness, only the results of the final choice of reducing both the stiffnesses by 25% is shown and discussed here.

Table 2.11
Frequency of driveline oscillations in sub-case 6

Jerk frequency from test vehicle	Jerk frequency from simulation	Error in jerk frequency
5.88 Hz.	6.67 Hz.	13.43 %

The simulation parameters for sub-case 6 are shown in Table 2.12. Fig. 2.16 shows the effect of reducing the propeller and axle shaft stiffness by 25%, in combination with the changes that were made in the previous sub-cases. Compared to the result of sub-case 5 (Fig. 2.15), there is a reduction in the error between the driveline oscillation frequency of the test vehicle and the simulation, as shown in Table 2.11. Since, frequency is also dependent on the inertia of the driveline elements (Eq. 2.27), the next sub-case deals with increasing the inertia of certain driveline components to match the oscillation frequency of jerk. This was exercised since there was a degree of uncertainty in the overall inertia of the driveline, due to some components that were not modeled. This is discussed in the next sub-case.

2.2.1.7 Sub-case 7: Engine, torque converter, and transmission inertia adjusted

The vehicle architecture being modeled in this work, has a 4WD variant. The test vehicle was a 4WD vehicle, whereas, the Amesim[®] model only considers a RWD

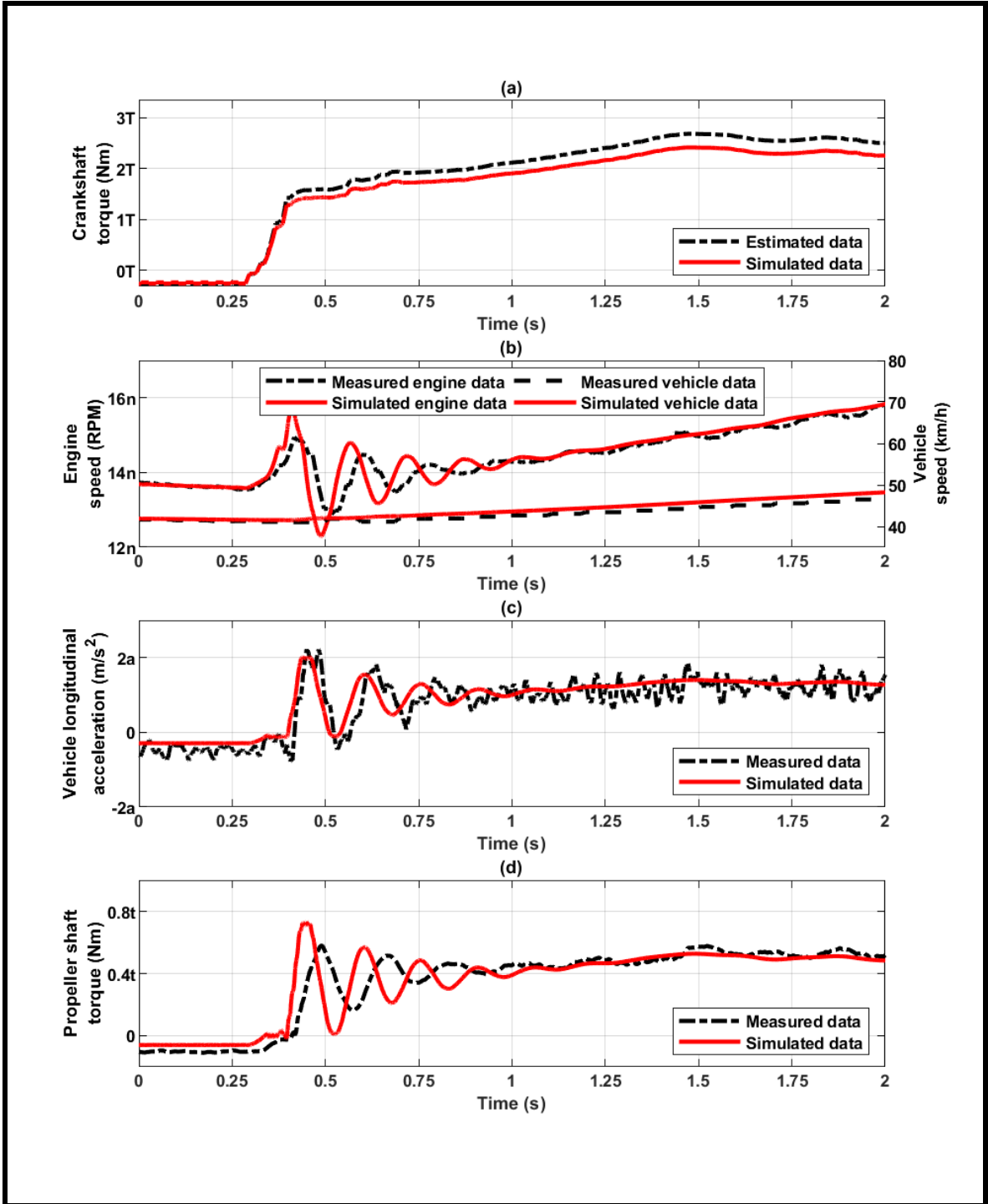


Figure 2.16: Results for sub-case 6 of model validation: Comparison between experimental and simulation data with reduced axle and propeller shaft stiffness (Table 2.12).

Table 2.12
Simulation parameters for sub-case 6

Parameter	Value
Gear state	5
TCC status	Locked
Input torque trajectory	Experimental crankshaft torque
Mass of vehicle	2884 kg
Coefficient of rolling resistance	0.01
Propeller shaft stiffness	Reduced by 25%
Axle shaft stiffness	Reduced by 25%
Engine inertia	Default value
Torque converter inertia	Default value
Transmission inertia	Default value

driveline. The transfer case present in a 4WD system, contributes significant inertia at the end of the transmission, which is not captured in the Amesim[®] model. Also, the crankshaft of the engine has a harmonic damper, which contributes significant inertia to the overall driveline. These components could not be included in the model as the sponsoring organization could not share this data. With this information, the inertia of the engine, torque converter and one node of the transmission had to be adjusted, in order to match the driveline jerk frequency observed on the test vehicle with the simulation data.

The simulation parameters for sub-case 7 are shown in Table 2.14. Fig. 2.17 shows the response of the driveline with 25% increase in the inertia of the engine, torque converter, and final node of the transmission. The error in the frequency of the jerk oscillation during tip-in, shown in Table 2.13, is negligible after these modifications.

Table 2.13
Frequency of driveline oscillations in sub-case 7

Jerk frequency from test vehicle	Jerk frequency from simulation	Error in jerk frequency
5.88 Hz.	5.84 Hz.	0.68 %

Table 2.14
Simulation parameters for sub-case 7

Parameter	Value
Gear state	5
TCC status	Locked
Input torque trajectory	Experimental crankshaft torque
Mass of vehicle	2884 kg
Coefficient of rolling resistance	0.01
Propeller shaft stiffness	Reduced by 25%
Axle shaft stiffness	Reduced by 25%
Engine inertia	Increased by 25%
Torque converter inertia	Increased by 25%
Transmission inertia	Increased by 25%

However, the propeller shaft torque still shows a phase difference between the measured and simulated data. This is addressed in sub-case 8.

2.2.1.8 Sub-case 8: Implementation of filter for propeller shaft torque

While validation results in the previous subsections show a phase difference between the measured and simulated values of propeller shaft torque, it was mentioned by

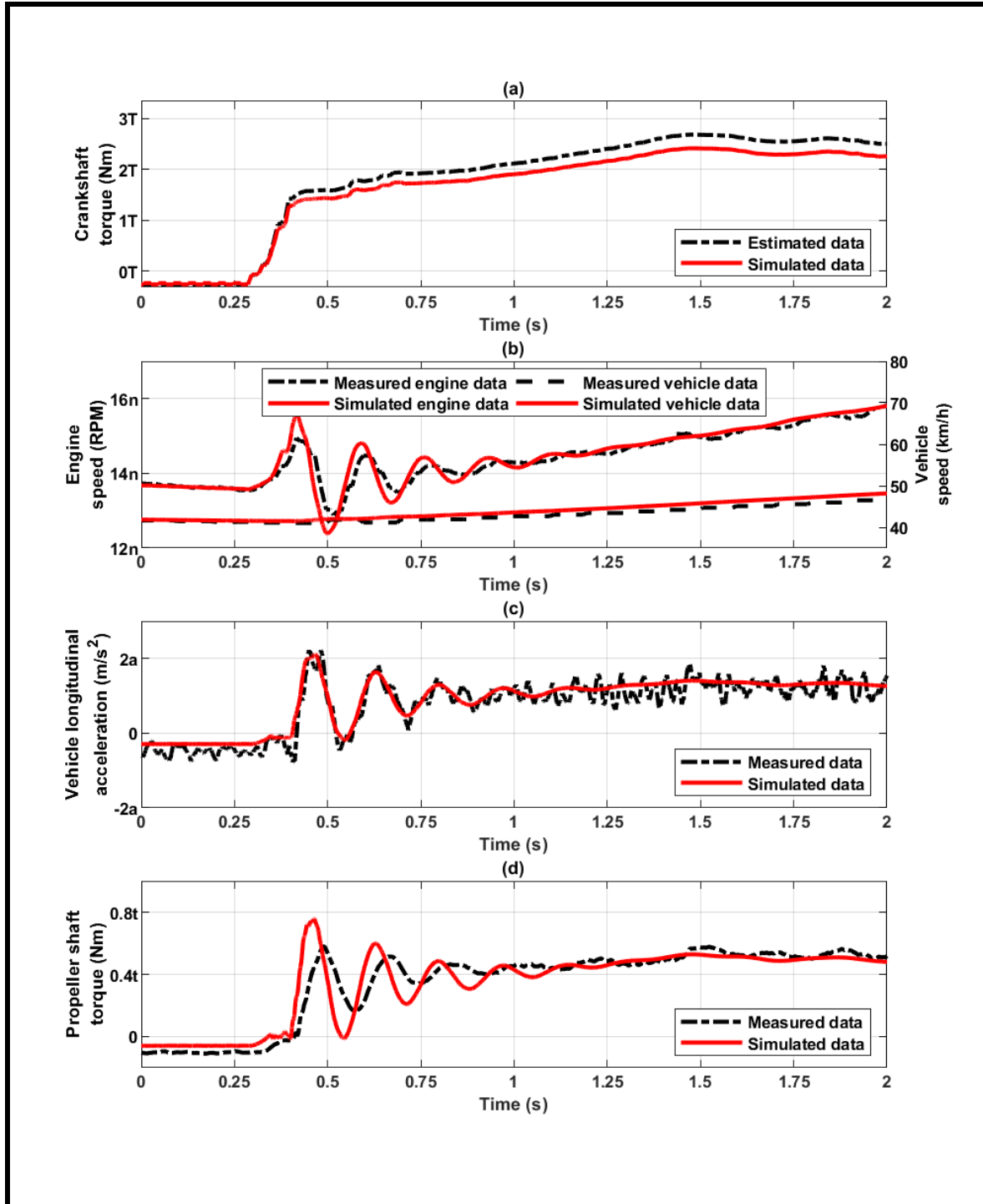


Figure 2.17: Results for sub-case 7 of model validation: Comparison between experimental and simulation data with crankshaft torque as input, reduced vehicle mass, reduced coefficient of rolling resistance, reduced drive shaft stiffness, and increased inertia of engine, torque converter and transmission (Table 2.14).

Table 2.15

Filter parameters used for filtering simulated propeller shaft torque

Parameter	Value
Response Type	Lowpass
Design Method	IIR - Chebyshev II
Sampling frequency	1000 Hz.
End frequency of passband	30 Hz.
Beginning frequency of stopband	35 Hz.
Passband ripple	1 dB
Stopband attenuation	120 dB

the sponsoring organization, that the telemetry device used for measuring the propeller shaft torque output, had an in-built low pass filter with a cutoff frequency of approximately 30 Hz. This contributed to the observed phase delay between the measured and simulated torque values. To this end, a Chebyshev filter was designed in MATLAB[®], with the specifications listed in Table 2.15.

From Fig. 2.18(d), it is evident that there was, in fact, a filter with a cutoff frequency of approximately 30 Hz., and implementing a filter on the simulated propeller shaft torque data matches the phase of the measured and simulated data.

2.2.2 Case 2: Torque converter lock-up clutch open

As already mentioned in the model development section, the torque converter model in this thesis, is based on a set of lookup tables for capacity factor, speed ratio, and

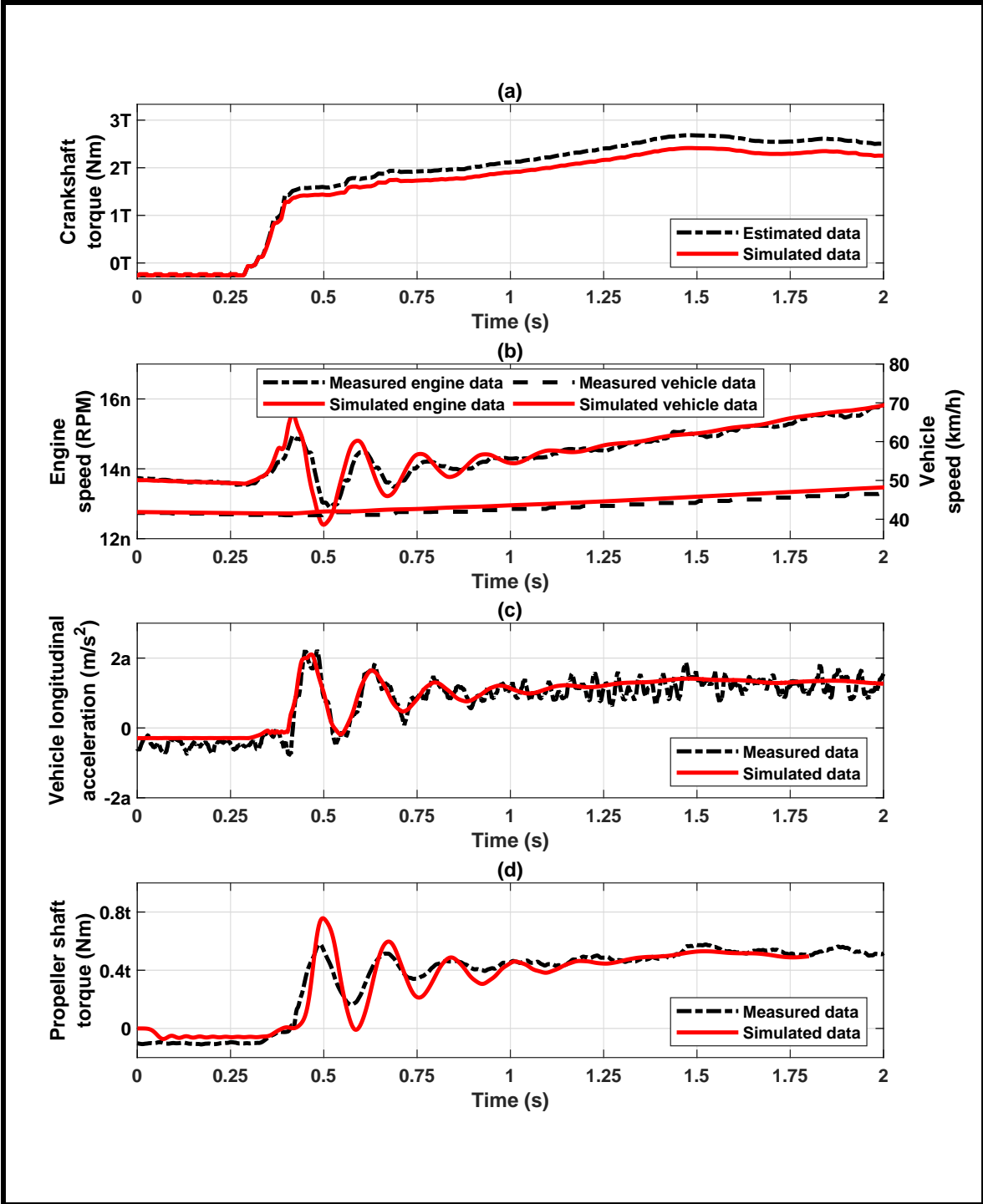


Figure 2.18: Simulation output in 5th gear with estimated crankshaft torque compensated for error as input to Amesim[®], modified vehicle mass, modified coefficient of rolling resistance, modified propeller shaft and axle shaft stiffness, and modified engine, torque converter and transmission inertia, and filtered driveshaft torque.

torque ratio. These tables can be classified into two types, based on whether the impeller is driving the turbine or the turbine is driving the impeller. The first case, called normal run, takes place during normal driving scenarios, when the engine is propelling the vehicle. The second case, called over run, takes place during coasting scenarios, when the wheels propel the vehicle, and the speed of the turbine is higher than the speed of the impeller. This causes the speed ratio of the torque converter to exceed 1, and therefore, a separate lookup table of capacity factor is usually required to accurately model its behavior. Lookup table data for the normal run case was provided by the sponsoring organization, but data for the over-run case could not be provided. Therefore, the over-run data had to be calculated based on information provided in the Amesim[®] manual [13].

Simulation was performed after adjusting the model parameters, based on the observations from the locked TCC validation. Since the TCC is required to be open throughout the run, the TCC capacity was set to 0 Nm, in the vehicle model.

Making use of calculated over-run lookup tables was good enough for the coasting scenarios, as indicated in all the subplots of Fig. 2.19. However, using a simple steady state torque converter model, based only on one- dimensional lookup tables, was not enough to capture the transient dynamics of the tip-in scenario. Amesim[®] has provision to use a transient torque converter model, which is more detailed, but requires geometric parameters like number of blades, blade angles, cross sectional area of flow

Table 2.16
Simulation parameters for Case 2: TCC open condition

Parameter	Value
Gear state	5
TCC status	Open
Input torque trajectory	Experimental crankshaft torque
Mass of vehicle	2884 kg
Coefficient of rolling resistance	0.01
Propeller shaft stiffness	Reduced by 25%
Axle shaft stiffness	Reduced by 25%
Engine inertia	Increased by 25%
Torque converter inertia	Increased by 25%
Transmission inertia	Increased by 25%

passage, and fluid properties, like viscous friction coefficient, shock loss coefficient etc. Since, these parameters were not available, the transient torque converter model could not be used in Amesim[®]. At the end of this chapter, next steps that are being taken to validate the model for transient torque converter events are discussed.

2.2.3 Case 3: Torque converter lock-up clutch slipping

In this case, the TCC is slipping during the tip-in scenarios, which means the flow of torque in the torque converter is split between the fluid path and the lock-up clutch path. The CAN signals from the experimental data contain an estimate of the amount of torque flowing through the fluid path. This estimate was utilized to define the lock-up clutch capacity in the Amesim[®] model, for this simulation.

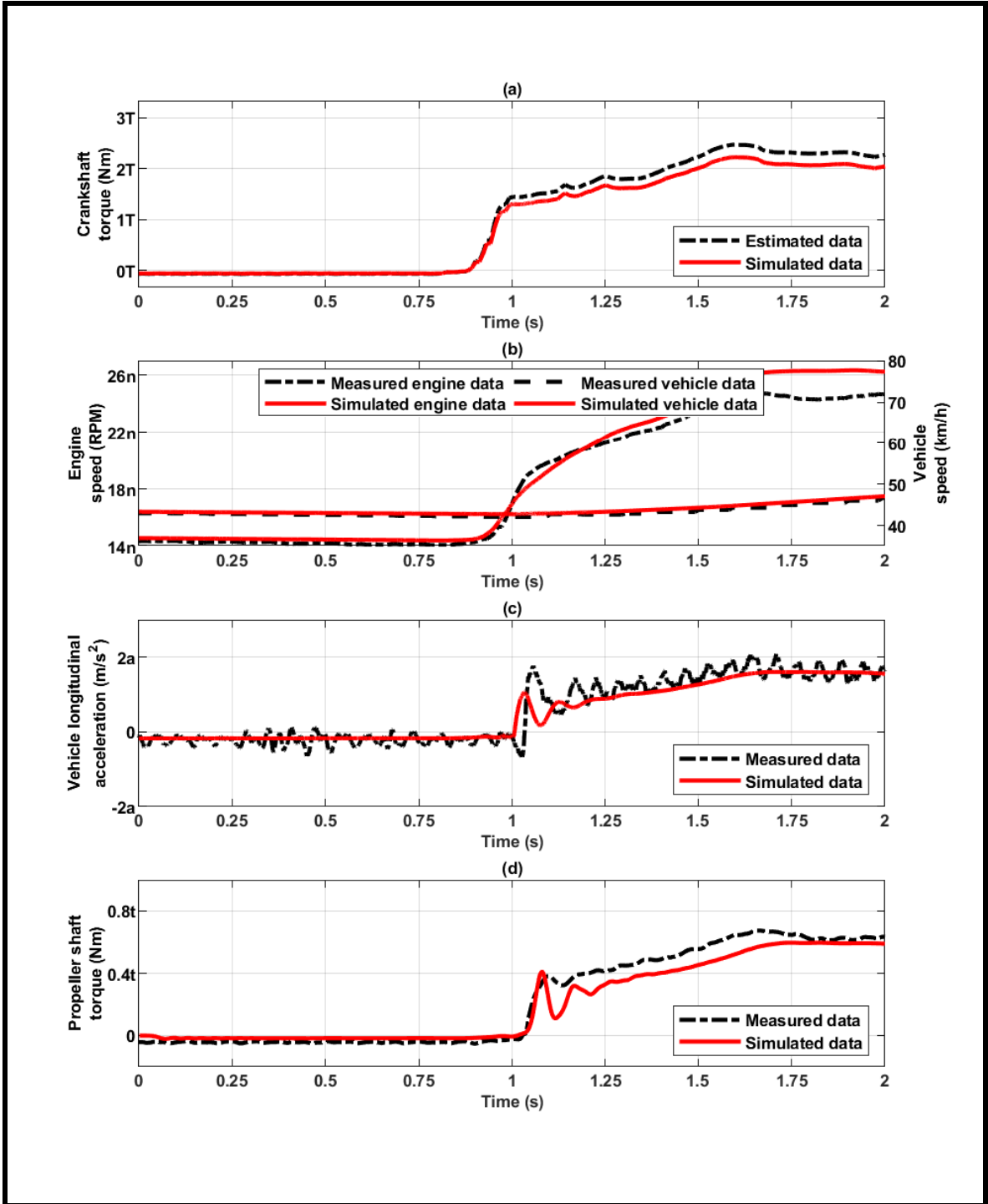


Figure 2.19: Results for the case of open torque converter clutch. Comparison between experimental and simulation data with adjusted parameters from previous section, with TCC status open(Table 2.16).

Table 2.17
Simulation parameters for Case 3: TCC slipping condition

Parameter	Value
Gear state	5
TCC status	Slipping
Input torque trajectory	Experimental crankshaft torque
Mass of vehicle	2884 kg
Coefficient of rolling resistance	0.01
Propeller shaft stiffness	Reduced by 25%
Axle shaft stiffness	Reduced by 25%
Engine inertia	Increased by 25%
Torque converter inertia	Increased by 25%
Transmission inertia	Increased by 25%

Table 2.17 shows the simulation parameters for case 3, and Fig. 2.20 shows the response of the driveline for this simulation. Similar to case 2, the torque converter model used in Amesim[®] was able to provide a good match for the coasting scenarios, but there is significant mismatch in the engine speed, vehicle longitudinal acceleration, and propeller shaft torque during and after tip-in. This is again attributed to the steady-state model of the torque converter that was used in Amesim[®].

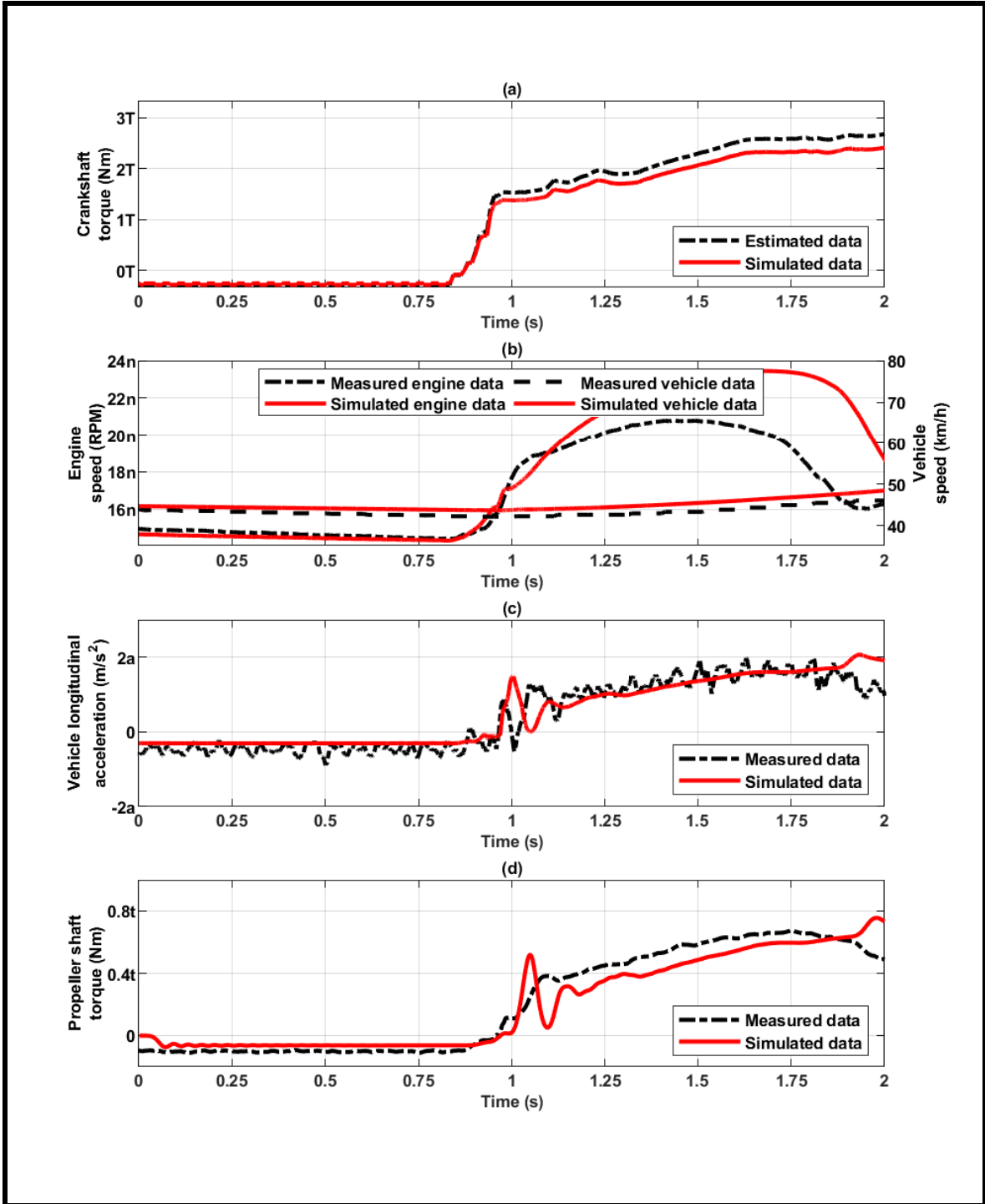


Figure 2.20: Results for the case of slipping torque converter clutch. Comparison between experimental and simulation data, with adjusted parameters from previous section, and with TCC status slipping (Table 2.17).

Proposed solution to improve torque converter model:

It is clear from the results of Case 2, and Case 3 of model validation, that a steady state torque converter model in Amesim[®] is ineffective in accurately capturing the required transient dynamics of the fluid path torque. Since, the geometric and fluid properties of the torque converter could not be made available, it was proposed that, as a next step, required parametric data would be collected from a parallel hardware project that is underway, on the same vehicle platform, at Michigan Technological University. Then, an accurate model of the torque converter, for the vehicle in this study, will be developed and integrated into the designed Amesim model in this thesis.

Chapter 3

Parametric Analysis of Driveline

Response

After model development and validation, parametric analysis of the model was performed to understand the significance of various driveline elements, on shuffle oscillations. Input torque ramp rate, transmission and final drive backlash size, propeller and axle shaft stiffnesses and damping coefficients were of particular interest for parametric analysis. Each of these is discussed in this section and corresponding plots are presented. This analysis was used to decide on the components to be considered while reducing the model order.

3.1 Effect of varying input torque ramp rate

As mentioned in the first chapter, the magnitude of torque input and the time period within which it is delivered, are major factors in defining the magnitude of oscillations that are induced due to the backlash in the driveline. This was investigated for various torque ramp rates from 150 Nm/s up to 1000 Nm/s. The results of two of these ramp rates, i.e., 150 Nm/s and 500 Nm/s, are discussed in this section. A ramp rate of 150 Nm/s represents a gradual torque request, and a ramp rate of 500 Nm/s represents a sudden torque request by the driver. The engine speed, vehicle longitudinal acceleration, transmission and final drive backlash traversal, and propeller shaft torque were plotted to understand the response of the driveline.

3.1.1 Tip-in scenarios

Torque ramp rate can be commanded for both tip-in and tip-out scenarios in the actual vehicle. Therefore, similar analysis was carried out, and this section presents the results of the tip-in scenarios. The tip-in scenario can further be classified based on the initial condition of backlash, and the status of the TCC. The initial condition of backlash can either be positive contact or negative contact, and the status of TCC can be (i) locked, (ii) slipping or (iii) open.

3.1.1.1 With backlash in positive contact and TCC locked

In this condition, the backlash is in positive contact, meaning the initial torque value commanded to the engine was a positive value, and the final torque value commanded is also positive. This case is analogous to a driver traveling on a highway with the cruise control turned ON, and increasing the speed of the vehicle through the cruise control system. Since the vehicle is at highway speeds, the TCC can be assumed to be locked.

In Fig. 3.1, the base and instantaneous command torque rise from 50 Nm to 350 Nm at a ramp rate of 150 Nm/s. The red line in Fig. 3.1 (a), is the delivered engine torque, and it includes the first-order lag and, base and instantaneous path delays, which is evident in its trajectory. Also, due to the included uncertainty in the engine model, it is observed that there is an error of 10% between the commanded torque and the delivered torque in steady state. Since the ramp rate is small, and the backlashes are in positive contact, oscillations are not induced into the system, which is comparable to an actual vehicle's behavior under these conditions.

In Fig. 3.2, the base and instantaneous command torque rise from 50 Nm to 350 Nm at a ramp rate of 500 Nm/s. Since, the torque uncertainty model uses a function of ramp rate of the command signal for calculating the delivered torque, a drop in engine delivered torque is observed at approximately 10.8 seconds. The increase in

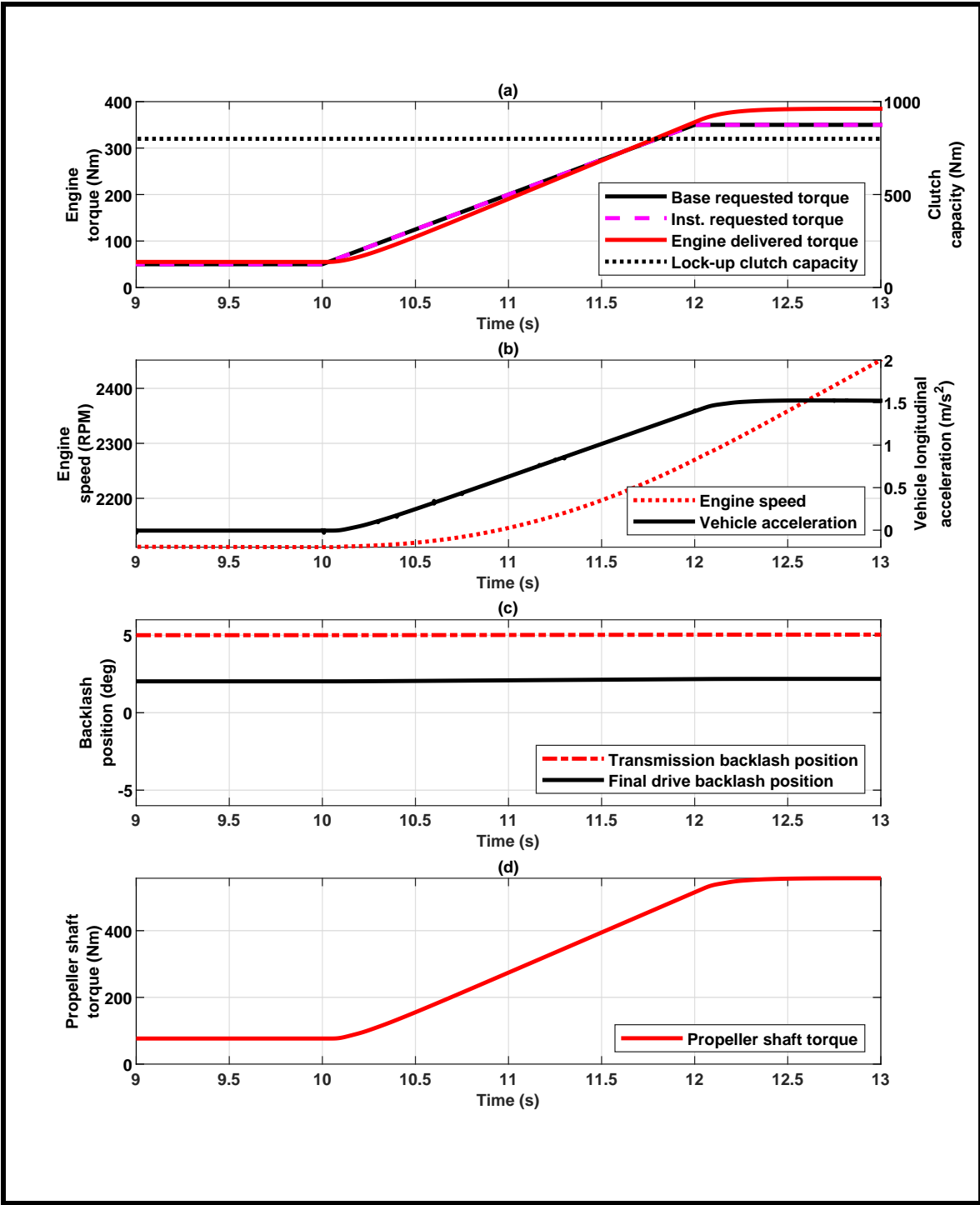


Figure 3.1: Driveline response for tip-in scenario with 150 Nm/s ramp rate, backlash in positive contact, and locked TCC.

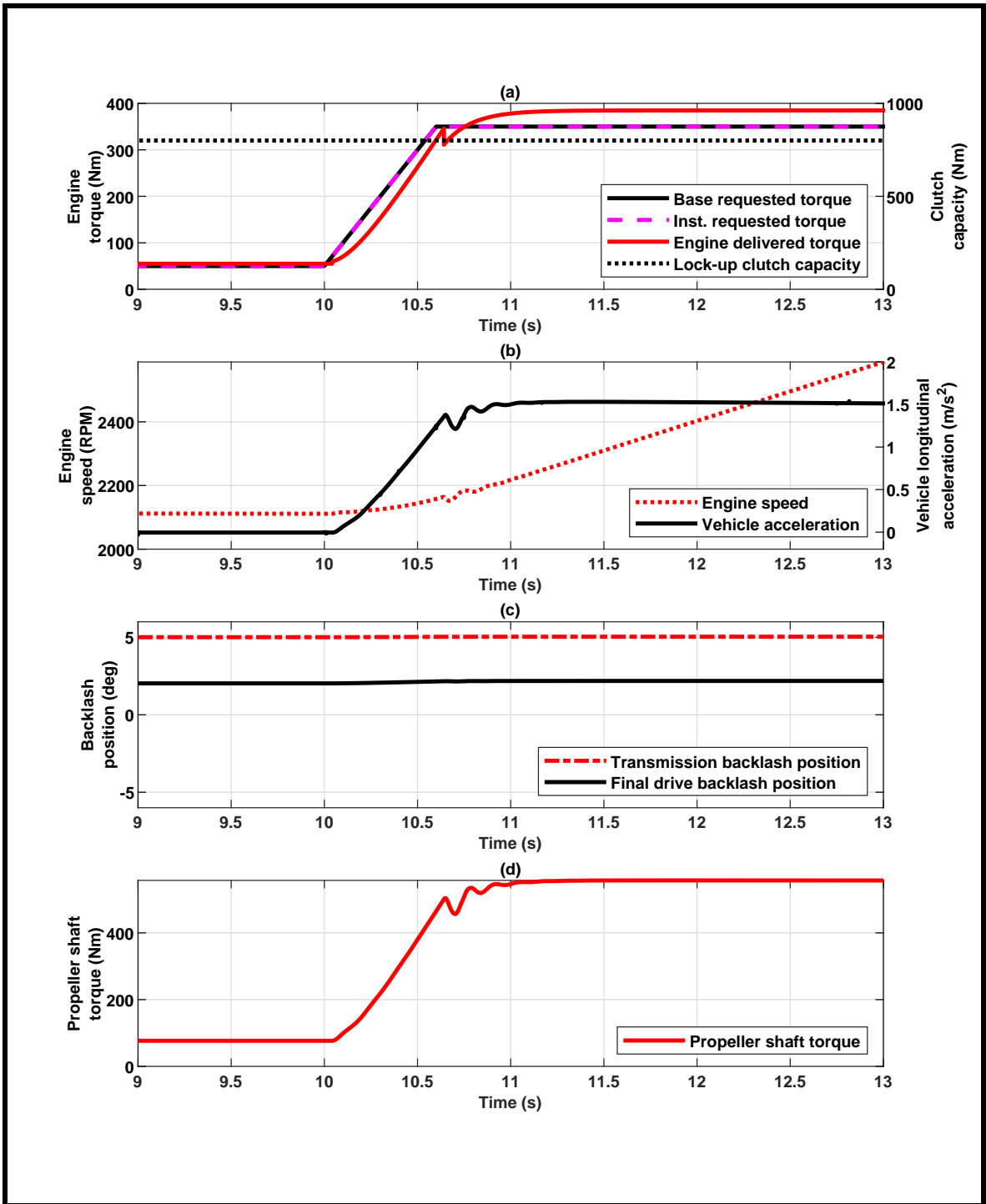


Figure 3.2: Driveline response for tip-in scenario with 500 Nm/s ramp rate, backlash in positive contact, and locked TCC.

torque ramp rate leads to oscillations of small amplitude in the driveline, as evidenced in the propeller shaft torque subplot (d) and, engine speed and vehicle acceleration in subplot (b).

3.1.1.2 With backlash in negative contact and TCC locked

Next, the case wherein backlash is initially in negative contact is analyzed. The initial torque command is in the negative domain, and it goes to positive domain when the driver requests torque from the engine. Change in domain of delivered torque causes the backlash to traverse from one side to the other. This case is analogous to a vehicle which is coasting at highway speeds, with the driver's foot off the accelerator pedal and the cruise control turned OFF, causing the vehicle's momentum to propel the vehicle. Then, the driver requests torque either through the accelerator pedal or through the cruise control, and the engine starts delivering torque to the driveline.

In Fig. 3.3, the base and instantaneous command torque rise from 50 Nm to 350 Nm at a ramp rate of 150 Nm/s, from negative contact of backlash to positive contact. Since the engine is providing torque, the backlash at the transmission traverses first, and as soon as it reaches positive contact, the backlash at the final drive traverses. Both these backlash elements cause an impact on making positive contact, and induce oscillations throughout the driveline, as evidenced in propeller shaft torque and vehicle acceleration in subplots Fig. 3.3(b) and (d) . Oscillations of the same frequency are

observed in the engine speed $\dot{\theta}_e$, which is being calculated in Amesim, using the formula:

$$J_e \ddot{\theta}_e = T_{(e,inst,brake)}(t) - T_{im} \quad (3.1)$$

wherein, J_e is the rotational inertia of the engine, $\ddot{\theta}_e$ is the rotational acceleration of the engine, from which rotational speed is computed and T_{im} is the load torque from the driveline, at the impeller of the torque converter. The load torque carries over the shuffle oscillations observed in the propeller shaft torque.

A similar tip-in scenario is shown in Fig. 3.4, with the the backlash in negative contact, and the TCC in locked position. However, the ramp rate of the input torque in this case is 500 Nm/s, which causes the backlash traversal to take place quicker than the previous case. This leads to an increased impact velocity at positive contact of the transmission and final drive backlash, causing the amplitude of the induced oscillations to be higher than the case where the input torque ramp rate is 150 Nm/s. The frequency of the oscillation, however, does not change, as it is related to the stiffness of the components of the driveline, rather than the input given to the system.

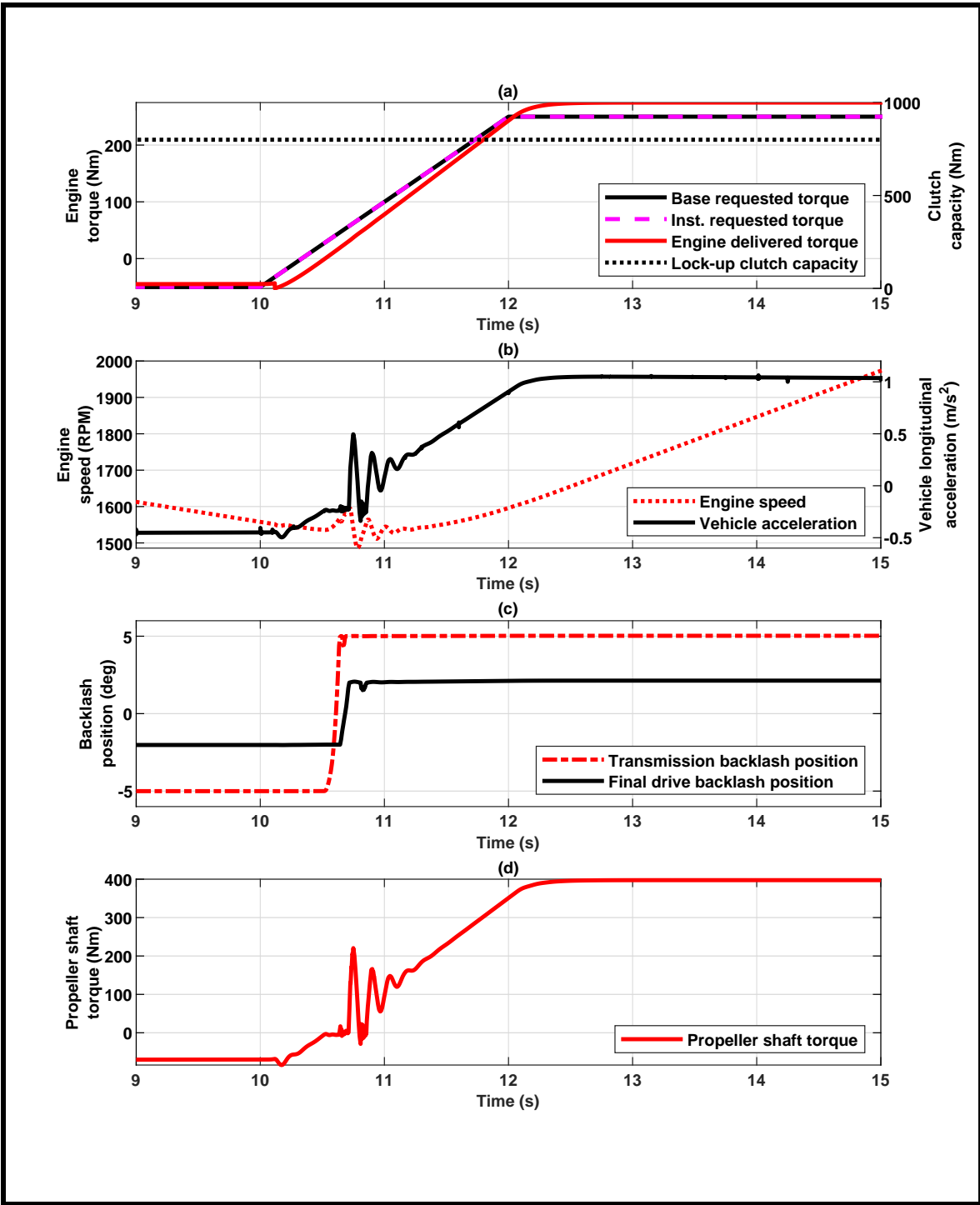


Figure 3.3: Driveline response for tip-in scenario with 150 Nm/s ramp rate, backlash in negative contact, and locked TCC.

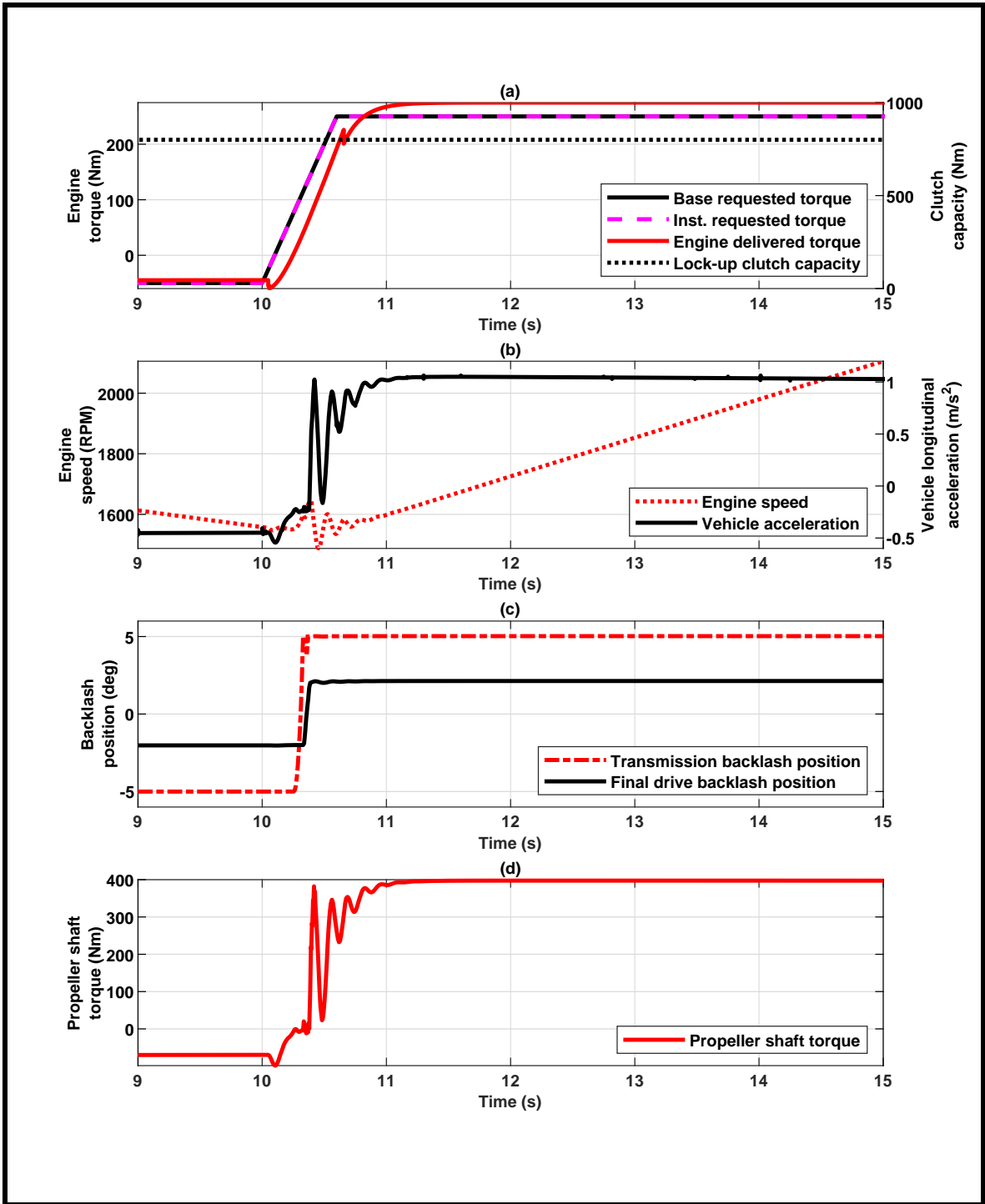


Figure 3.4: Driveline response for tip-in scenario with 500 Nm/s ramp rate, backlash in negative contact, and locked TCC.

3.1.1.3 With backlash in negative contact and TCC slipping

The fluid path of the torque converter is capable of damping out the oscillations induced into the driveline due to backlash traversal. In fact, this property can be utilized as a means of mitigating the jerk in the driveline. This was tested by reducing the clutch capacity of the system from 800 Nm (Locked case), to 100 Nm (Slipping case), and providing a base and instantaneous torque command at a ramp rate of 500 Nm/s. Fig. 3.5 shows the response of the driveline for this scenario. The torque converter lock up clutch is in the locked position until a torque value of 100 Nm from the engine, and above that it starts to slip, meaning the flow of torque in the torque converter model is distributed between the fluid path and the lock-up clutch path. Both the propeller shaft torque and the vehicle longitudinal acceleration show reduced oscillations compared to the case where the torque converter lock up clutch was locked. In an actual vehicle, the pressure command to the torque converter lock up clutch can be varied during backlash traversal, such that the jerk in the driveline is further reduced.

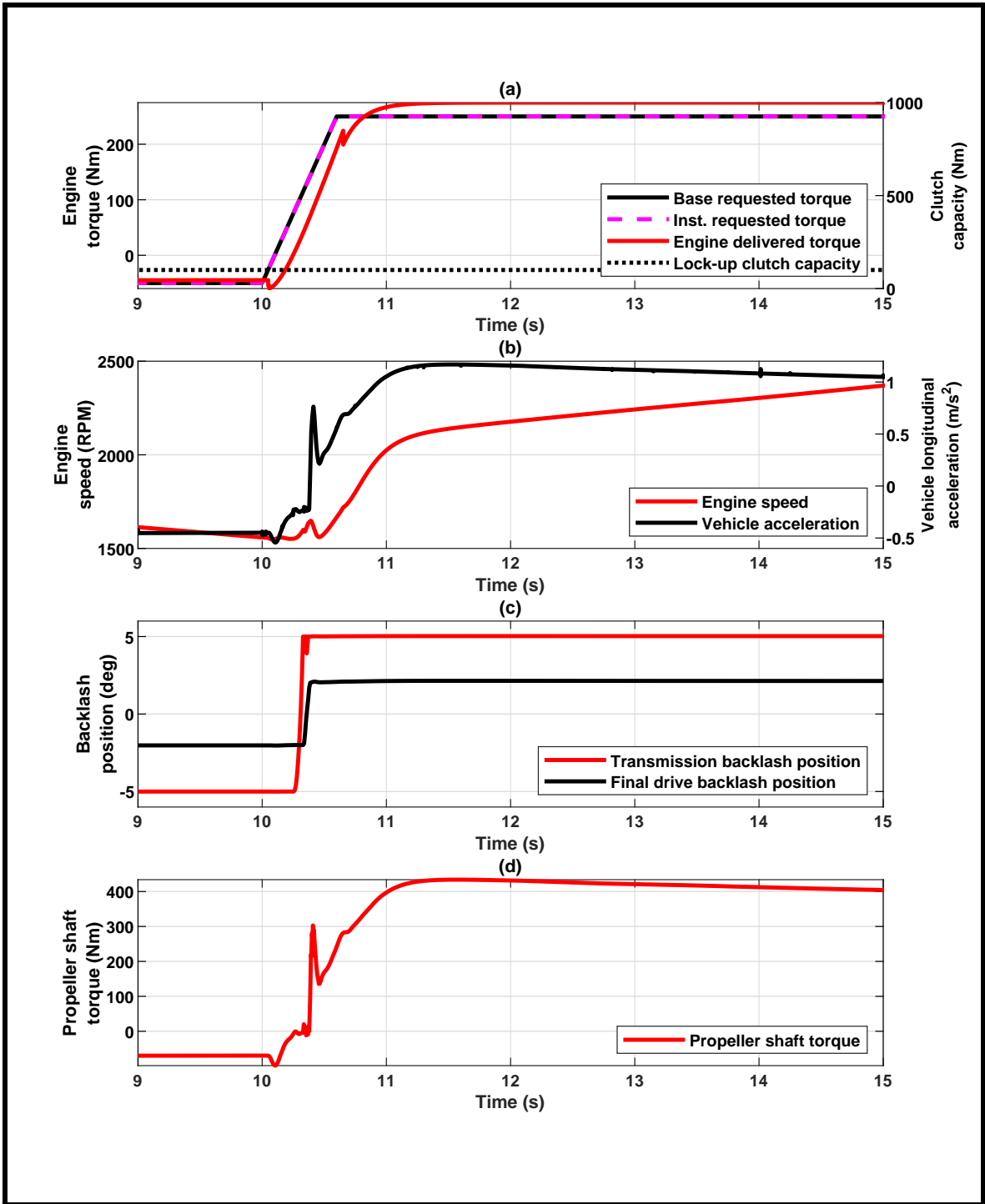


Figure 3.5: Driveline response for tip-in scenario with 500 Nm/s ramp rate, backlash in negative contact, and slipping TCC.

3.1.2 Tip-out scenarios

It is possible to experience clunk and shuffle even during tip-out scenarios, and therefore requires a separate set of algorithms for managing backlash traversal when the driver lifts his/her foot off the accelerator pedal, or the cruise control stops requesting torque from the engine. It is necessary to understand the behavior of the driveline during such scenarios, to aid the development of the required control strategy.

While it has already been established in the subsection 3.1.1, that unlocking the TCC during backlash traversal is beneficial for reducing jerk, it is not always recommended from a fuel economy point of view. Therefore, tip-out scenarios were also sub-classified into cases when the TCC is locked, and when it is slipping or open, to understand the effect each of these cases has on the driveline response.

3.1.2.1 With backlash in positive contact and TCC locked

In Fig. 3.6, the base and instantaneous torque command fall from 350 Nm to 50 Nm at a ramp rate of 150 Nm/s, with the backlash in positive contact, and the TCC in locked position. Since the torque command is in the positive domain throughout the scenario, backlash traversal does not take place, and therefore, the response of the driveline is smooth, and similar to the tip-in case with locked TCC and positive

contact of backlash.

3.1.2.2 With backlash in negative contact and TCC locked

In Fig. 3.7, the base and instantaneous command torque fall from 250 Nm to -50 Nm at a ramp rate of 150 Nm/s, from positive contact of backlash to negative contact, with the TCC locked. In this case, the final drive backlash traverses first, and as soon as it makes negative contact, transmission backlash traversal takes place. This causes clunk and shuffle in the system, just as in the case of tip-in scenarios. Since, the backlash traversal takes place after the delivered engine torque changes domain, it is only required to control the engine delivered torque as it reaches a value close to 0 Nm.

3.1.2.3 With backlash in negative contact and TCC open

In Fig. 3.8, the base and instantaneous command torque fall from 250 Nm to -50 Nm at a ramp rate of 150 Nm/s, from positive contact of backlash to negative contact, with the TCC capacity set to 0 Nm. Therefore, the TCC remains open throughout the scenario, and the entire torque flows through the fluid path of the torque converter. Just as in the case of tip-in scenario with slipping lock up clutch inside the torque converter, having an open lock up clutch during tip-out scenario also reduces jerk in

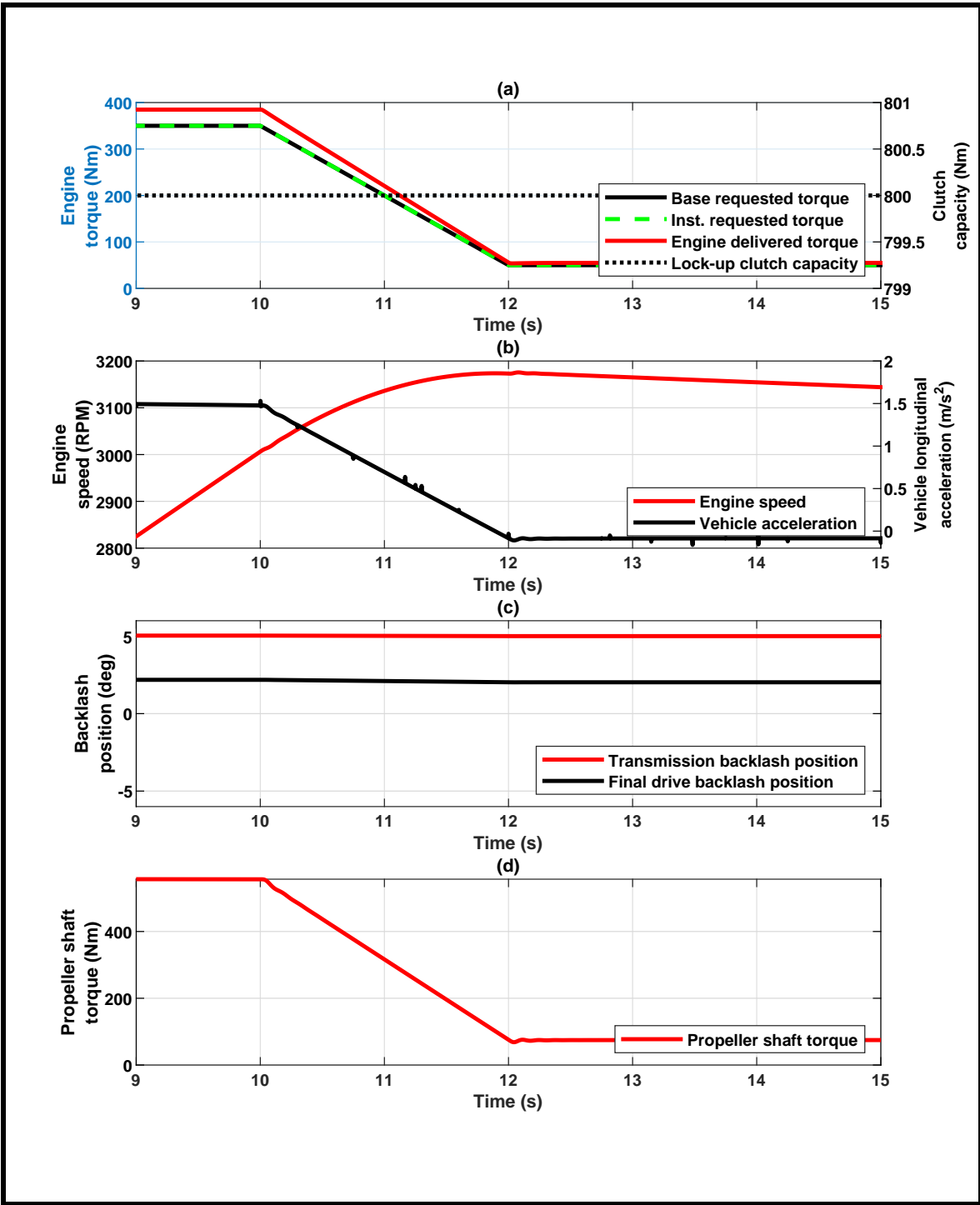


Figure 3.6: Driveline response for tip-out scenario with 150 Nm/s ramp rate, backlash in positive contact, and locked TCC.

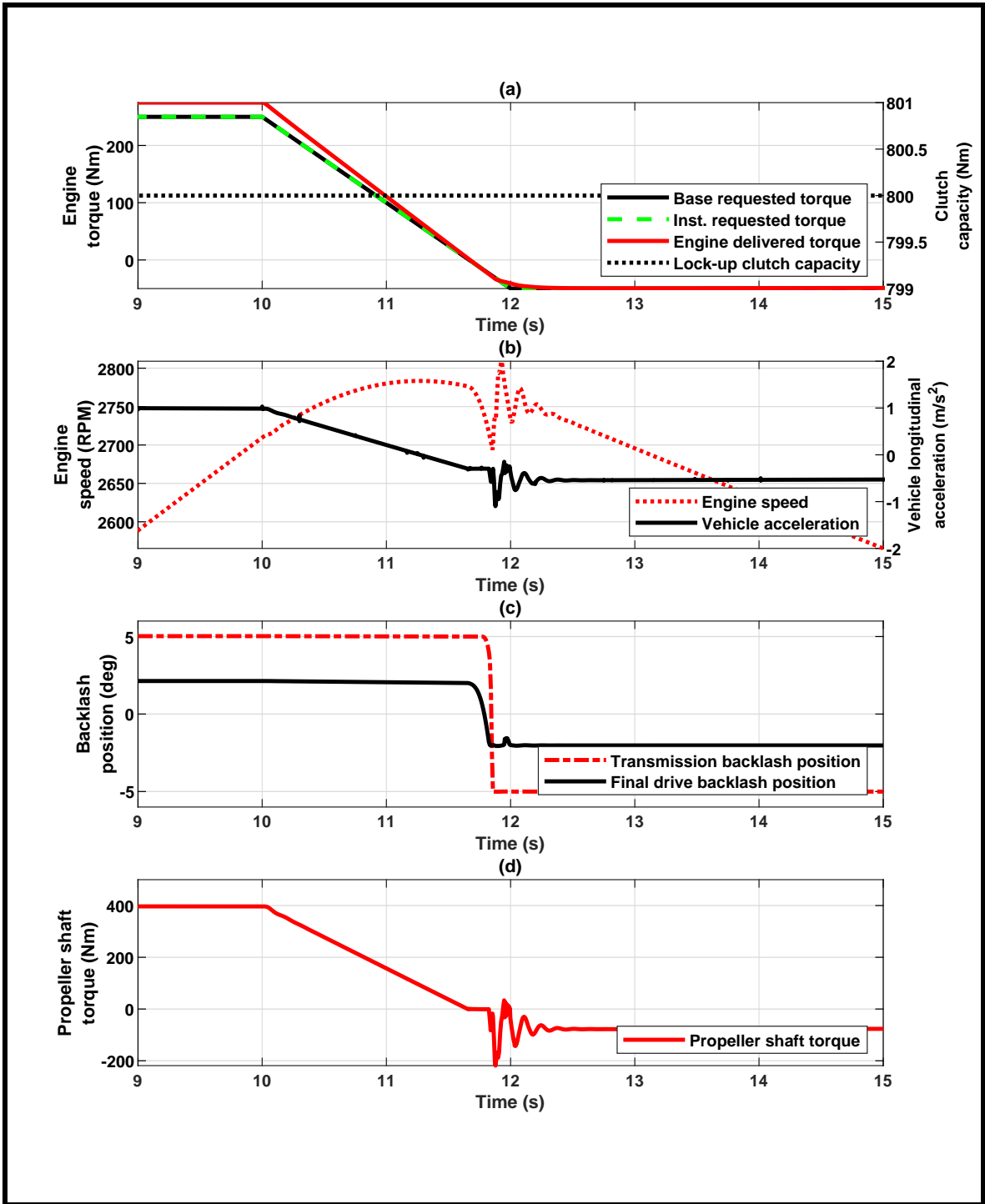


Figure 3.7: Driveline response for tip-out scenario with 150 Nm/s ramp rate, backlash in negative contact, and locked TCC.

the system.

3.1.3 During backlash traversal

From the previous analyses in this chapter, it is evident that controlling the speed with which backlash traversal takes place, is essential for reducing clunk and shuffle in the driveline. Therefore, varying the torque ramp rate is carried out in such a way, that the impact velocity on the positive contact of backlash is reduced.

In Fig. 3.9, the base torque command rises from -50 Nm to 250 Nm at a ramp rate of 500 Nm/s, while the instantaneous torque command first rises at the same ramp rate, and then suddenly drops during backlash traversal, and then rises again to merge with the base torque command. The TCC is locked in this condition, and therefore, there is no damping from the fluid path of the torque converter. Compared to Fig. 3.4, the amplitude of oscillation in vehicle longitudinal acceleration is reduced by nearly 50 %, and in propeller shaft torque it is reduced by nearly 30 %. As the instantaneous path torque command controls the spark during combustion, it is capable of handling such quick dynamics. However, the effect of drop in instantaneous path torque command, on other parameters like fuel economy has to be studied.

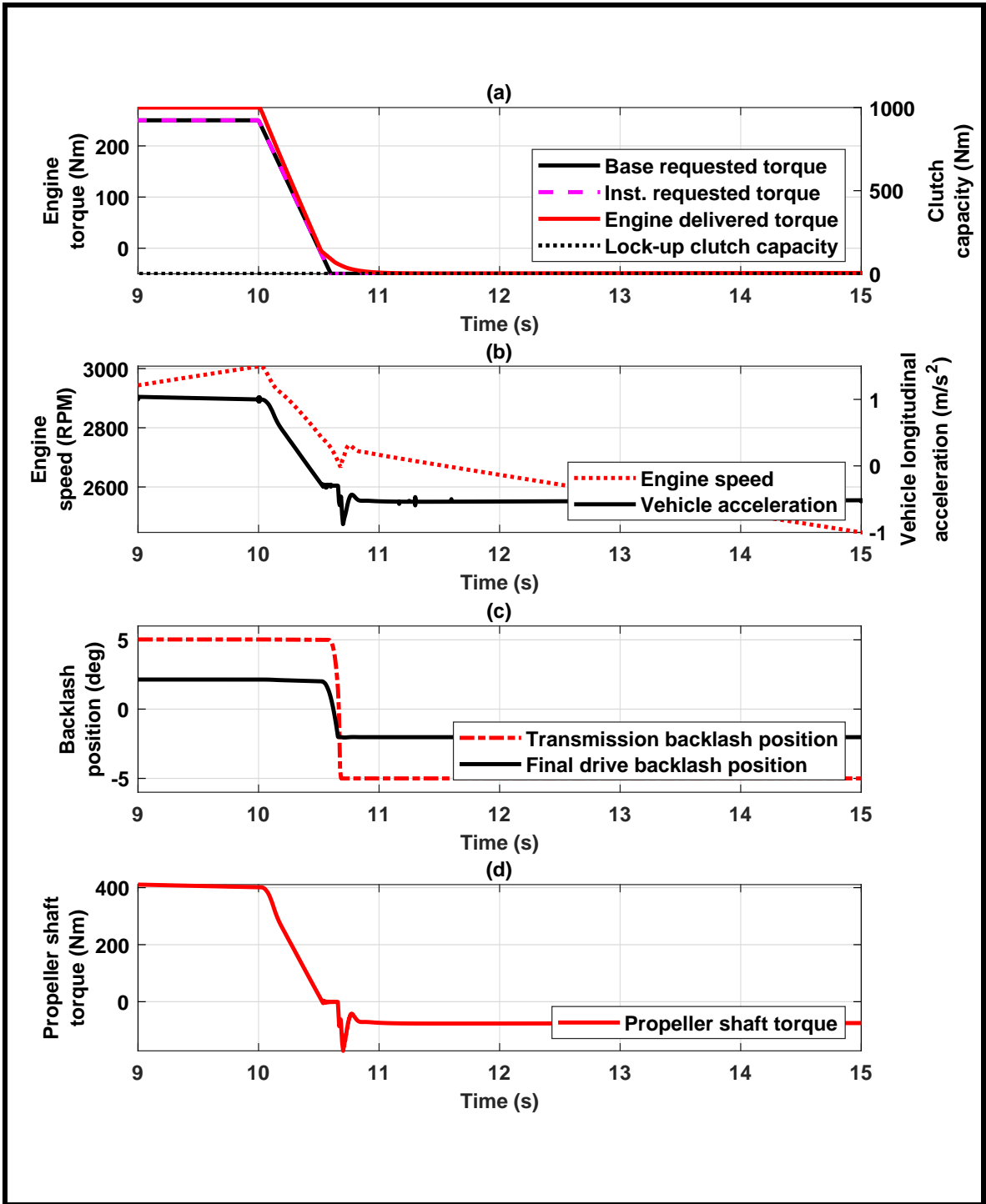


Figure 3.8: Driveline response for tip-out scenario with 150 Nm/s ramp rate, backlash in negative contact, and open TCC.

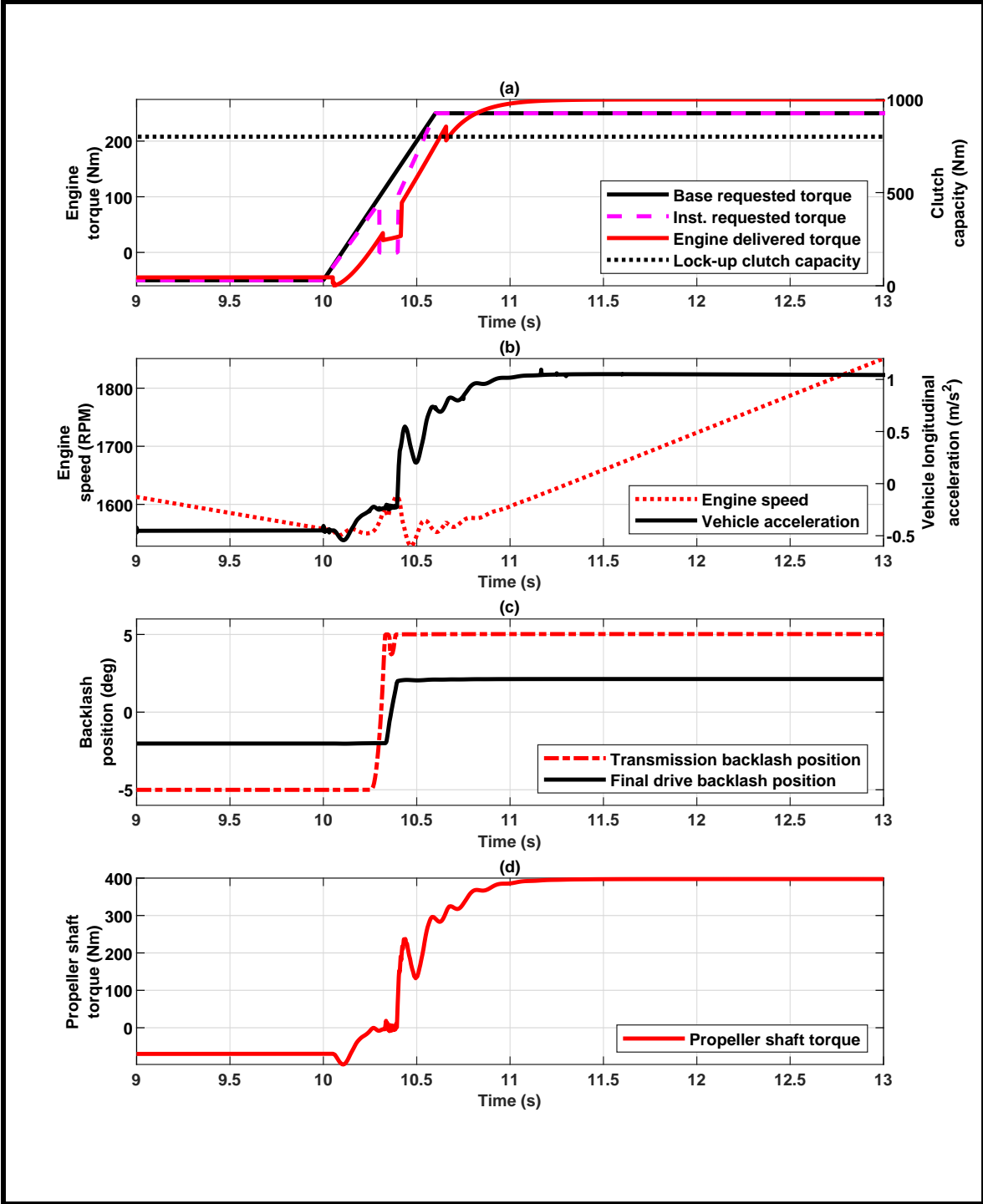


Figure 3.9: Driveline response for tip-in scenario with torque ramp rate varying during backlash traversal. The backlash is initially in negative contact, and TCC is locked.

3.2 Effect of varying backlash size

3.2.1 Variation in transmission backlash

In an automobile, the size of the backlash is dependent on factors such as the construction of the gear element, the wear and tear in the components, etc. Also, the transmission may have different backlash sizes for different gear states. Therefore, it is necessary to understand the effect of variation in backlash size of both the transmission backlash, and the final drive backlash. This would give an idea as to where the lumped backlash element in the reduced-order model (ROM) should be placed.

Transmission backlash varies from gear state to gear state, because of the construction of the gear train in the transmission assembly. The effect of variation in the transmission backlash is comparatively analyzed in Fig. 3.10. A torque input of 500 Nm/s is provided, and the commanded torque goes from -50 Nm to 250 Nm. The backlash is in negative contact initially, and the TCC is locked throughout the simulation. In case A, the transmission backlash size was 10 deg., and in case B, the transmission backlash size was increased to 20 deg. Having a larger backlash size naturally increases the response time of the system, but the difference for these cases is nominal. There is an increase of 8 % in the oscillation amplitude of propeller shaft

torque in Case B, as compared to Case A, and an increase of 9.8 % in the oscillation amplitude of vehicle longitudinal acceleration in Case B, as compared to Case A. This increase can be attributed to the increased travel that the transmission backlash in case B has to traverse, giving it a higher impact velocity.

3.2.2 Variation in final drive backlash

The final drive backlash can vary due to wear and tear of the components, leading to a gradual increase in its size. The effect of variation in the final drive backlash is comparatively analyzed in Fig. 3.11. The simulation conditions were same as in the case of varying the transmission backlash size. The final drive backlash size was 4 deg. in case A, and 8 deg. in case B. From the results in Fig. 3.11, it is clear that an increase in the final drive backlash size makes the response of the system significantly slower compared to an increase in transmission backlash. Also, the amplitude of oscillations of vehicle acceleration increased by an average of 37 % in Case B, compared to Case A. This can be attributed to the fact that the torque flowing through the final drive backlash is higher than the torque flowing through the transmission backlash, as torque multiplication takes place within the system, leading to larger amplitude of oscillation. Also, the rotational speed at the final drive backlash is comparatively less than the speed at the transmission backlash, which explains the delay in system response.

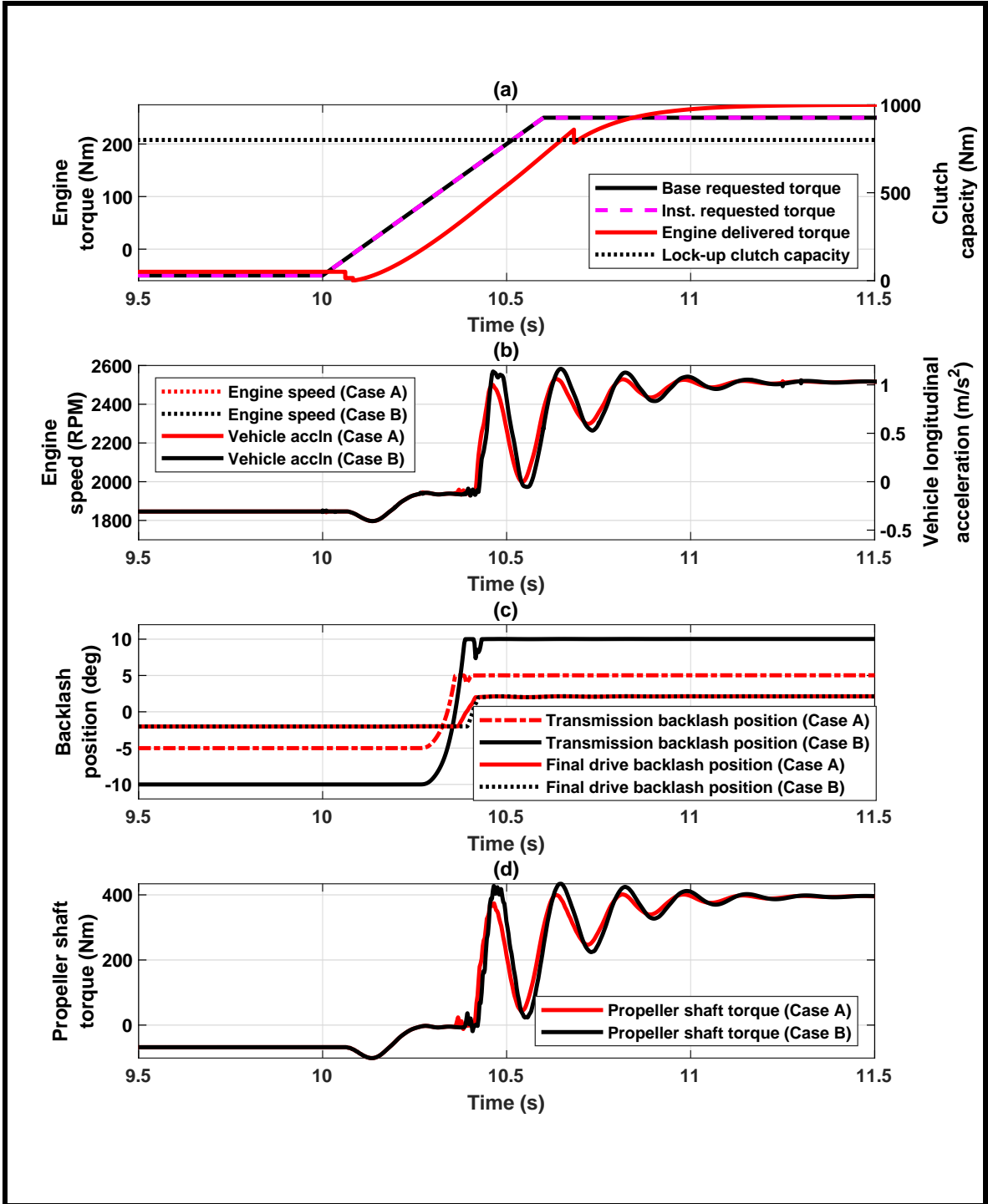


Figure 3.10: Effect of changing the transmission backlash on driveline response. Case A represents condition where transmission backlash is 10 deg. Case B represents condition where transmission backlash is 20 deg.

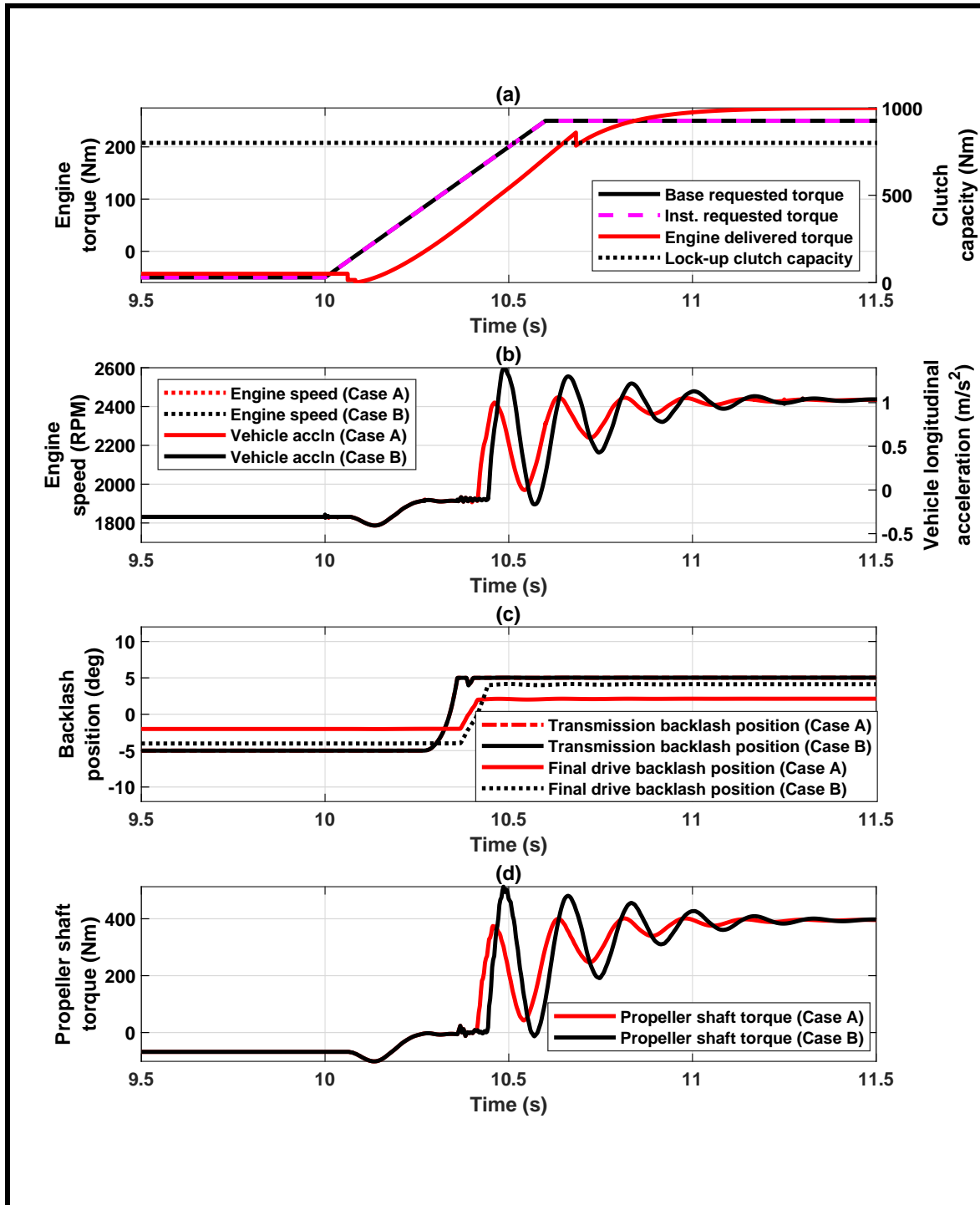


Figure 3.11: Effect of increasing the final drive backlash on driveline response. Case A represents condition where final drive backlash is 4 deg. Case B represents condition where final drive backlash is 8 deg.

3.3 Effect of varying propeller and axle shaft properties

In a rear wheel driven vehicle powertrain, the propeller shaft and axle shafts are prone to the highest elastic deformations, making them the most compliant elements of the driveline. Therefore, the effect of changing the individual properties of these shafts, on the response of the vehicle driveline was studied. Though it is known that a change in stiffness of the shaft would bring about a change in the damping coefficient of the shaft, it was assumed in these analyses that they can be individually modified. The results of this analysis was used to determine the location of the lumped stiffness and damping coefficient elements in the ROM.

3.3.1 Effect of varying propeller shaft stiffness

The natural frequency of a system is based on its stiffness and mass (or inertia in this case). Since the inertia of the propeller shaft is low compared to the other inertial elements in the driveline, the stiffness of the propeller shaft was varied to analyze its impact on the response of the driveline, and a comparative result of this analysis is shown in Fig. 3.12. An input torque is commanded from -50 Nm to 250 Nm, at a ramp rate of 500 Nm/s, the backlash is initially in negative contact, and the TCC is locked.

In case A, the propeller shaft stiffness is decreased by 25% from its final modified value in Chapter 2, and in case B, it is increased by 25%. Since, the frequency is directly proportional to the stiffness, it was observed that increasing the stiffness of the propeller shaft, increased the frequency of oscillations, and vice versa. In case A, the oscillation frequency in propeller shaft torque decreased by 1.97%, and in case B, the oscillation frequency is increased by 1.43%. It was also observed that changing the stiffness, does not have an effect on the amplitude of oscillations.

3.3.2 Effect of varying axle shaft stiffness

Similar analysis was carried out on the axle shaft, by increasing and decreasing its stiffness by 25% of the final value considered for model validation in Chapter 2. The input conditions for the simulations were similar to the previous case of propeller shaft stiffness analysis. The results of this analysis are shown in Fig. 3.13. The driveline response was similar as in the case of modified propeller shaft stiffness, but it was observed that the change in frequency of oscillations, with a change in axle shaft stiffness, was higher. In case A, for a decrease in axle shaft stiffness by 25%, a decrease in oscillation frequency of propeller shaft torque by 4.49% was observed. In case B, for an increase in axle shaft stiffness by 25%, an increase in oscillation frequency of propeller shaft torque by 3.95% was observed. This can be attributed to the increased magnitude of torque flowing through the axle shafts, compared to

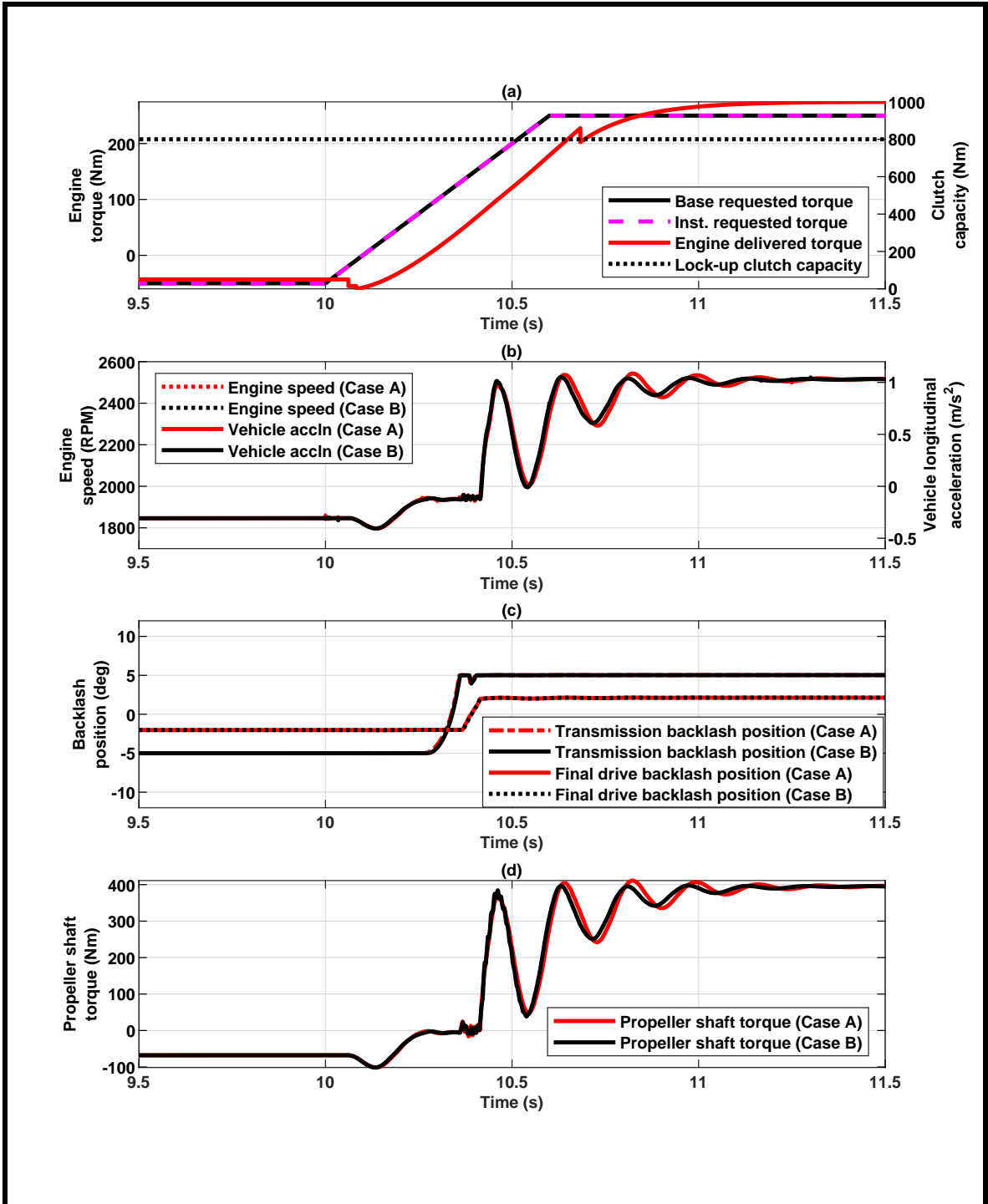


Figure 3.12: Effect of changing propeller shaft stiffness on overall driveline response. Case A represents condition where propeller shaft stiffness is decreased by 25%. Case B represents condition where propeller shaft stiffness is increased by 25%.

the propeller shaft. Even though the axle shafts are stiffer than the propeller shaft, the ratio of difference in torques flowing through them is higher than the ratio of difference in stiffness.

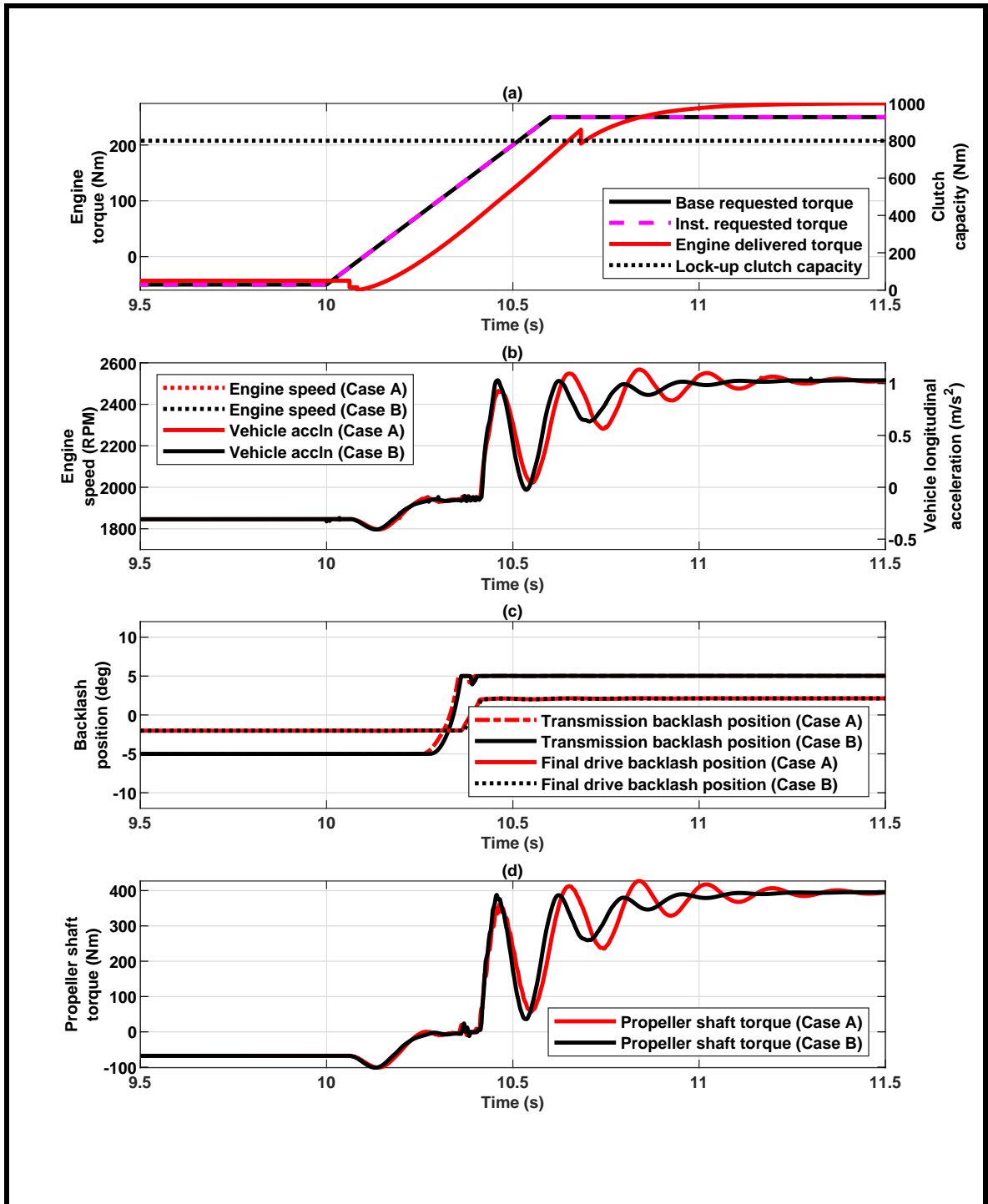


Figure 3.13: Effect of changing axle shaft stiffness on overall driveline response. Case A represents condition where axle shaft stiffness is increased by 25%. Case B represents condition where axle shaft stiffness is decreased by 25%.

3.4 Effect of varying propeller and axle shaft damping coefficient

The damping coefficient in propeller and axle shafts was increased and decreased by 25 %, in a similar fashion as the modifications in the shaft stiffnesses were carried out. However, there is no significant change due to variation in the damping coefficient, due to the minor contribution these shaft elements make in the overall damping of the vehicle. Fig. 3.14 shows the effect of increasing the axle shaft damping coefficient by 25%, in case A, and the effect of decreasing the axle shaft damping coefficient by 25%, in case B. There is no noticeable effect whatsoever, in either the frequency or amplitude of the oscillations.

From the analysis of varying the propeller and axle shaft stiffnesses and damping coefficients, it was inferred that the compliance of the axle shaft had relatively substantial effect on the driveline oscillations. However, since the experimental validation data utilizes a torque meter on the propeller shaft, it was decided to lump all the stiffnesses and damping coefficients in the ROM at the propeller shaft.

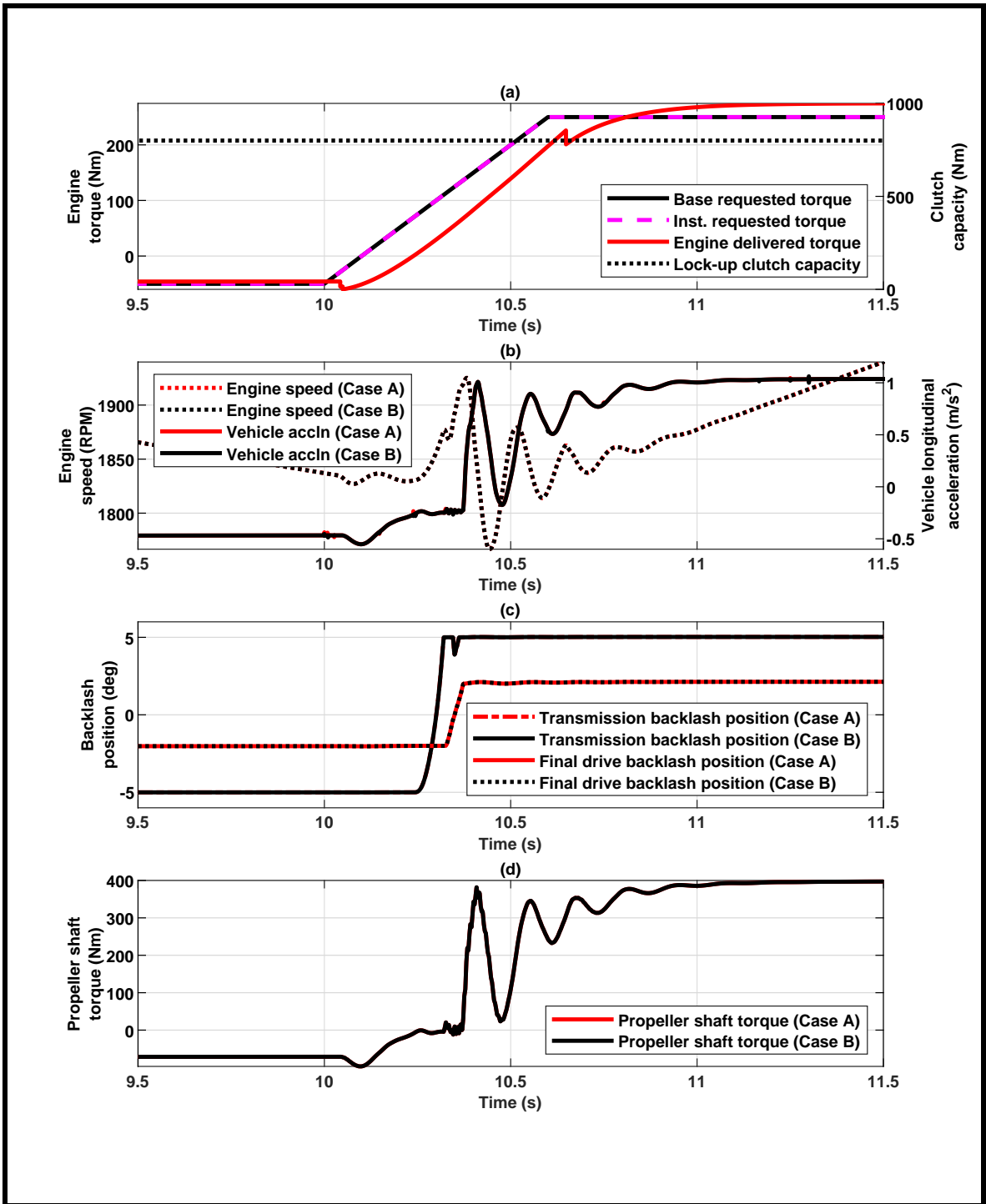


Figure 3.14: Effect of changing axle shaft damping on driveline response. Case A represents condition where axle shaft damping is increased by 25%. Case B represents condition where axle shaft damping is decreased by 25%.

Chapter 4

Reduced-order model (ROM):

Development and validation

4.1 Introduction

Though the full-order model, described in Chapter 2, provides a relatively accurate analysis of the vehicle behavior, using the same model for estimator and control system development would be impractical, due to the computational load a full-order model would place, for real-time control. In addition, the full-order model may require time-varying parameters such as backlash size at the transmission and final drive. These parameters are often not easily available, and can be found using

real-time estimators, if there are enough measurement sensors. If the system does not have enough sensors, meaning that the system is not observable, then the model needs to be simplified. This demands for a low order driveline model for estimation and real-time control. Therefore, a reduced-order model (ROM) is derived from the full-order model, which replicates the response of the full-order model without being computationally expensive.

Most of the previous works in driveline jerk control, discussed in the literature review section, have considered a two mass model approach, where all the inertia components in the driveline are lumped into two mass elements, the backlash is lumped into a single element near the final drive, and the propeller shaft and axle shafts are lumped into a single stiffness and damping element [7], [9], [10], [18], [44]. While this approach is favorable for developing control systems, it may not always replicate the full-order model accurately. This is due to the significant effect multiple backlashes and tire dynamics have, on the response of the driveline.

The effect of tire slip and damping is included in some ROM designs in literature [6], [29], [34]. The benefit of modeling the tire dynamics as an individual element have been shown in [45]. The slippage between the tire and road, at the contact patch, is a reason for significant damping in the vehicle driveline, causing the amplitude of the shuffle oscillations to reduce quickly. This type of ROM, increases the complexity of the control system, but it provides a fairly accurate estimate of the damping effect

of the tire contact patch. This information may be utilized as a feedback by the controller, thereby timing the control strategy to be active only for the required period.

In this chapter, two ROMs are presented, and a comparative validation is performed with respect to the FOM, highlighting the accuracy of each in replicating the behavior of the driveline during tip-in scenarios. The first ROM is a two-mass model, in which the torsional stiffness and damping characteristics of the tire are lumped along with the propeller and axle shafts, and the second ROM is two-mass model, in which the characteristics of the tire are modeled separately.

4.2 ROM with lumped tire parameters

4.2.1 ROM I development

In this case, the model includes two rotational mass elements, each of which incorporates the inertias of the engine, torque converter, transmission, propeller shaft and final drive lumped into one mass element, and the inertias of the axle shaft, tires, and vehicle body lumped into the other mass element respectively. The transmission and final drive backlashes are lumped into one backlash element, at the end of the final drive. The stiffnesses and damping coefficients of the torque converter clutch

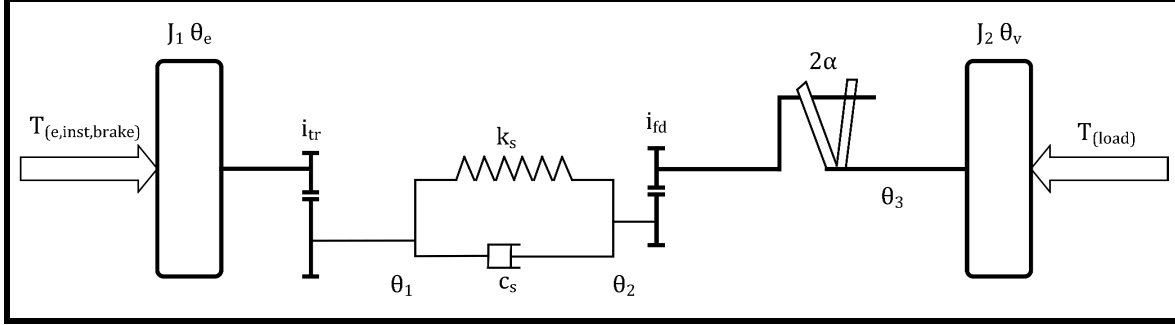


Figure 4.1: ROM with lumped tire parameters.

damper, transmission input shaft, axle shafts and tire, are lumped at the propeller shaft. A schematic of this model is shown in Fig. 4.1.

As used in the model validation and parametric analysis section, $T_{e,inst,brake}$ provides the engine torque trajectory for the ROM. J_1 is the lumped inertia of the engine, the torque converter, the transmission, the propeller shaft, and the final drive. J_2 is the lumped inertia of the axle shafts, the tires including the wheel hub, and the vehicle. i_{tr} and i_{fd} are the gear ratios of the transmission and the final drive, respectively. While k_s is the equivalent torsional stiffness of the torque converter clutch damper, the transmission input shaft, the propeller shaft, the axle shafts, and the tires, c_s is the equivalent damping coefficient of these components. 2α is the lumped backlash size of both the transmission and final drive backlashes. The model equations for the ROM with lumped tire parameters are:

$$J_1 \ddot{\theta}_e = T_{e,inst,brake} + \frac{T_s}{i_{tr}} \quad (4.1)$$

$$J_2\ddot{\theta}_v = T_s i_{fd} - T_{load} \quad (4.2)$$

$$T_s = k_s(\theta_1 - \theta_2) + c_s(\dot{\theta}_1 + \dot{\theta}_2) \quad (4.3)$$

4.2.2 ROM I validation

The developed ROM with lumped tire parameters was validated against the full-order model that was developed in Chapter 2. For validation, same crankshaft torque trajectory was provided as an input to both the FOM and the ROM, and the response of the driveline in both the models was observed by comparing output engine speed, vehicle speed, vehicle acceleration, and driveshaft torque. Fig. 4.2 shows the observed response for a tip-in scenario. The torque trajectory mimics a coasting scenario before the tip-in event. The response during the coasting scenario in ROM matches exactly with the response of the FOM. However, at tip-in, it was observed that there is significant variation in the amplitude and frequency of oscillations in the ROM. Also, the response seems to indicate that the overall damping of the ROM is significantly lower than the FOM. Activity analysis was carried out on the FOM, using in-built tools in Amesim. It was observed that after rolling resistance, and aerodynamic resistance components of the vehicle model, tire damping coefficient had the most

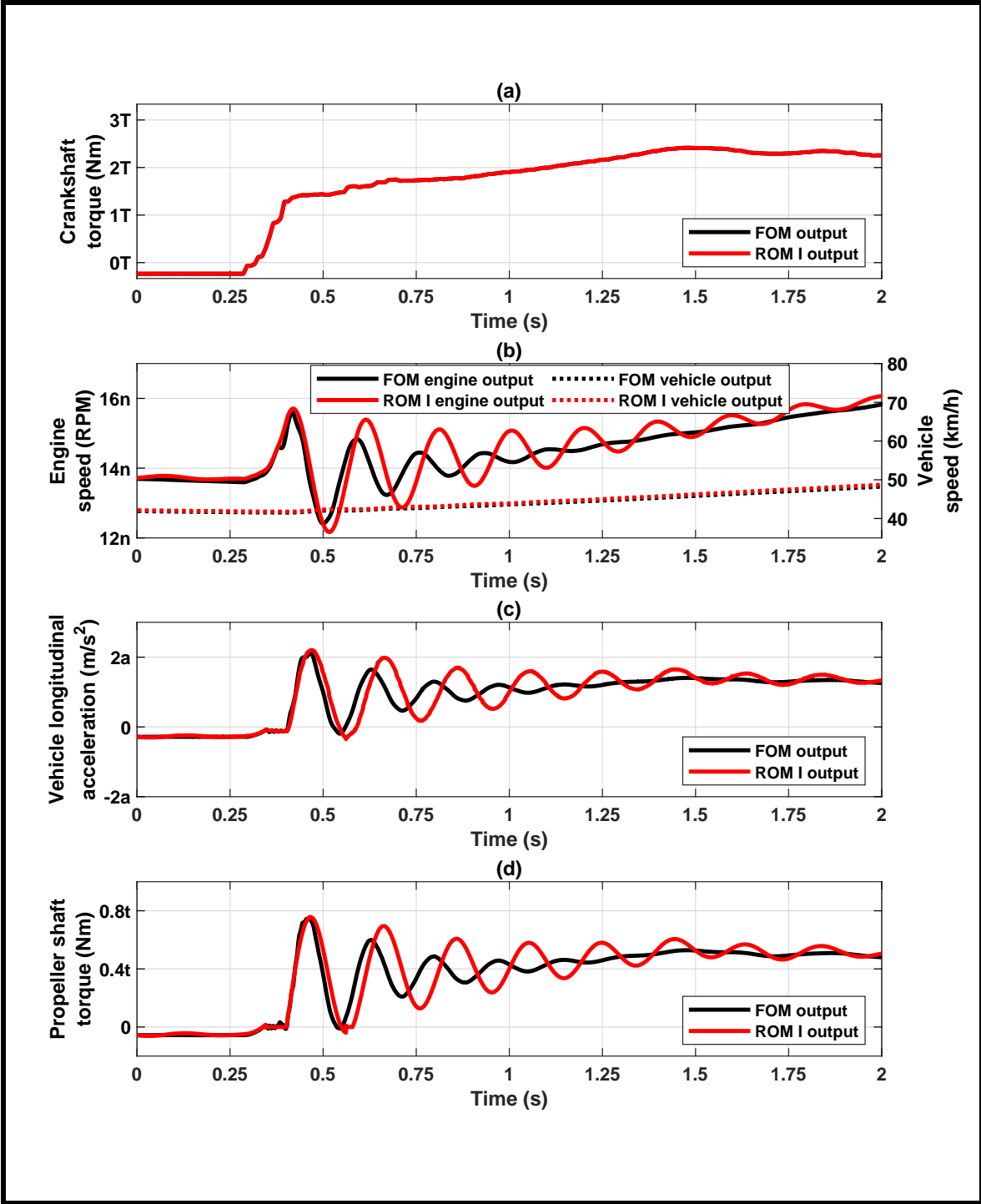


Figure 4.2: Comparison of ROM I with lumped tire parameters' driveline response with FOM, for a tip-in scenario.

substantial activity in the model. Therefore, the next section deals with including the tire parameters separately in the ROM.

4.3 ROM with separate tire parameters

4.3.1 ROM II development

Including the tire damping in the equivalent damping coefficient c_s , as seen in the previous sub-section, may be beneficial from a controls perspective. It leads to the formulation of fewer state variables, thereby reducing the complexity of the controller. However, it does not replicate the dynamics of the driveline that is observed in the full-order model, because the effect of tire slip, which is represented by the tire model using torsional stiffness and damping coefficient, is significant in reducing the oscillations observed in the driveline. Therefore, in this section, another ROM is developed with the tire parameters represented separately, as shown in Fig. 4.3.

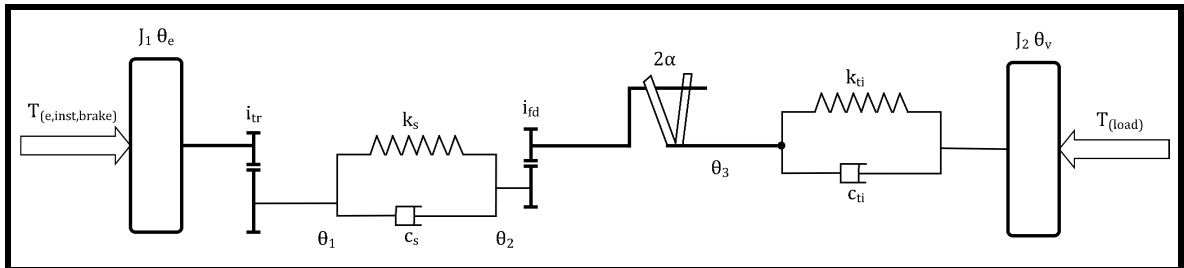


Figure 4.3: ROM with separate tire parameters.

The inputs to the model, and outputs from the model remain similar to the case with lumped tire parameters. The model equations for this ROM are:

$$J_1 \ddot{\theta}_e = T_{e,inst,brake} + \frac{T_s}{i_{tr}} \quad (4.4)$$

$$J_2 \ddot{\theta}_v = T_v - T_{load} \quad (4.5)$$

$$T_v = T_s i_{fd} \quad (4.6)$$

$$T_s = k_s(\theta_1 - \theta_2) + c_s(\dot{\theta}_1 + \dot{\theta}_2) \quad (4.7)$$

$$T_v = k_{ti}(\theta_v - \theta_3) + c_{ti}(\dot{\theta}_v + \dot{\theta}_3) \quad (4.8)$$

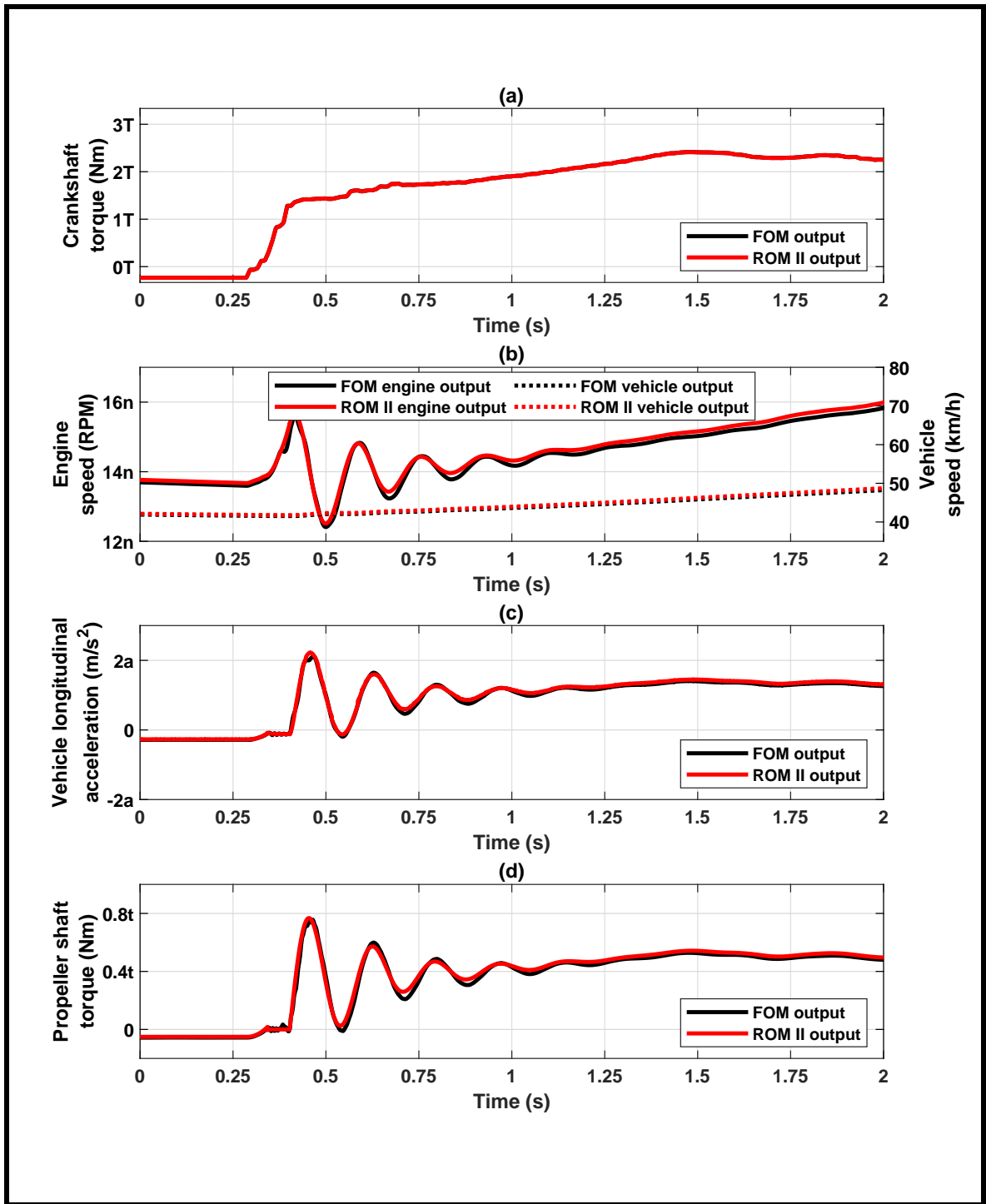


Figure 4.4: Comparison of ROM II with separate tire parameters' driveline response with FOM, for a tip-in scenario.

4.3.2 ROM II validation

The second ROM was also validated against the response of the FOM, for a tip-in scenario in 5th gear, and the corresponding engine speed, vehicle speed, vehicle longitudinal acceleration, and propeller shaft torque were plotted. Fig. 4.4 clearly shows that this ROM is able to match all the parameters of interest, from the FOM, including the amplitude and frequency of shuffle oscillations.

Similar analysis was carried out for a tip-in scenario in the 3rd gear, and the comparison between the FOM and ROM for this case is shown in Fig. 4.5. The response of the ROM shows a good match in any gear state of the transmission.

4.3.3 Effect of lumping backlashes in the ROM

For both the ROMs discussed in sections 4.2 and 4.3, transmission and final drive backlash have been lumped together into a single element, taken at the end of the final drive. Fig. 4.6 shows a comparative analysis of the effect of lumping the backlash at the final drive on the response of the driveline, during a tip-in scenario, using ROM with separate tire parameters. Lumping the backlash elements, requires the size of the backlash to be translated based on the position it is being placed at. For example, the size of the transmission backlash in the split backlash FOM is assumed to be 10

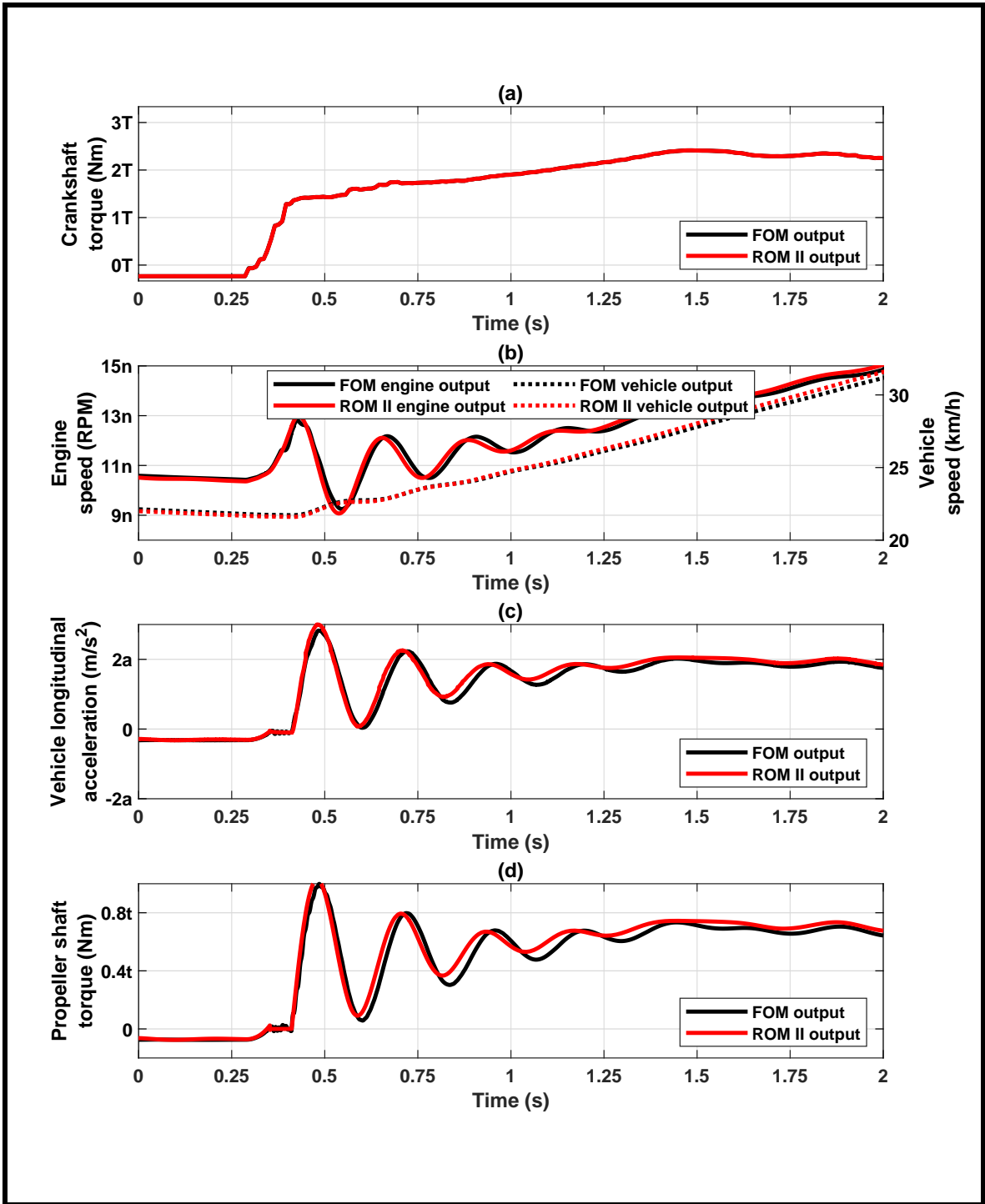


Figure 4.5: Comparison of ROM with separate tire parameters' driveline response with FOM, in 3rd gear, for a tip-in scenario.

deg., and the size of the final drive backlash is assumed to be 4 deg. But when these backlashes are lumped at the final drive, the transmission backlash has to be adjusted for the gear ratios of the transmission, and the final drive, making the lumped element to have a backlash size of 6 deg. From Fig. 4.6, it is clear that even after lumping the backlashes at a single element, the ROM is able to capture the frequency and amplitude of the shuffle oscillations to a satisfactory level of accuracy. As evident in Fig. 4.6 (b), the rebound in the transmission backlash, after the clunk impact, observed in the FOM, was not reproduced in the ROM with the lumped backlash. This has to be taken care of, while developing the controller, so that rebounds in the backlash elements do not take place.

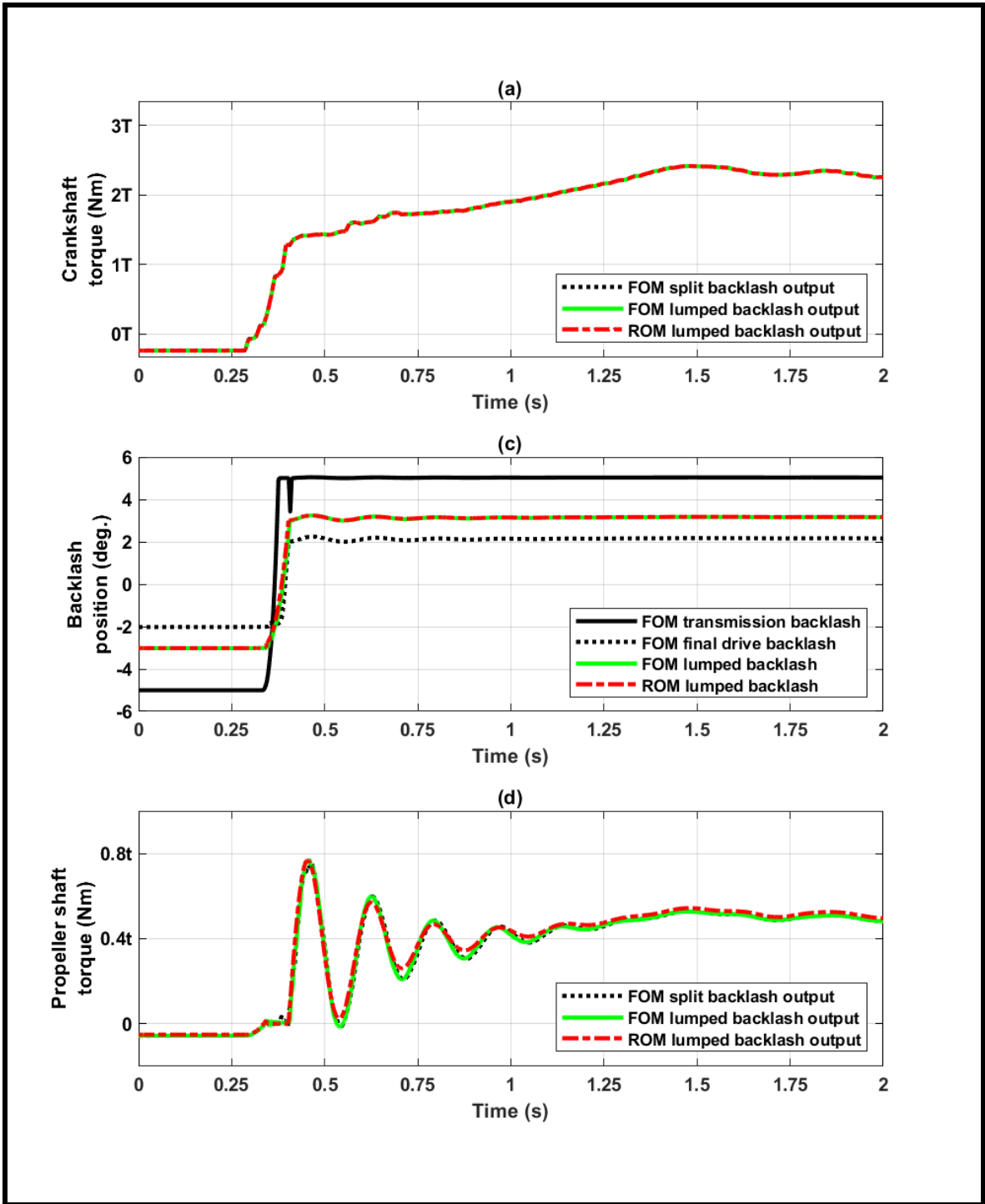


Figure 4.6: Comparison of lumped and split backlash models in full-order and reduced-order models.

4.4 Estimation of model parameters for ROM

For both the ROM's described in Section 4.2 and 4.3, model parameters like inertias, stiffnesses and damping coefficients for lumped systems had to be estimated using available data for the individual components. A brief overview of the methodology used, for finding the lumped parameters is described in this section.

The engine, torque converter, transmission, propeller shaft, final drive, and the differential can be assumed to be in a series connection with one another. After the differential, the axle shafts on the left side, and right side of the driveline, and the tires on the left side, and right side of the driveline, can be assumed to be parallel to their respective element. After lumping the left and right side axle shaft, and tire, the lumped elements are assumed to be in series again.

Irrespective of the assumed connections, the equivalent moment of inertia is obtained by simply adding the inertias together. If there is a gear ratio (e.g. transmission gear ratio, final drive gear ratio) between two inertias that need to be lumped, then the square of the gear ratio was considered while calculating the lumped inertia. As an example, the procedure for lumping moment of inertias of the propeller shaft, axle shafts, and the tires is shown:

$$J_{axle\ shafts} = J_{left\ axle} + J_{right\ axle} \quad (4.9)$$

$$J_{lumped\ axle\ and\ tire} = J_{axle\ shafts} + J_{tires} \quad (4.10)$$

$$J_{lumped\ propeller,\ axle\ and\ tire} = J_{propeller} + \frac{J_{lumped\ axle\ and\ tire}}{i_{fd}^2} \quad (4.11)$$

The stiffness and damping coefficients are lumped like a spring element. The parameters of connections in parallel (e.g., the axle shafts on left and right side) are lumped directly, whereas parameters of connections in series (e.g., lumped axle shafts and lumped tires) are lumped by adding their inverses. The square of the gear ratio was considered for elements that were lumped across the transmission or the final drive. As an example, the procedure for lumping the stiffnesses of the propeller shaft, axle shafts, and the tires is shown:

$$k_{axle\ shafts} = k_{left\ axle} + k_{right\ axle} \quad (4.12)$$

$$k_{lumped\ axle\ and\ tire} = \frac{k_{axle\ shafts} \times k_{tires}}{k_{axle\ shafts} + k_{tires}} \quad (4.13)$$

$$k_{lumped\ propeller,\ axle\ and\ tire} = \frac{k_{propeller} \times \frac{k_{lumped\ axle\ and\ tire}}{i_{fd}^2}}{k_{propeller} + \frac{k_{lumped\ axle\ and\ tire}}{i_{fd}^2}} \quad (4.14)$$

For lumping the damping coefficients, the same procedure used in Eq. 4.12, 4.13 and 4.14 was used.

4.5 Application of ROM for controls

The ROM with separate tire parameters will later be used for developing an estimator and a controller for reducing the shuffle oscillations. The estimator will help in estimating backlash states in the driveline, whereas the controller will shape the torque trajectory to reduce impact at gear faces after backlash traversal.

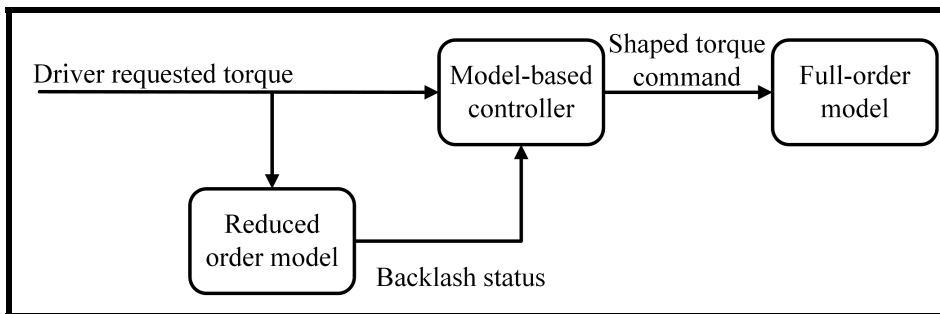


Figure 4.7: Schematic showing a simple control system, utilizing the output of the ROM, for controlling the torque delivered to the plant(Full-order model).

A simple controls application of the ROM in reducing the shuffle oscillations is demonstrated here. The schematic of this simple control system is shown in Fig. 4.7. The torque requested by the driver, through the accelerator pedal, is received as a command signal by the controller, as well as the ROM. Based on the driver requested torque, the ROM estimates the position of the backlash continuously. When the backlash is in either negative contact, or positive contact, the controller does not modify the torque requested by the driver. As soon as the backlash traversal starts to take place in the ROM, the status of the backlash becomes inlash, and a signal is sent to the controller. The controller, then uses a multiplication factor to reduce the ramp rate of driver requested torque, which is sent to the virtual plant, represented by the full-order model for showing this result. To avoid the torque request from increasing rapidly after backlash traversal, the multiplication factor is integrated with time, which leads to a smooth increase in torque. This approach is used based on the effect observed in Chapter 3, of reduced driveline oscillation amplitude, with a reduction in ramp rate of torque input, and learnings from [46]. The mathematical equation for the approach used is shown below:

$$\frac{dT_{shaped}(t)}{dt} = T_{driver}(t) \int_{0.05}^1 F(t)dt \quad (4.15)$$

where, T_{shaped} is the shaped engine torque, T_{driver} is the driver requested torque, and F is the multiplication factor that is used for reducing the ramp rate of the delivered

torque.

Fig. 4.8 shows a comparative response of the driveline oscillations in the virtual plant for two cases. In case A, torque output from the engine is obtained from the driver requested torque, and therefore, it is not externally shaped by the controller. The trajectory of torque output observed in case A, is due to the air charge dynamics discussed in Chapter 2. Consequently, the amplitude of shuffle oscillations is higher, as seen in propeller shaft torque and vehicle longitudinal acceleration. In case B, the torque output from the engine is shaped, based on the input received from the ROM, about the status of the backlash. Since, the torque shaping reduces the ramp rate of the engine output torque, a 53% reduction in amplitude of oscillations of vehicle acceleration is observed. Moreover, the backlash traversal time also increases in both the transmission and final drive backlash. This demonstrates the ability of the ROM for controls applications.

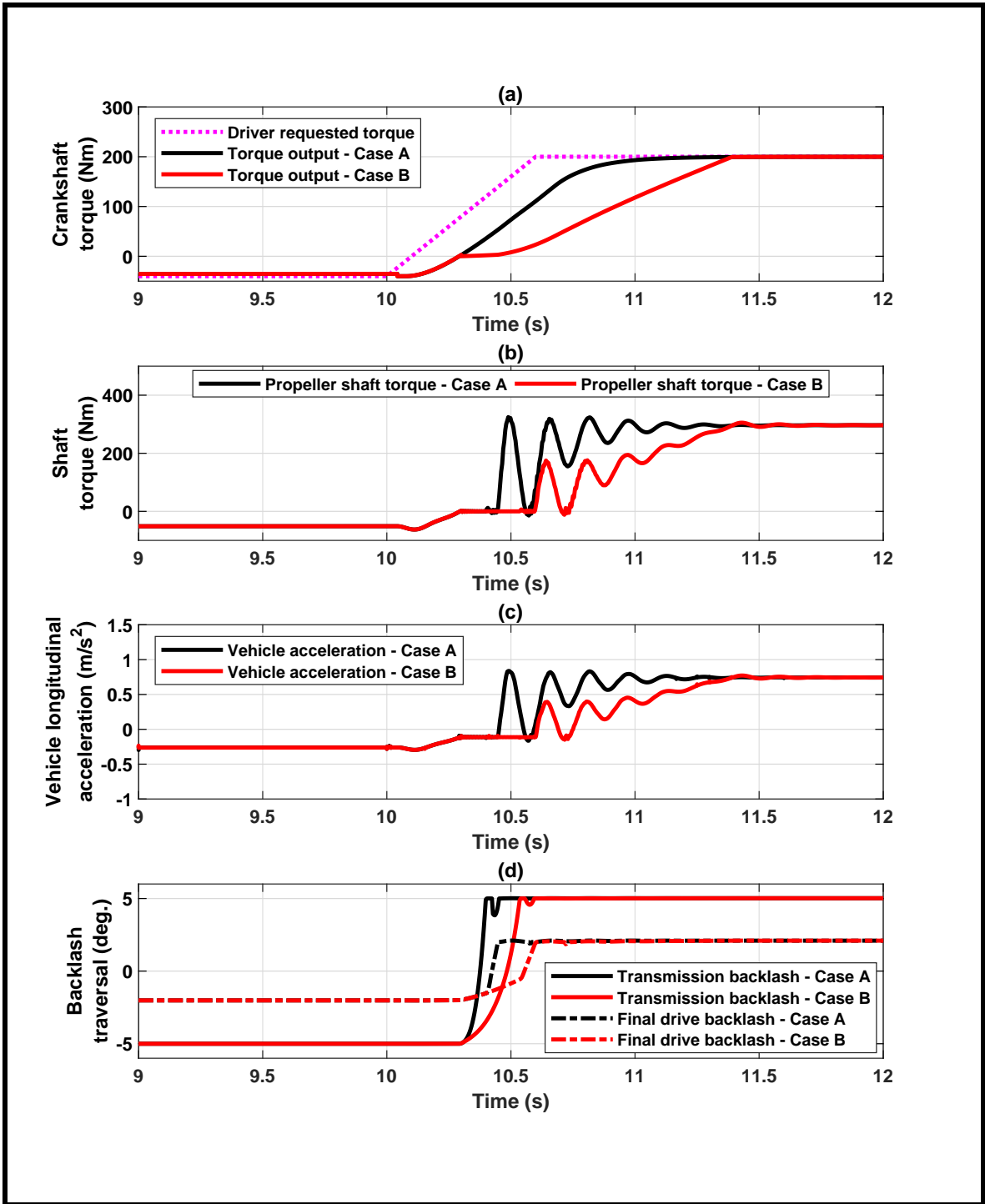


Figure 4.8: Comparison of driveline response for two cases of torque input. Case A: Torque input without shaping. Case B: Torque input with shaping.

Chapter 5

Conclusion and Future work

5.1 Conclusions

† A full-order model of a current generation vehicle based on an SUV/pick-up truck platform was developed, using an Amesim[®] - Simulink[®] interface. Model parameters for the powertrain were provided by the sponsoring organization. Literature review was carried out in modeling and controls domain for simulating and reducing driveline oscillations during tip-in and tip-out scenarios in automobiles.

† The actual torque delivered by an engine is bound to have an error, compared to the ECU estimated values, due to the reasons discussed in Chapter 2. It

is essential to take this error into account since the ramp rate of the delivered torque, directly affects the magnitude of driveline oscillations.

† The developed model was validated for three different use modes: (i) locked torque converter clutch, (ii) open torque converter clutch and (iii) slipping torque converter clutch. Experimental data was collected and provided by the sponsoring organization, for tip-in and tip-out scenarios. Some of the observations made during model validation were:

- For the case of a locked TCC, the parameters of the developed full-order model had to be modified, in order to match the behavior of the driveline, during tip-in condition, as observed in the experimental data. The stiffness of the propeller and axle shafts had to be reduced by 25%, and the inertia of the engine, torque converter, and final node of the transmission had to be increased by 25%, to account for the components that could not be modeled due to lack of parametric data, but which had an impact on the oscillation frequency.
- For the scenarios where the flow of torque in a torque converter, takes place in either the fluid path or in a combination of fluid and lock-up clutch path, a simple look-up table for capacity factor and torque ratio, as a function of speed ratio, is not enough to capture the dynamics inside the torque converter during transient events like tip-in. A detailed model which takes into account the geometrical parameters like number of blades,

blade angles etc., and fluid flow properties, is required for replicating the dynamics inside the torque converter accurately during transient scenarios.

† Parametric analysis was performed on the full-order model, to analyze the effect of elements such as backlashes, shaft stiffnesses etc., on driveline oscillations. The results are summarized below:

- The ramp rate of the provided torque input is a prime factor that affects the amplitude of the shuffle oscillations that are induced due to both backlash and shaft flexibility. A higher ramp rate leads to a higher amplitude of oscillation and vice-versa.
- The effect of variation in the final drive backlash size is more significant on the shuffle oscillation amplitude, compared to a similar variation in the transmission backlash.
- The effect of variation of axle shaft stiffness is more significant on the shuffle frequency, compared to a similar variation in the propeller shaft. There is no influence on the amplitude of shuffle oscillations in either case.
- The effect of variation in damping coefficient of both propeller and axle shafts is negligible on the frequency and amplitude of shuffle oscillations, which is due to their low contribution, in the overall damping of the system.

† The full-order model was simplified into a reduced-order model, to be used in controls work in the future. Two reduced-order model designs were investigated,

based on the how the tire parameters were considered in the model. Some of the findings are:

- It is necessary to include the tire parameters as a separate entity in the model, for retaining most of the fidelity of the full-order model. Lumping the tire parameters within the model might still provide some insight into the behavior of the actual vehicle’s driveline, but it may not be useful for developing precise controls.
- Lumping the backlashes at the transmission and the final drive into a single element might make it easier to develop and implement an effective estimator and controller in future, but it might not be able to accurately replicate driveline scenarios where the driver requests a small amount of torque for a short period of time, causing the transmission backlash to traverse, but not the final drive backlash. It is important to take that into account, so that the developed control system can take the required steps to mitigate such driveline clunk scenarios.
- Implementing the developed ROM in a simple control system, with the full-order model as a virtual plant, showed the application capability of the ROM. Using a simple, factor-based torque shaping technique, driveline oscillation amplitude was successfully reduced by 53.44 % in vehicle longitudinal acceleration.

5.2 Future work

While this work was based on the effect of backlash traversal and shaft flexibility for inducing shuffle oscillations, the model can be improved for studying the effect of road disturbances on the driveline. Similarly, the tire model can be modified for studying the effect of sudden variations in road friction on the driveline. Considering the main objective of the current thesis, the future work includes:

- † Verifying the validity of some of the assumed model parameters to further improve the accuracy of the full-order and reduced-order models. This will be accomplished through an ongoing Ph.D. thesis at Michigan Tech.
- † Development and validation of a dynamic torque converter model, such that transient events can be accurately replicated, during the slipping and open modes of the torque converter lock-up clutch.
- † Development and validation of state estimators, based on Kalman filtering techniques, such that backlash state and position can be estimated in real-time, without having to rely on alternative algorithms to provide an approximation.
- † Sensitivity analysis of vehicle parameters that can vary due to the availability of different model variants of a vehicle, e.g., mass of the vehicle, overall inertia of the vehicle, tire properties of the vehicle etc., on driveline oscillations.

Parameters having significant impact will be included with parameters to be estimated using state estimators.

† Development and validation of a robust model-based anti-jerk controller, that can utilize the outputs from the state estimator, and shape the torque to be delivered in such a way that the impact velocity at the end of backlash traversal is significantly reduced, and therefore the NHV characteristics of the vehicle are improved. The controller will need to be robust to changes in vehicle parameters, without requiring additional calibration, thereby reducing current calibration time and effort.

† Analysis of effect of tire slip on driveline oscillations, and possible integration of strategies for both slip-induced and backlash-induced jerk control.

† Implementation of the estimator and the controller on a test rig, which is currently under development at Michigan Tech, to study their effectiveness during actual drive scenarios.

References

- [1] Cain, T., 2017. U.S. auto sales in calendar year 2016, by vehicle category. <http://www.goodcarbadcar.net/2017/01/usa-auto-sales-by-vehicle-type-2016-char/>. Accessed on 8 January 2018, [Online].

- [2] PwC, 2017. Projected vehicle sales in China, the U.S. and the EU between 2017 and 2030, by propulsion technology (in million vehicles). <https://www.statista.com/statistics/264754/worldwide-vehicle-sales-by-propulsion-technology-2025/>. Accessed on 8 January 2018, [Online].

- [3] &, S., and PwC, 2017. Projected sales of autonomous vehicles, classified by level of automation. <https://www.strategyand.pwc.com/media/file/2017-Strategyand-Digital-Auto-Report.pdf>. Accessed on 8 January 2018, [Online].

- [4] GearHeads, 2010. Backlash. Used under Creative Commons Attribution-Share Alike 3.0 Unported license.
- [5] Papageorgiou, D., Blanke, M., Niemann, H. H., and Richter, J. H., 2017. “Backlash estimation for industrial drive-train systems”. *IFAC-PapersOnLine*, **50**(1), pp. 3281–3286.
- [6] Baumann, J., Torkzadeh, D. D., Ramstein, A., Kiencke, U., and Schlegl, T., 2006. “Model-based predictive anti-jerk control”. *Control Engineering Practice*, **14**(3), pp. 259–266.
- [7] Grotjahn, M., Quernheim, L., and Zemke, S., 2006. “Modelling and identification of car driveline dynamics for anti-jerk controller design”. In 2006 IEEE International Conference on Mechatronics. Budapest, Hungary.
- [8] Lagerberg, A., and Egardt, B., 2002. “Evaluation of control strategies for automotive powertrains with backlash”. In 6th International Symposium on Advanced Vehicle Control. Hiroshima, Japan.
- [9] Lagerberg, A., and Egardt, B., 2007. “Backlash estimation with application to automotive powertrains”. *IEEE Transactions on Control Systems Technology*, **15**(3), pp. 483–493.
- [10] Lagerberg, A., and Egardt, B., 2005. “Model predictive control of automotive powertrains with backlash”. In IFAC Proceedings Volumes, Vol. **38**, pp. 1–6.

- [11] Templin, P., and Egardt, B., 2011. “A powertrain LQR-torque compensator with backlash handling”. *Oil & Gas Science and Technology—Revue d'IFP Energies nouvelles*, **66**(4), pp. 645–654.
- [12] Baumann, J., Swarnakar, A., Kiencke, U., and Schlegl, T., 2005. “A robust controller design for anti-jerking”. SAE Technical Paper 2005-01-0041.
- [13] Siemens Industry Software NV, 2017. *LMS Amehelp - User Manual for LMS.Amesim 15.2*. LMS.Amesim, Plano, TX.
- [14] Goleski, G. D., and Thomas, S. G., 2014. Paths for supplying fluid to clutches of an automatic transmission, Sept. 16. US Patent 8,834,310.
- [15] Oman, C. M., 1990. “Motion sickness: a synthesis and evaluation of the sensory conflict theory”. *Canadian journal of physiology and pharmacology*, **68**(2), pp. 294–303.
- [16] Griffin, M. J., 2012. *Handbook of human vibration*. Academic press.
- [17] Crowther, A. R., Zhang, N., and Singh, R., 2005. “Development of a clunk simulation model for a rear wheel drive vehicle with automatic transmission”. SAE Technical Paper 2005-01-2292.
- [18] Lagerberg, A., and Egardt, B., 2003. “Estimation of backlash with application to automotive powertrains”. In Proceedings of 42nd IEEE International Conference on Decision and Control. Maui, HI, USA.

- [19] Cho, D., and Hedrick, J. K., 1989. “Automotive powertrain modeling for control”. *Journal of dynamic systems, measurement, and control*, **111**(4), pp. 568–576.
- [20] Hrovat, D., and Tobler, W., 1991. “Bond graph modeling of automotive power trains”. *Journal of the Franklin Institute*, **328**(5-6), pp. 623–662.
- [21] Pettersson, M., 1997. *Driveline modeling and control*. Department of Electrical Engineering, Linköping University.
- [22] Hayat, O., Lebrun, M., and Domingues, E., 2003. “Powertrain driveability evaluation: analysis and simplification of dynamic models”. SAE Technical paper 2003-01-1328.
- [23] Karlsson, J., and Fredriksson, J., 1999. “Cylinder-by-cylinder engine models vs mean value engine models for use in powertrain control applications”. SAE Technical Paper 1999-01-0906.
- [24] Sorniotti, A., 2008. “Driveline modeling, experimental validation and evaluation of the influence of the different parameters on the overall system dynamics”. SAE Technical Paper 2008-01-0632.
- [25] Bartram, M., Mavros, G., and Biggs, S., 2010. “A study on the effect of road friction on driveline vibrations”. *Proceedings of the Institution of Mechanical Engineers, Part K: Journal of Multi-body Dynamics*, **224**(4), pp. 321–340.

- [26] Dridi, S., Salem, I. B., and El Amraoui, L., 2017. “Dynamic modeling of non-linear longitudinal automotive system using graphically based techniques”. In Information and Digital Technologies (IDT), 2017 International Conference on, IEEE, pp. 349–354.
- [27] Sun, G., Wei, M., Shao, J., and Pei, M., 2007. “Automotive powertrain modeling and simulation based on amesim”. SAE Technical Paper 2007-01-3464.
- [28] Lagerberg, A., 2001. “A literature survey on control of automotive powertrains with backlash”. *Technical report no R013/2001; Department of Signals and Systems, Chalmers University of Technology, Gothenburg, Sweden*, pp. 1–15.
- [29] Templin, P., 2008. “Simultaneous estimation of driveline dynamics and backlash size for control design”. In IEEE International conference on Control Applications. San Antonio, Texas, USA.
- [30] Templin, P., and Egardt, B., 2009. “An LQR torque compensator for driveline oscillation damping”. In IEEE Conference on Control Applications. St. Petersburg, Russia.
- [31] Karikomi, T., Itou, K., Okubo, T., and Fujimoto, S., 2006. “Development of the shaking vibration control for electric vehicles”. In 2006 SICE-ICASE International Joint Conference. Busan, Korea.
- [32] Kawamura, H., Ito, K., Karikomi, T., and Kume, T., 2011. “Highly-responsive

- acceleration control for the nissan leaf electric vehicle”. pp. 1–6. SAE Technical Paper 2011-01-0397.
- [33] Mohit Batra, Anson Maitland, J. M., and Azad, N. L., 2018. “Non-linear model predictive anti-jerk cruise control for electric vehicles with slip-based constraints”. In American Control Conference. Milwaukee, USA.
- [34] Canova, M., Rostiti, C., D’Avico, L., Stockar, S., Chen, G., Prucka, M., and Dourra, H., 2017. “Model-based wheel torque and backlash estimation for drivability control”. *SAE International Journal of Engines*, **10**, pp. 1318–1327.
- [35] Formentini, A., Oliveri, A., Marchesoni, M., and Storace, M., 2017. “A switched predictive controller for an electrical powertrain system with backlash”. *IEEE Transactions on Power Electronics*, **32**(5), pp. 4036–4047.
- [36] Di Cairano, S., Doering, J., Kolmanovsky, I. V., and Hrovat, D., 2014. “Model predictive control of engine speed during vehicle deceleration”. *IEEE Transactions on Control Systems Technology*, **22**(6), pp. 2205–2217.
- [37] Wang, J., Michelini, J., Wang, Y., and Shelby, M. H., 2017. Time to torque optimization by evolutionary computation methods. Tech. rep., SAE Technical Paper 2017-01-1629.
- [38] Alkeilani, A., Wang, L. Y., and Ying, H., 2016. “Direct torque feedback for accurate engine torque delivery and improved powertrain performance”. *Journal of Engineering for Gas Turbines and Power*, **138**(11), p. 112801.

- [39] Schwab, M., 1990. “Electronically-controlled transmission systems-current position and future developments”. In *Vehicle Electronics in the 90’s: Proceedings of the International Congress on Transportation Electronics, 1990, IEEE*, pp. 335–342.
- [40] Pacejka, H. B., and Bakker, E., 1992. “The magic formula tire model”. *Vehicle System Dynamics*, **21**(sup001), pp. 1–18.
- [41] Mozharovskii, V. V., Shil’ko, S. V., Anfinogenov, S. B., and Khot’ko, A. V., 2007. “Determination of resistance to rolling of tires in dependence on operating conditions. part 1. method of multifactorial experiment”. *Journal of Friction and Wear*, **28**(2), Apr, pp. 154–161.
- [42] Pscoa, J., Brojo, F., Charrua Santos, F., and Fael, P., 2012. “An innovative experimental on-road testing method and its demonstration on a prototype vehicle”.
- [43] Toolbox, E., 2008. Rolling resistance. https://www.engineeringtoolbox.com/rolling-friction-resistance-d_1303.html. (Accessed on 16 July, 2018). [Online].
- [44] Lagerberg, A., 2004. “Control and estimation of automotive powertrains with backlash”. PhD thesis, Chalmers University of Technology, Sweden.
- [45] Hao, D., Zhao, C., and Huang, Y., 2018. “A reduced-order model for active

suppression control of vehicle longitudinal low-frequency vibration”. *Shock and Vibration*, **2018**.

- [46] Krenz, R., 1985. “Vehicle response to throttle tip-in/tip-out”. pp. 45–52. SAE Technical Paper 850967.

Appendix A

Amesim-Simulink Interface

For setting up the interface between Amesim and Simulink, specific versions of their packages had to be used with Visual C++ compiler. At the time of writing this thesis, the following versions of the softwares were being used:

LMS Amesim:

Version → 15.2 (63896-58725) 2017

Platform → Windows 7/8/10

Library → Standard Amesim library

MATLAB/Simulink:

Version → MATLAB - 9.4.0.885841 (R2018a) Update 3

→ Simulink - 9.1 (R2018a)

Microsoft Visual Studio:

Version → 12.0.21005.1 REL

Microsoft Visual C++:

Version → 2013

Code to load Amesim libraries in Simulink

```
>addpath(fullfile(getenv('AME'),'scripting','matlab','amesim'));
```

```
>ameml
```

Appendix B

Engine Torque Uncertainty

After reviewing the results of the torque measurements, that were carried out by the sponsoring organization, for various tip-in and tip-out conditions, it was found that using a fixed transfer function for representing the dynamics of air flow into the cylinders is not adequate. Variations in the experimentally observed torque trajectories were significant, and to simplify replication of those variations, torque calculations by the engine model in this work include a term T_{unc} .

Four different scenarios are shown here, which include one tip-in scenario with relatively small driver torque request, one tip-in scenario with relatively large driver torque request, one tip-in scenario with maximum driver torque request, and one tip-out scenario. The transfer function used in each scenario is mentioned on the plots.

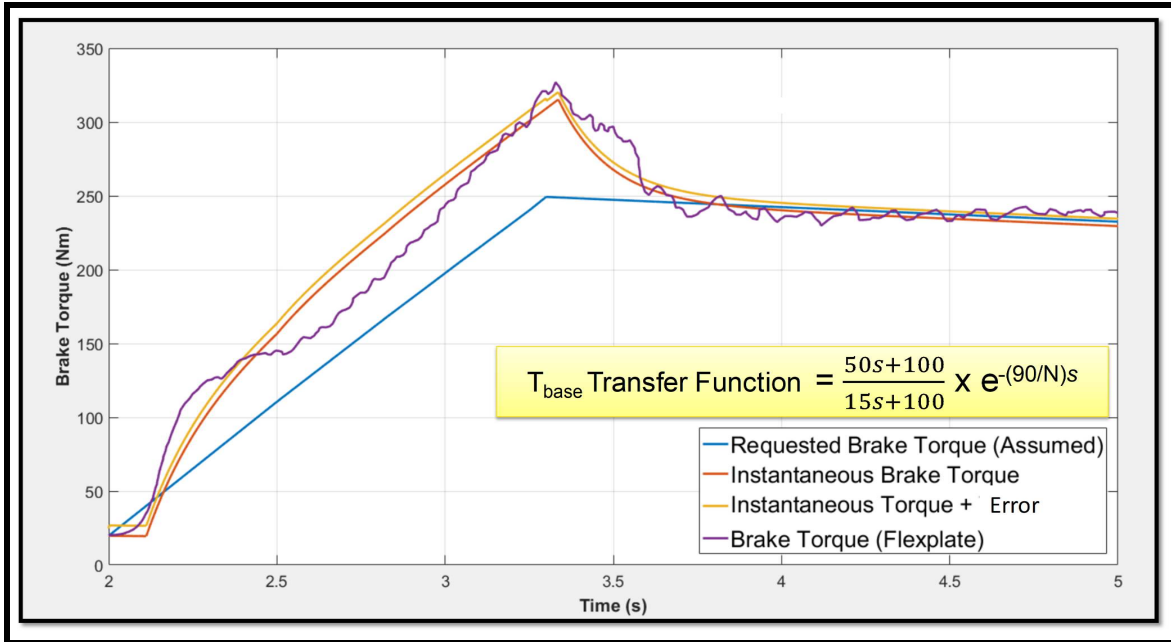


Figure B.1: Observed engine torque response for a throttle input of 0 → 100%

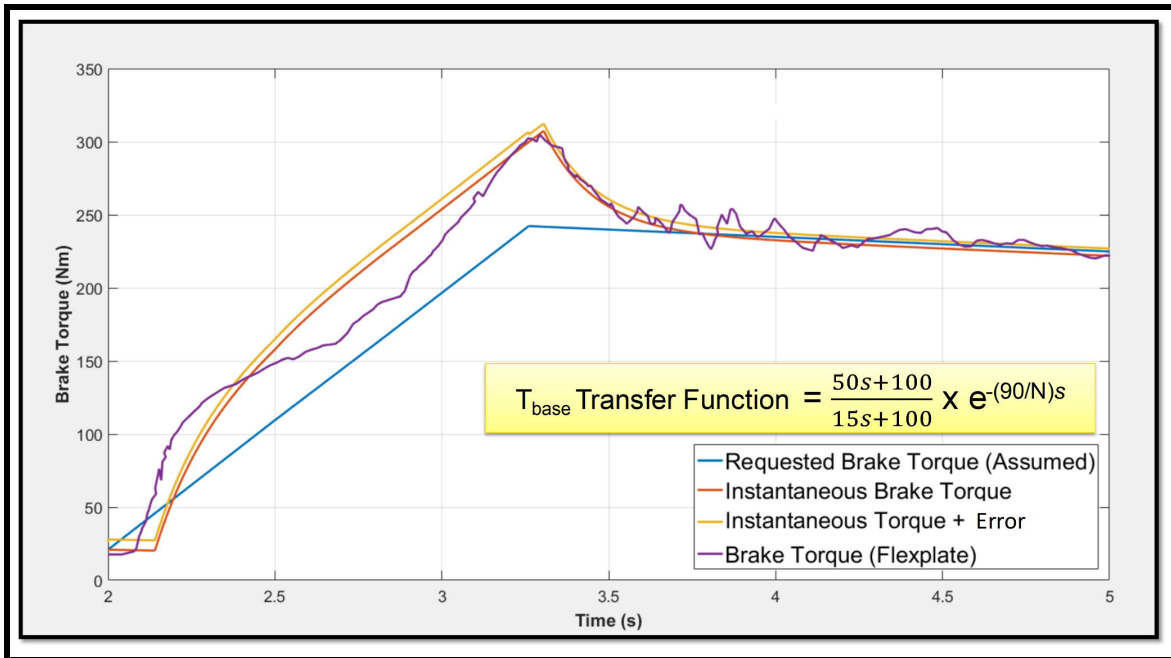


Figure B.2: Observed engine torque response for a throttle input of 0 → 60%

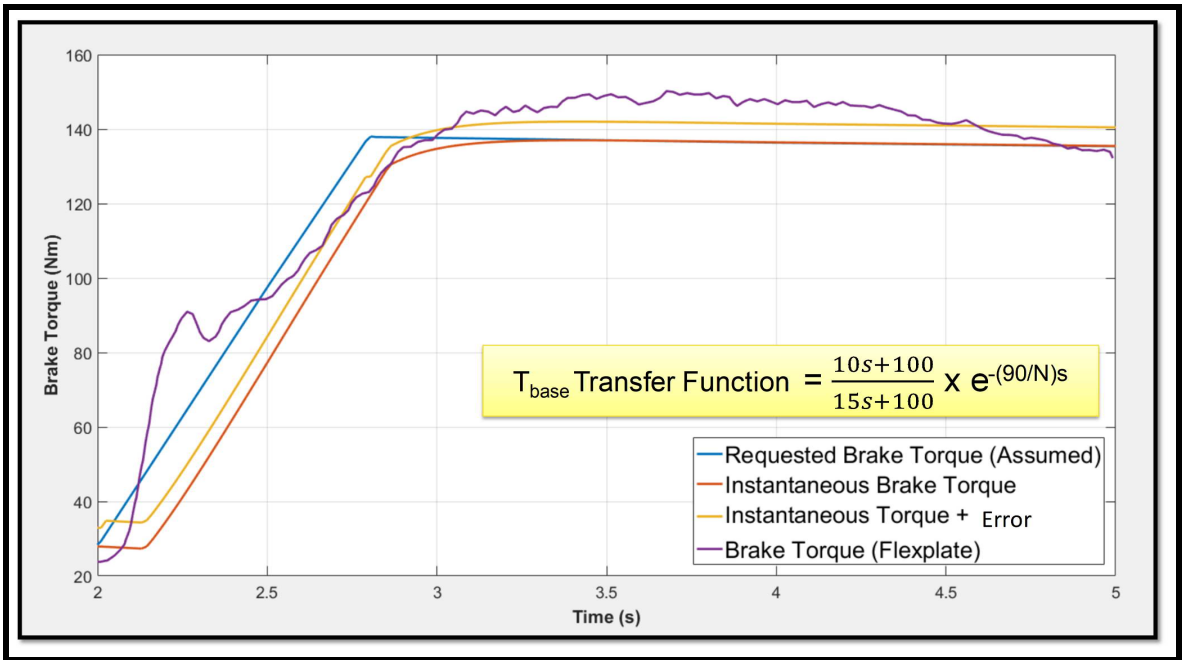


Figure B.3: Observed engine torque response for a throttle input of 0 → 20%

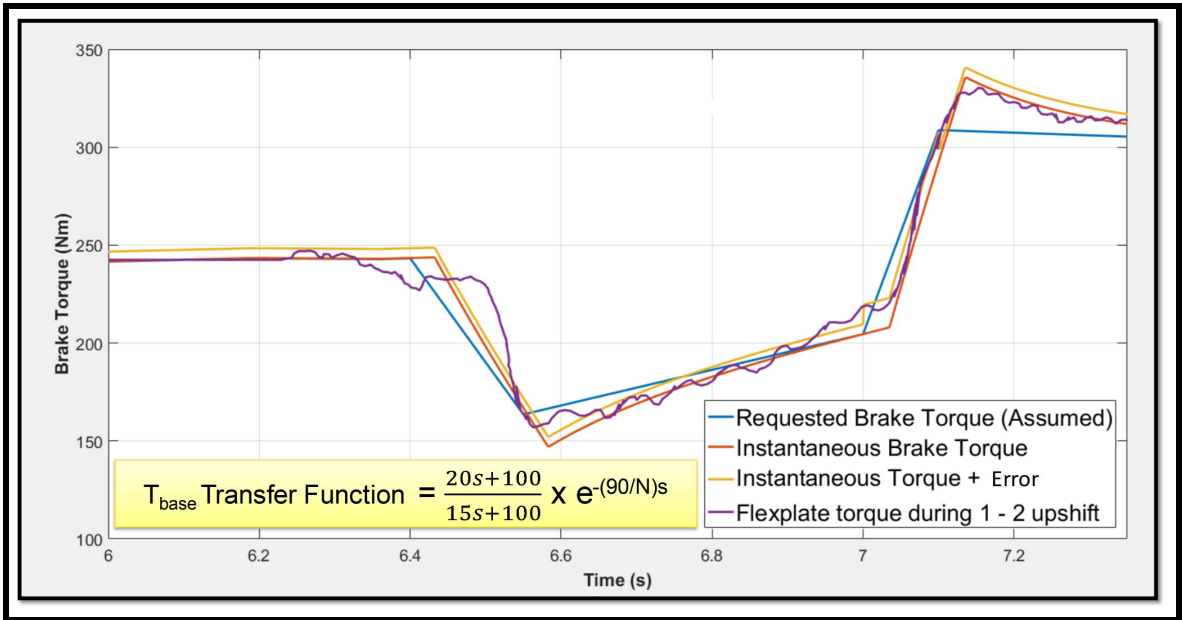


Figure B.4: Observed response for a throttle tip-out scenario

Each of the plot in Fig. B.1 - Fig. B.4 shows flexplate brake torque, which is adapted from the experimental data that the sponsoring organization shared, requested brake torque, which was the assumed simulation input for the engine model, instantaneous brake torque and instantaneous brake torque with error included, which are the observed outputs of the engine model for the transfer functions mentioned on the plots.

Appendix C

Program and Data File Summary

Following image and model files were used for this thesis, organized as per the chapter they were used in:

C.1 Chapter 1

Table C.1
Chapter 1 figure files

File name	File description
Fig_1_1.jpg	Figure 1.1
Fig_1_2.jpg	Figure 1.2
Fig_1_3.jpg	Figure 1.3
Fig_1_4.vsdX	Figure 1.4
Fig_1_5.jpg	Figure 1.5
Fig_1_6.bmp	Figure 1.6
Fig_1_7.bmp	Figure 1.7
Fig_1_8.bmp	Figure 1.8
Fig_1_9.bmp	Figure 1.9
Fig_1_10.vsdX	Figure 1.10

C.2 Chapter 2

Table C.2
Chapter 2 figure files

File name	File description
Fig_2_1.vsd	Figure 2.1
Fig_2_2.bmp	Figure 2.2
Fig_2_3.bmp	Figure 2.3
Fig_2_4.jpg	Figure 2.4
Fig_2_5.jpg	Figure 2.5
Fig_2_6.bmp	Figure 2.6
Fig_2_7.jpg	Figure 2.7
Fig_2_8.jpg	Figure 2.8
Fig_2_9.jpg	Figure 2.9
Fig_2_10.vsd	Figure 2.10
Fig_2_11.fig	Figure 2.11
Fig_2_12.fig	Figure 2.12
Fig_2_13.fig	Figure 2.13
Fig_2_14.fig	Figure 2.14
Fig_2_15.fig	Figure 2.15
Fig_2_16.fig	Figure 2.16
Fig_2_17.fig	Figure 2.17
Fig_2_18.fig	Figure 2.18
Fig_2_19.fig	Figure 2.19
Fig_2_20.fig	Figure 2.20

Table C.3
Chapter 2 model files

File name	File description
Driveline_model_final.ame	Amesim file of full-order driveline model
Torque_shaping_final_model.slx	Simulink file of engine model
Plot_code_model_validation_lockedTCC.m	Code for model validation graphs of locked TCC
Plot_code_model_validation_openTCC.m	Code for model validation graphs of open TCC
Plot_code_model_validation_slippingTCC.m	Code for model validation graphs of slipping TCC

Table C.4
Chapter 2 model validation files

File name	File description
Locked_press_override.rec	Experimental vehicle data for locked TCC
Slipping.rec	Experimental vehicle data for slipping TCC
Open.rec	Experimental vehicle data for open TCC

C.3 Chapter 3

Table C.5
Chapter 3 figure files

File name	File description
Fig_3_1.fig	Figure 3.1
Fig_3_2.fig	Figure 3.2
Fig_3_3.fig	Figure 3.3
Fig_3_4.fig	Figure 3.4
Fig_3_5.fig	Figure 3.5
Fig_3_6.fig	Figure 3.6
Fig_3_7.fig	Figure 3.7
Fig_3_8.fig	Figure 3.8
Fig_3_9.fig	Figure 3.9
Fig_3_10.fig	Figure 3.10
Fig_3_11.fig	Figure 3.11
Fig_3_12.fig	Figure 3.12
Fig_3_13.fig	Figure 3.13
Fig_3_14.fig	Figure 3.14

Table C.6
Chapter 3 model files

File name	File description
Driveline_model_final.ame	Amesim file of full-order driveline model
Torque_shaping_parametric_analysis.slx	Simulink file of engine model with inputs defined for parametric analysis
Plot_code_parametric_analysis_torque_ramp_rate.m	Code for parametric analysis plots for variation in input torque ramp rate
Plot_code_parametric_analysis_backlash_size.m	Code for parametric analysis plots for variation in backlash size
Plot_code_parametric_analysis_shaft_stiffness.m	Code for parametric analysis plots for variation in shaft stiffness
Plot_code_parametric_analysis_shaft_damping.m	Code for parametric analysis plots for variation in shaft damping coefficient

C.4 Chapter 4

Table C.7
Chapter 4 figure files

File name	File description
Fig_4.1.vsd	Figure 4.1
Fig_4.2.fig	Figure 4.2
Fig_4.3.vsd	Figure 4.3
Fig_4.4.fig	Figure 4.4
Fig_4.5.fig	Figure 4.5
Fig_4.6.fig	Figure 4.6
Fig_4.7.vsd	Figure 4.6
Fig_4.8.fig	Figure 4.8

Table C.8
Chapter 4 model files

File name	File description
Driveline_model_ROM.ame	Amesim file of reduced-order driveline model
Torque_shaping_final_model.slx	Simulink file of engine model
Torque_shaping_ROM_model.slx	Simulink file ROM controls
Plot_code_ROM_validation.m	Code for validation of ROM with FOM
Plot_code_ROM_controls.m	Code for comparison of ROM in controls

C.5 Appendix B

Table C.9
Appendix B figure files

File name	File description
Fig_B.1.bmp	Figure B.1
Fig_B.2.bmp	Figure B.2
Fig_B.3.bmp	Figure B.3
Fig_B.4.bmp	Figure B.4